Editors' Suggestion

Noncommutativity between the low-energy limit and integer dimension limits in the ϵ expansion: A case study of the antiferromagnetic quantum critical metal

Andrés Schlief,[1,2] Peter Lunts,[3] and Sung-Sik Lee[1,2]

[1]*Perimeter Institute for Theoretical Physics, 31 Caroline St. N., Waterloo ON, Canada N2L 2Y5*

[2]*Department of Physics & Astronomy, McMaster University, 1280 Main St. W., Hamilton ON, Canada L8S 4M1*

[3]*Center for Computational Quantum Physics, Flatiron Institute, 162 5th Avenue, New York, New York 10010, USA*

(Received 22 May 2018; published 23 August 2018)

We study the field theory for the SU(N_c) symmetric antiferromagnetic quantum critical metal with a one-dimensional Fermi surface embedded in general space dimensions between two and three. The asymptotically exact solution valid in this dimensional range provides an interpolation between the perturbative solution obtained from the ϵ expansion near three dimensions and the nonperturbative solution in two dimensions. We show that critical exponents are smooth functions of the space dimension. However, physical observables exhibit subtle crossovers that make it hard to access subleading scaling behaviors in two dimensions from the low-energy solution obtained above two dimensions. These crossovers give rise to noncommutativities, where the low-energy limit does not commute with the limits in which the physical dimensions are approached.

DOI: 10.1103/PhysRevB.98.075140

I. INTRODUCTION

Quantum critical points (QCPs) host exotic quantum states that do not support well-defined single-particle excitations [1]. Universal long-distance physics of such critical states are often described by interacting quantum field theories that cannot be diagonalized in any known single particle basis. In two space dimensions, strong quantum fluctuations make it hard to extract universal low-energy data from interacting theories. In the presence of supersymmetry [2] or conformal symmetry [3,4], kinematic constraints can be strong enough to fix some dynamical properties. However, nonperturbative tools are scarce for strongly interacting nonrelativistic quantum field theories (QFTs) in general.

For this reason, it has been theoretically challenging to understand non-Fermi liquid metals that arise near itinerant QCPs in two dimensions [5–48]. Couplings between particle-hole excitations and critical order parameter fluctuations present at QCPs invalidate Landau Fermi liquid theory that is built on the quasiparticle paradigm [49]. As a result of abundant low-energy excitations that amplify infrared quantum fluctuations, even perturbative expansions become subtle in the presence of small parameters. The $1/N$ expansion, where N is the number of flavors of fermions that form Fermi surfaces, does not give a controlled expansion in two-dimensional non-Fermi liquids [21,24]. The ϵ expansions pose different types of challenges. In the dimensional regularization scheme which tunes the dimension of space with a fixed codimension of the Fermi surface [28,50], it is hard to access the physics in two dimensions from higher dimensions because of a spurious ultraviolet (UV)/infrared (IR) mixing caused by the size of the Fermi surface [51]. If one tunes the codimension of the Fermi surface, one usually has to go beyond the one-loop order to capture the leading order physics correctly [34,52,53]. Although the ϵ expansion gives a controlled expansion, extrapolating perturbative results obtained near the upper critical dimension to strongly coupled theories in two spatial dimensions is a highly nontrivial task. For a brief review of recent progress in field theories of non-Fermi liquids, see Ref. [54]. For recent discussions on subtle issues in the ϵ expansion for relativistic QFTs [55,56], see Refs. [57–59].

In the past two decades, the non-Fermi liquids realized at the antiferromagnetic (AFM) QCP have been extensively studied both analytically [15,17,18,24–26,30,33,34,37,38,40,42,47,60,61] and numerically [62–68] because correlated metals such as electron doped cuprates [69], iron pnictides [70], and heavy fermion compounds [71] exhibit strong AFM fluctuations. In Fig. 1 we show a schematic phase diagram for metals that exhibit AFM quantum phase transitions. Recently, the field theory that describes the metallic AFM QCP with the SU(2) symmetry and a C_4-symmetric Fermi surface has been solved both perturbatively near $d = 3$ based on the ϵ expansion [34,53] and nonperturbatively in $d = 2$ [72], where d is the space dimension. The availability of both the perturbative solution valid near the upper critical dimension and the nonperturbative solution for the two-dimensional theory provides a rare opportunity to test the extent to which the ϵ expansion is applicable to strongly coupled theories in which $\epsilon \sim 1$.

In this paper we test the dimensional regularization scheme (and the ϵ expansion) as a methodology using the field theory for AFM quantum critical metals as a model theory. We solve the theory in general dimensions between two and three to understand how the perturbative solution obtained from the ϵ expansion near the upper critical dimension evolves as nonperturbative effects become stronger with decreasing dimension. From this we expose both strengths and weaknesses of the dimensional regularization scheme. On the one hand, the exact critical exponents are smooth functions of the space dimension, and the ϵ expansion can provide a useful ansatz for the exact exponents in two dimensions. On the other hand, it is difficult to capture full scaling behaviors in two dimensions from the low-energy solution obtained above two dimensions

 ©2018 American Physical Society

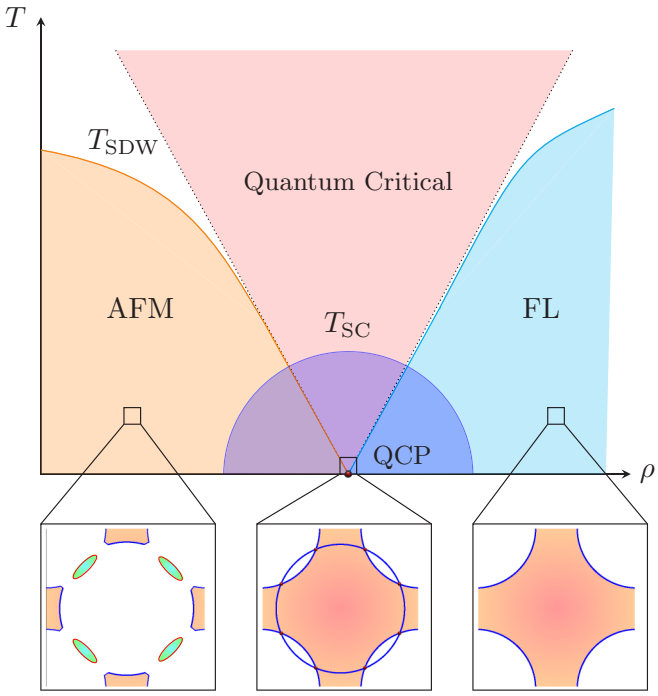

FIG. 1. A schematic phase diagram for metals that undergo antiferromagnetic quantum phase transitions. T denotes temperature and ρ denotes a tunning parameter that drives the transition from a paramagnetic Fermi liquid (FL) to an antiferromagnetically ordered Fermi liquid (AFM). The dome near the critical point represents a superconducting phase. The physics in the quantum critical region is dictated by the underlying quantum critical point (QCP).

because the low-energy limit and the $d \to 2$ limit do not commute.

This paper is organized as follows. In Sec. II we review the field theory that describes AFM quantum critical metals in space dimensions between two and three [34,53]. In Sec. III we begin by summarizing the scaling forms of the low-energy Green's functions. Table I encapsulates the main result of this paper: *physical observables exhibit noncommutativities in the sense that the low-energy limit and the limit in which physical dimensions are approached do not commute.* After the summary, we provide details that lead to such scaling forms. We first review the one-loop solution valid in $d = 3$, and discuss how the solution fails to capture the low-energy physics in $d = 3 - \epsilon$ for any nonzero ϵ. This is caused by a noncommutativity between the low-energy limit and the $d \to 3$ limit. We then move on to the general solution valid in any $2 < d < 3$, which shows how nonperturbative effects become important as the space dimension is lowered. Finally, we compare this solution with the nonperturbative solution obtained at $d = 2$. While critical exponents vary smoothly in d, the full low-energy Green's functions in $d = 2$ *cannot* be obtained by taking the $d \to 2$ limit of the low-energy Green's function obtained in $d > 2$ due to a noncommutativity between the $d \to 2$ limit and the low-energy limit. We finish this paper by making some concluding remarks in Sec. IV.

II. FIELD THEORY IN $2 \leqslant d \leqslant 3$

The minimal theory for the SU(2) symmetric AFM quantum critical metal in two dimensions is written as [15,17,24,34]

$$\begin{aligned} S_{d=2} = & \sum_{n=1}^{4} \sum_{\sigma=\uparrow,\downarrow} \int dk \overline{\Psi}_{n,\sigma}(k)[i\gamma_0 k_0 + i\gamma_1 \varepsilon_n(\vec{k}; v)]\Psi_{n,\sigma}(k) \\ & + \frac{1}{4}\int dq \left(q_0^2 + c^2|\vec{q}|^2\right) \mathrm{Tr}[\Phi(-q)\Phi(q)] \\ & + ig \sum_{n=1}^{4} \sum_{\sigma,\sigma'=\uparrow,\downarrow} \int dk \int dq \overline{\Psi}_{\bar{n},\sigma}(k+q) \\ & \times \Phi_{\sigma\sigma'}(q)\gamma_1 \Psi_{n,\sigma'}(k) \\ & + \frac{u}{4}\left[\prod_{i=1}^{3}\int dq_i\right] \mathrm{Tr}[\Phi(q_1+q_3)\Phi(q_2-q_3)] \\ & \times \mathrm{Tr}[\Phi(-q_1)\Phi(-q_2)]. \end{aligned} \tag{1}$$

Here $k = (k_0, \vec{k})$ with k_0 denoting fermionic Matsubara frequency and $\vec{k} = (k_x, k_y)$, the two-dimensional momentum measured from each of the eight hot spots (points on the C_4-symmetric Fermi surface connected

TABLE I. Scale-dependent universal crossover functions and renormalized velocities in the low-energy limit for each fixed d. Here $\ell \equiv \log(\Lambda/\mu)$ is a logarithmic length scale associated with a running energy scale μ, and a UV cutoff Λ. β_d, $\zeta(d)$, $\mathfrak{F}_z(d)$, $\mathfrak{F}_\Phi(d)$, and $\mathfrak{B}(d)$ are smooth and positive functions defined in Eqs. (13), (23), (31), (33), and (D21), respectively. It is noted that $\beta_2 = \sqrt{\pi/2}$, $\zeta(2) = (2\pi)^{-1}$, $\mathfrak{F}_z(2) = \sqrt{2}$, $\mathfrak{F}_\Phi(2) = 2\sqrt{2}$, and $\mathfrak{B}(2) = (4\pi^2)^{-1}$ in $d = 2$, and $\beta_{3-\epsilon} = \sqrt{4\pi\epsilon}$, $\zeta(3-\epsilon) = \epsilon/2$, $\mathfrak{F}_z(3) = 3/(2^{14}h_5^*)^{1/3}$, $\mathfrak{F}_\Phi(3) = 3/(2^8 h_5^*)^{1/3}$, and $\mathfrak{B}(3) = 2h_5^*$ with $h_5^* \approx 5.7\times10^{-4}$ [53] in $d = 3 - \epsilon$ to leading order in $\epsilon \ll 1$.

	$d = 2$	$2 < d < 3$	$d = 3$
$F_z(\mu)$	$\exp\left(2\sqrt{N_c^2-1}\,\frac{\ell^{1/2}}{\log(\ell)}\right)$	$\exp\left[(d-2)\mathfrak{F}_z(d)\left(N_c^2-1\right)^{\frac{1}{d}}\ell^{\frac{1}{d}}\right]$	$\ell^{\frac{(N_c^2+N_cN_f-1)}{2(N_c^2+N_cN_f-3)}}$
$F_\Psi(\mu)$	$\ell^{3/8}$	$\sqrt{\ell}$	$\sqrt{\log(\ell)}$
$F_\Phi(\mu)$	$\exp\left(\frac{2\ell^{1/2}}{\sqrt{N_c^2-1}}\right)$	$\exp\left(-\frac{\mathfrak{F}_\Phi(d)}{2}\frac{[(d-2)N_c^2-d]}{\left(N_c^2-1\right)^{\frac{d-1}{d}}}\ell^{\frac{1}{d}}\right)$	$\log(\ell)$
$v(\mu)$	$\frac{\pi^2 N_c N_f}{2(N_c^2-1)\ell\log(\ell)}$	$\frac{\pi N_c N_f(d-2)}{4(N_c^2-1)\zeta(d)(d-1)\ell}$	$\frac{\pi N_c N_f(N_c^2-N_cN_f-3)}{4(N_c^2-1)(N_c^2+N_cN_f-1)\log(\ell)}$
$c(\mu)$	$\frac{\pi}{4\sqrt{N_c^2-1}}\frac{1}{\sqrt{\ell}}$	$\left[\frac{\pi\beta_d^4\mathfrak{B}(d)}{(3-d)(d-1)\zeta(d)\left(N_c^2-1\right)}\right]^{\frac{1}{d}}\frac{1}{\ell^{\frac{1}{d}}}$	$\frac{\pi(N_c^2-N_cN_f-3)}{4(N_c^2-1+N_cN_f)}\frac{1}{\log(\ell)}$

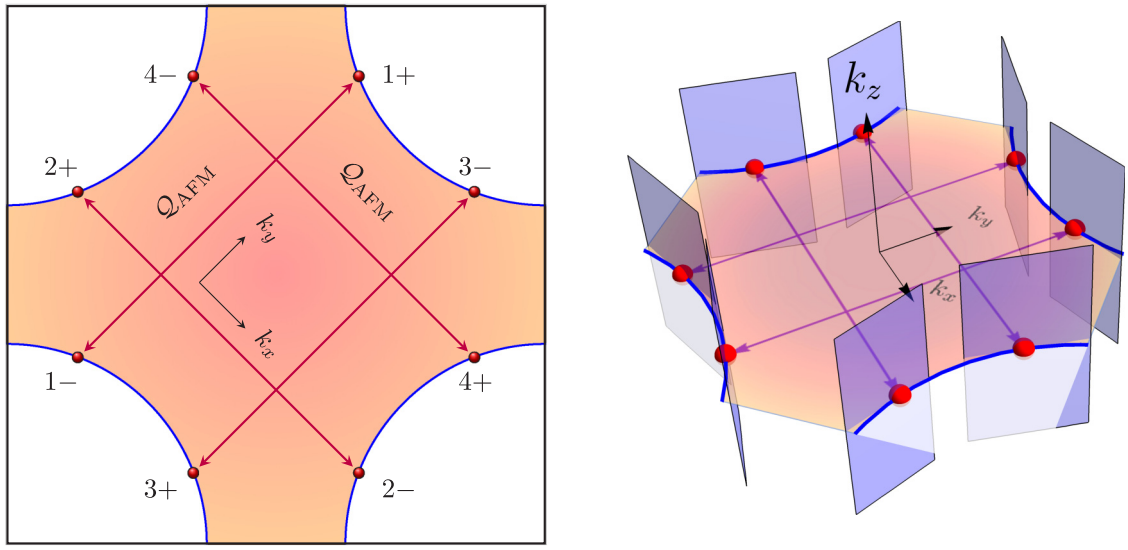

(a) (b)

FIG. 2. (a) A Fermi surface with C_4 symmetry in two dimensions. The (red) dots represent the hot spots connected by the AFM wave vector which is chosen to be $\mathcal{Q}_{\rm AFM} = \pm\sqrt{2}\pi\hat{k}_x$ or $\mathcal{Q}_{\rm AFM} = \pm\sqrt{2}\pi\hat{k}_y$ up to reciprocal lattice vectors $\sqrt{2}\pi(\hat{k}_x \pm \hat{k}_y)$. (b) One-dimensional Fermi surface embedded in a three-dimensional momentum space. The (blue) planes correspond to locally flat patches that include line nodes (blue lines) near the hot spots.

by the commensurate wave vector $\mathcal{Q}_{\rm AFM}$), as shown in Fig. 2. We use a simplified notation $dk = \frac{dk_0}{(2\pi)}\frac{d\vec{k}}{(2\pi)^2}$ for the integration measure. The four two-component spinors are given by $\Psi_{1,\sigma}(k) = (\psi^{(+)}_{1,\sigma}(k), \psi^{(+)}_{3,\sigma}(k))^{\rm T}$, $\Psi_{2,\sigma}(k) = (\psi^{(+)}_{2,\sigma}(k), \psi^{(+)}_{4,\sigma}(k))^{\rm T}$, $\Psi_{3,\sigma}(k) = (\psi^{(-)}_{1,\sigma}(k), -\psi^{(-)}_{3,\sigma}(k))^{\rm T}$, and $\Psi_{4,\sigma}(k) = (\psi^{(-)}_{2,\sigma}(k), -\psi^{(-)}_{4,\sigma}(k))^{\rm T}$, where $\psi^{(m)}_{n,\sigma}(k)$ is the Grassmanian field representing electrons near the hot spots labeled by $n = 1, 2, 3, 4$ and $m = \pm$, and with spin $\sigma = \uparrow, \downarrow$. $\gamma_0 = \sigma_y$ and $\gamma_1 = \sigma_x$ are the 2×2 Pauli matrices, and $\overline{\Psi}_{n,\sigma}(k) = \Psi^{\dagger}_{n,\sigma}(k)\gamma_0$. The energy dispersion relations of the fermions are given by $\varepsilon_1(\vec{k}; v) = vk_x + k_y$, $\varepsilon_2(\vec{k}; v) = -k_x + vk_y$, $\varepsilon_3(\vec{k}; v) = vk_x - k_y$, and $\varepsilon_4(\vec{k}; v) = k_x + vk_y$, where v measures the component of the Fermi velocity perpendicular to $\mathcal{Q}_{\rm AFM}$. The component of the Fermi velocity parallel to $\mathcal{Q}_{\rm AFM}$ is set to one. $q = (q_0, \vec{q})$ denotes the bosonic Matsubara frequency and two-dimensional momentum $\vec{q} = (q_x, q_y)$ measured relative to $\mathcal{Q}_{\rm AFM}$. The bosonic matrix field representing the collective spin fluctuations is written in the defining representation of SU(2): $\Phi(q) = \sum_{a=1}^{3}\phi^a(q)\tau^a$, where τ^a denotes the three generators of SU(2). We choose the normalization of the generators as ${\rm Tr}[\tau^a\tau^b] = 2\delta^{ab}$. $\Phi(q)$ carries momentum $\vec{q} + \mathcal{Q}_{\rm AFM}$, and c denotes the velocity of the AFM spin fluctuations. The coupling between the collective mode and the fermions is denoted by g. $\overline{n}$ denotes the hot spot connected to n via $\mathcal{Q}_{\rm AFM}$, that is, $\overline{1} = 3, \overline{2} = 4, \overline{3} = 1$, and $\overline{4} = 2$. Finally, u sources the quartic interaction between the collective modes.

Now we write down the theory defined in $2 \leqslant d \leqslant 3$, where d is the space dimension [29,34,42,53]. Here the codimension of the Fermi surface is tuned while keeping its dimension fixed to be one. This choice of dimensional regularization scheme maintains locality in real space, and avoids the UV/IR mixing that arises through couplings between different patches of the Fermi surface when its dimension is greater than one [51]. The theory in $2 \leqslant d \leqslant 3$ is written as

$$
\begin{aligned}
S_d = &\sum_{n=1}^{4}\sum_{\sigma=1}^{N_c}\sum_{j=1}^{N_f}\int dk\overline{\Psi}_{n,\sigma,j}(k)[i\boldsymbol{\Gamma}\cdot\mathbf{K} + i\gamma_{d-1}\varepsilon_n(\vec{k}; v)] \\
&\times \Psi_{n,\sigma,j}(k) + \frac{1}{4}\int dq(|\mathbf{Q}|^2 + c^2|\vec{q}|^2){\rm Tr}[\Phi(-q)\Phi(q)] \\
&+ \frac{ig}{\sqrt{N_f}}\sum_{n=1}^{4}\sum_{\sigma,\sigma'=1}^{N_c}\sum_{j=1}^{N_f}\int dk\int dq\overline{\Psi}_{\overline{n},\sigma,j}(k+q) \\
&\times \Phi_{\sigma\sigma'}(q)\gamma_{d-1}\Psi_{n,\sigma',j}(k) \\
&+ \frac{1}{4}\left[\prod_{i=1}^{3}\int dq_i\right]\{u_1{\rm Tr}[\Phi(q_1+q_3)\Phi(q_2-q_3)] \\
&\times {\rm Tr}[\Phi(-q_1)\Phi(-q_2)] + u_2 \\
&\times {\rm Tr}[\Phi(q_1+q_3), \Phi(q_2-q_3)\Phi(-q_1)\Phi(-q_2)]\}. \qquad (2)
\end{aligned}
$$

Here $k = (\mathbf{K}, \vec{k})$, where $\mathbf{K}$ denotes the $(d-1)$-dimensional vector composed of the Matsubara frequency and $(d-2)$ momentum components that represent the extra space dimensions and $\vec{k} = (k_x, k_y)$. The integration measure is denoted as $dk = \frac{d\mathbf{K}}{(2\pi)^{d-1}}\frac{d\vec{k}}{(2\pi)^2}$. In $2 \leqslant d \leqslant 3$, the number of spinor components is fixed to be two. $(\boldsymbol{\Gamma}, \gamma_{d-1}) = (\gamma_0, \gamma_1, \ldots, \gamma_{d-2}, \gamma_{d-1})$ denotes 2×2 gamma matrices that satisfy the Clifford algebra: $\{\gamma_\mu, \gamma_\nu\} = 2\delta_{\mu\nu}\mathbb{I}_{2\times2}$ with $\mathbb{I}_{2\times2}$ being the identity matrix. The fermionic kinetic term in Eq. (2) describes a metal with a one-dimensional Fermi surface embedded in a d-dimensional momentum space. We choose $\gamma_0 = \sigma_y$ and $\gamma_{d-1} = \sigma_x$ without loss of generality. For completeness, the fermion flavor is promoted to $j = 1, 2, \ldots, N_f$. We also generalize the SU(2) spin

group to SU(N_c) such that $\sigma = 1, 2, \ldots, N_c$. Accordingly, the boson field is written as $\Phi(q) = \sum_{a=1}^{N_c^2-1} \phi^a(q)\tau^a$, where τ^a denotes the $(N_c^2 - 1)$ generators of SU(N_c) subject to the normalization $\mathrm{Tr}[\tau^a\tau^b] = 2\delta^{ab}$. u_1 and u_2 source two possible quartic interactions which are independent from each other for $N_c \geqslant 4$. In what follows, we consider the theory for general $N_c \geqslant 2$ and $N_f \geqslant 1$. However, the validity of the solution presented in this paper does not rely on N_c or N_f being large.

$$G_1(k;d) = \frac{1}{iF_\Psi(|\mathbf{K}|)} \frac{1}{F_z(|\mathbf{K}|)\boldsymbol{\Gamma}\cdot\mathbf{K} + \gamma_{d-1}[v(|\mathbf{K}|)k_x + k_y]}, \tag{3}$$

$$D(k;d) = \frac{1}{F_\Phi(|\mathbf{K}|)} \frac{1}{F_z(|\mathbf{K}|)^{d-1}|\mathbf{K}|^{d-1} + c(|\mathbf{K}|)^{d-1}(|k_x|^{d-1} + |k_y|^{d-1})}, \tag{4}$$

for $\frac{\vec{k}}{|\mathbf{K}|F_z(|\mathbf{K}|)} \sim 1$. $G_1(k;d)$ denotes the fermion Green's function at hot spot $n = 1$ in d space dimensions. The Green's functions at other hot spots are related to $G_1(k;d)$ through the C_4 symmetry of the theory. $D(k;d)$ is the Green's function for the AFM collective mode. Here the condition $\vec{k}/[|\mathbf{K}|F_z(|\mathbf{K}|)] \sim 1$ is chosen so that the forms of the Green's functions are invariant (up to the weak scale dependence of the velocities) under scale transformations in which momentum and frequency are simultaneously taken to zero. If the dynamical critical exponent was fixed, the scale invariance of the Green's function would be manifest under the rescaling in which $\vec{k}/|\mathbf{K}|^{1/z}$ is fixed, where z is the dynamical critical exponent. In the present case, the dynamical critical exponent depends weakly on the scale, and it flows to $z = 1$ in the low-energy limit, as will be shown later. At finite energy scales, the Green's functions are invariant under the scale transformation in which $\vec{k}/[|\mathbf{K}|F_z(|\mathbf{K}|)]$ is fixed, where $F_z(|\mathbf{K}|)$ is a function that encodes the scale dependence of the dynamical critical exponent. The leading power-law dependencies of the Green's functions in energy and momentum reflect the dynamical critical exponent ($z = 1$), and the scaling dimensions of the fermion ($[\Psi(k)] = -(d+2)/2$) and the collective mode ($[\Phi(k)] = -d$) at the fixed point. The full Green's functions deviate from the perfect power-law behaviors due to a scale dependence of marginally irrelevant operators. In $d < 3$, the ratio between velocities,

$$w(\mu) \equiv v(\mu)/c(\mu) \tag{5}$$

controls quantum corrections, where $v(\mu)$ and $c(\mu)$ are the renormalized velocities that depend on the energy scale μ. As will be shown later, a slow flow of $w(\mu)$ generates superlogarithmic corrections captured by $F_z(\mu)$, $F_\Psi(\mu)$, and $F_\Phi(\mu)$, that is, corrections that are smaller than a power law but larger than any fixed power of a logarithm in energy. $F_\Psi(\mu)$ [$F_\Phi(\mu)$] represents the correction to the scaling dimension of the fermion (boson) field. In $d = 3$, quantum corrections are controlled by g^2/v, which yield logarithmic corrections to the power-law scalings. The scale dependencies of $v(\mu)$, $c(\mu)$, $F_z(\mu)$, $F_\Psi(\mu)$, and $F_\Phi(\mu)$ in each dimension are summarized in Table I.

Although the critical exponents that characterize the fixed point are smooth functions of d, $v(\mu)$, $c(\mu)$, $F_z(\mu)$, $F_\Psi(\mu)$, and $F_\Phi(\mu)$, evaluated in the small μ limit, are not, as is shown in Table I. This leads to discontinuities of $\lim_{k\to 0} G_1(k;d)$ and $\lim_{k\to 0} D(k;d)$ as functions of d. The discontinuities are caused by a lack of commutativity between the low-energy limit and the limits in which d approaches the physical dimensions,

$$\lim_{k\to 0}\lim_{d\to 2,3} G_1(k;d) \neq \lim_{d\to 2,3}\lim_{k\to 0} G_1(k;d), \tag{6}$$

and similarly for $D(k;d)$. Since the Green's functions diverge at $k = 0$, Eq. (6) makes sense only if the small k limit is viewed as the asymptotic limit of the Green's functions. In other words, $\lim_{k\to 0} G_1(k;d)$ should be understood as the asymptote of $G_1(k;d)$ in the small k limit, that is, the k-dependent function that $G_1(k;d)$ asymptotically approaches in the small k limit at a fixed d rather than $G_1(0;d)$. With this, Eq. (6) implies that the low-energy asymptote of $G_1(k;d)$ at $d = 2, 3$ cannot be reproduced by taking the $d \to 2, 3$ limits of the low-energy asymptotes of $G_1(k;d)$ obtained in $2 < d < 3$.

The expressions in Table I are obtained by taking the low-energy limit at a fixed dimension. Because of the noncommutativity in Eq. (6), $\lim_{k\to 0} G_1(k;d)$ is not a continuous function of d at $d = 2$ and $d = 3$. The noncommutativity arises because of the existence of crossover energy scales that vanish in the $d \to 2, 3$ limits. In the plane of spatial dimension and energy scale, there are three distinct regions divided by these crossover energy scales as is shown in Fig. 3. The first crossover energy scale is given by $E_1(d) \sim \Lambda e^{-\frac{(N_c N_f)^{3/2}}{(N_c^2-1)}(3-d)^{-3/2}}$ which vanishes exponentially as d approaches three, where Λ is a UV energy scale. The second scale $E_2(d) \sim \Lambda e^{-(d-2)^2\frac{(N_c N_f)^2}{(N_c^2-1)}e^{\frac{2}{d-2}}}$ vanishes in a doubly exponential fashion as d approaches two. The three regions divided by $E_1(d)$ and $E_2(d)$ are governed by different physics.

In region I of Fig. 3 [$\mu > E_1(d)$], the low-energy physics is described at the one-loop order by a quasilocal marginal Fermi liquid, where v and c flow to zero as $1/\log[\log(\Lambda/\mu)]$ with $w \sim O(1)$ [34]. Because the velocities flow to zero, the magnitude of higher-loop diagrams is not only determined by the number of vertices, but also by enhancement factors of $1/v$ and $1/c$ that originate from the fact that modes become dispersionless at low energies. In particular, the one-loop fixed point is controlled only when g^2 flows to zero faster than v and c. In $d = 3$, the one-loop results become asymptotically exact at low energies because $\lambda \equiv g^2/v$ flows to zero much faster

Finally, we note that the field theory in $2 \leqslant d \leqslant 3$ inherits the underlying C_4 symmetry of the Fermi surface.

III. NONCOMMUTATIVITY BETWEEN THE LOW ENERGY AND THE PHYSICAL DIMENSION LIMITS

In this section we first summarize the main results of the paper without derivation. The scaling form of the Green's functions in $2 \leqslant d \leqslant 3$ is given by

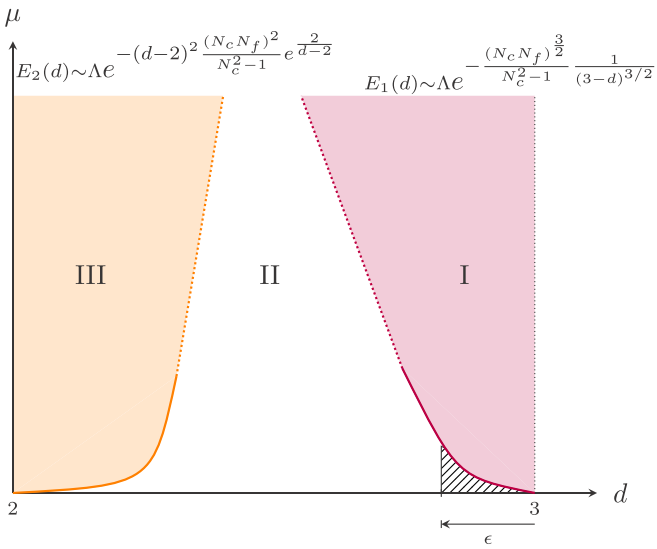

FIG. 3. Two crossover energy scales that divide the plane of spatial dimension (d) and energy scale (μ) into three regions. At low energies, $w(\mu)$ flows to an order one number in region I, while it flows to zero in regions II and III. Region III is distinguished from region II by the fact that physical observables receive additional logarithmic corrections.

than any power of the velocities. While the quasilocal marginal Fermi liquid behavior persists down to the zero energy limit in $d = 3$, the low-energy physics becomes qualitatively different below three dimensions. In $d = 3 - \epsilon$ with $\epsilon > 0$, λ becomes order of ϵ, while v and c still flow to zero logarithmically at the one-loop order. Due to the enhanced quantum fluctuations associated with the vanishing velocities and nonvanishing λ, higher-loop effects become qualitatively important at energies below the crossover energy scale $E_1(d)$ [34,53]. For any nonzero $\epsilon < 1$, the theory flows into a new region (region II) in which leading order quantum fluctuations are no longer contained within the one-loop order. The noncommutativity between the $d \to 3$ and $\mu \to 0$ limits arises because $E_1(d)$ vanishes as $d \to 3$.

It turns out that it is sufficient to include a two-loop quantum correction in addition to the one-loop quantum corrections to the leading order in $\epsilon \ll 1$ because all other higher-loop corrections are suppressed by ϵ in the shaded area of region II shown in Fig. 3 [42,53]. The physics below $E_1(d)$ is qualitatively different from that of region I. In particular, w flows to zero in the low-energy limit in $d = 3 - \epsilon$ due to the two-loop effect that modifies the flow of the velocities. The fact that quantum corrections are not organized by the number of loops even close to the upper critical dimension is a feature caused by the emergent quasilocality where velocities flow to zero in the low-energy limit.

As d decreases further away from three, an infinite set of diagrams, which are suppressed by higher powers of ϵ near three dimensions, becomes important. Although it is usually hopeless to include all higher-order quantum corrections, in the present case one can use w as a control parameter since w dynamically flows to zero in the low-energy limit. In the small w limit, only the diagrams in Figs. 7(a), 7(b) and 8 remain important even when $\epsilon \sim 1$ [53]. In there, the double wiggly line represents the renormalized boson propagator which is self-consistently dressed with the diagrams in Figs. 7(a) and 7(b). The propagator of the collective mode becomes $D(q) = \frac{1}{|\mathbf{Q}|^{d-1}+c(v)^{d-1}(|q_x|^{d-1}+|q_y|^{d-1})}$, where $c(v)$ is the velocity of the incoherent collective mode given by $c(v)^d \sim \frac{v}{d-2}$.

The behavior in region II does not extend smoothly to $d = 2$ because of another crossover set by an energy scale $E_2(d)$ that vanishes in the $d \to 2$ limit. The existence of the crossover is expected from the fact that the relation $c(v)^d \sim \frac{v}{d-2}$ valid in region II becomes ill-defined in $d = 2$. The UV divergence in the $d \to 2$ limit is caused by the incoherent nature of the AFM collective mode which has significant low-energy spectral weight even at large momenta. At $d = 2$, the divergence gives rise to a logarithmic enhancement of $c(v)$ as $c(v)^2 \sim v \log[1/w(v)]$. The extra logarithmic correction causes the additional set of diagrams in Fig. 9 to become important in region III. This gives rise to a lack of commutativity between the $d \to 2$ limit and the low-energy limit.

In what follows, we elaborate on the points summarized in this section starting from $d = 3$. Sections III A and III C are mostly summaries of Refs. [34,53] and [72] for regions I and III, respectively. Section III B is devoted to region II, which is the main new result of the present paper.

A. Region I: From $d = 3$ to $d = 3 - \epsilon$

In three dimensions, the Yukawa coupling is marginal under the Gaussian scaling. The one-loop quantum corrections shown in Figs. 4(a) to 4(e) drive all parameters of the theory (g, v, c, u_i) to flow to zero in such a way that the ratios defined by $\lambda = g^2/v$, $w = v/c$, and $\kappa_i = u_i/c^2$ become [34]

$$\lambda^* = 0, \quad c^* = 0, \quad w^* = \frac{N_c N_f}{N_c^2 - 1}, \quad \text{and} \quad \kappa_i^* = 0 \tag{7}$$

in the low-energy limit. As is shown in Table I, the velocities flow to zero as $v(\ell), c(\ell) \sim 1/\log(\ell)$ in the logarithmic length scale $\ell \equiv \log(\Lambda/\mu)$, while the rescaled coupling flows to zero as $\lambda(\ell) \sim 1/\ell$. Because λ flows to zero faster than both v and c, the ratios g^{2n}/c^m and g^{2n}/v^m, which control the perturbative expansion, flow to zero for any $n, m > 1$. This implies that all higher-order corrections are suppressed at low energies. The physical observables receive only logarithmic quantum corrections compared to the Gaussian scaling. The crossover functions that capture the corrections are given by

$$F_z(|\mathbf{K}|) = [\log(\Lambda/|\mathbf{K}|)]^{\frac{(N_c^2+N_cN_f-1)}{2(N_c^2+N_cN_f-3)}}, \tag{8}$$

$$F_\Psi(|\mathbf{K}|) = \sqrt{\log[\log(\Lambda/|\mathbf{K}|)]}, \tag{9}$$

$$F_\Phi(|\mathbf{K}|) = \log[\log(\Lambda/|\mathbf{K}|)], \tag{10}$$

in the small $|\mathbf{K}|$ limit with $\frac{\vec{k}}{|\mathbf{K}|F_z(|\mathbf{K}|)} \sim 1$ fixed. See Appendix A for details.

For $d < 3$, $\lambda = g^2/v$ no longer flows to zero, although v and c still do under the one-loop renormalization group (RG) flow. This puts the control of the one-loop analysis in peril even close to three dimensions. Due to the enhanced infrared quantum fluctuations caused by the modes that become increasingly dispersionless at low energies, some higher-loop diagrams,

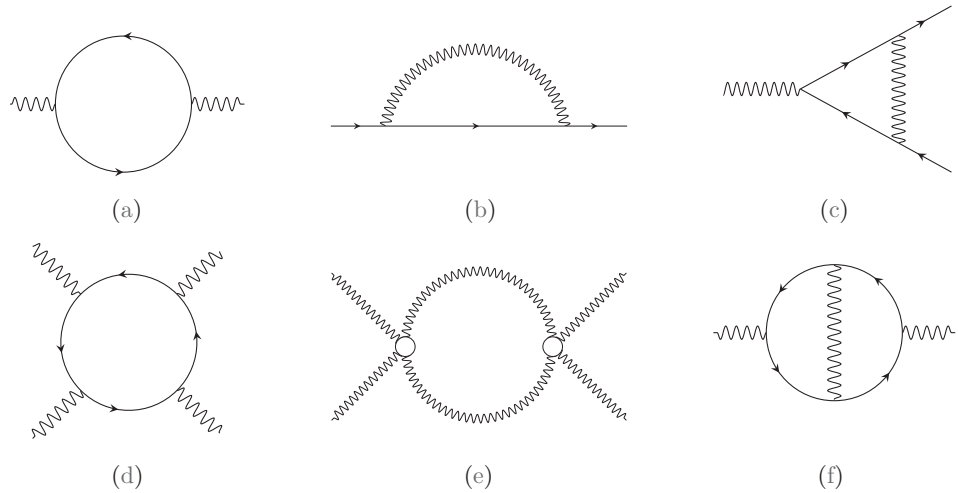

FIG. 4. Quantum corrections at the modified one-loop order.

albeit suppressed by powers of ϵ, diverge at the one-loop fixed point. The divergence is cured only after the two-loop correction in Fig. 4(f) is included. The energy scale below which the two-loop effect becomes qualitatively important marks the crossover energy scale $E_1(d) \sim \Lambda \exp\left(-\frac{(N_c N_f)^{3/2}}{(N_c^2-1)}\epsilon^{-3/2}\right)$. At energies below $E_1(d)$, the two-loop self-energy speeds up the collective mode such that v and c flow to zero with a hierarchy $c \gg v$, with $c^3 \sim \epsilon v/N_c N_f$ [53]. The low-energy fixed point is characterized by

$$\lambda^* = 4\pi\epsilon, \quad x^* = \frac{N_c N_f}{16\pi \mathfrak{B}(3)}, \quad w^* = 0, \quad \text{and} \quad \kappa_i^* = 0, \quad (11)$$

where $x \equiv g^2/c^3$ and $\mathfrak{B}(3) \approx 0.0012434$ (see Appendix D for details). It can be shown that all other higher-loop corrections remain finite and they are suppressed by ϵ at the modified one-loop (M1L) fixed point where the two-loop effect is taken into account in addition to the one-loop corrections [53]. The shaded area of region II in Fig. 3 is where the M1L description is valid at low energies.

Comparing these results with those obtained in three dimensions shows a qualitative change in the low-energy physics. Especially, the fixed point value of w is not a continuous function of d. In region I, the one-loop effect causes w to flow to the $O(1)$ value given in Eq. (7). Below the crossover energy scale $E_1(d)$, w flows to zero as $w(\ell) = \frac{N_c N_f}{2^{10/3}\mathfrak{B}(3)^{1/3}(N_c^2-1)^{2/3}}\epsilon^{-1}\ell^{-2/3}$ [53]. For small but nonzero ϵ, the M1L description is controlled, and w flows to zero at sufficiently low energies. Thus, the low-energy fixed point below three dimensions is qualitatively different from the fixed point that the theory flows into in three dimensions. This discrepancy shows that the low-energy limit does not commute with the $d \to 3$ limit. The change in the flow of w is responsible for the disparity between the low-energy physical observables in $d = 3 - \epsilon$ in the $\epsilon \to 0$ limit and those in $d = 3$.

There are two relatively well separated stages of the RG flow in the space of λ, x, w, and κ_i for $\epsilon > 0$ and $\mu < E_1(d)$. In the first stage, the RG flow converges towards a one-dimensional manifold, where deviations away from the manifold die out as a power law in the energy scale. The one-dimensional manifold can be parametrized by one of the parameters, say w, where λ, x, and κ_i take w-dependent values. Once the RG flow converges to the one-dimensional manifold, all couplings are controlled by a slow sublogarithmic flow of w [53]. This is shown in Fig. 5. At low energies, we can keep only one coupling, although the microscopic theory has five independent parameters.

At the IR fixed point, the fermion keeps the Gaussian scaling dimension $[\Psi(k)] = -(d+2)/2$, while the collective mode acquires an anomalous dimension which gives $[\Phi(k)] = -d$. Interestingly, the scaling dimensions of the fields are set such that the fermion kinetic term and the Yukawa coupling

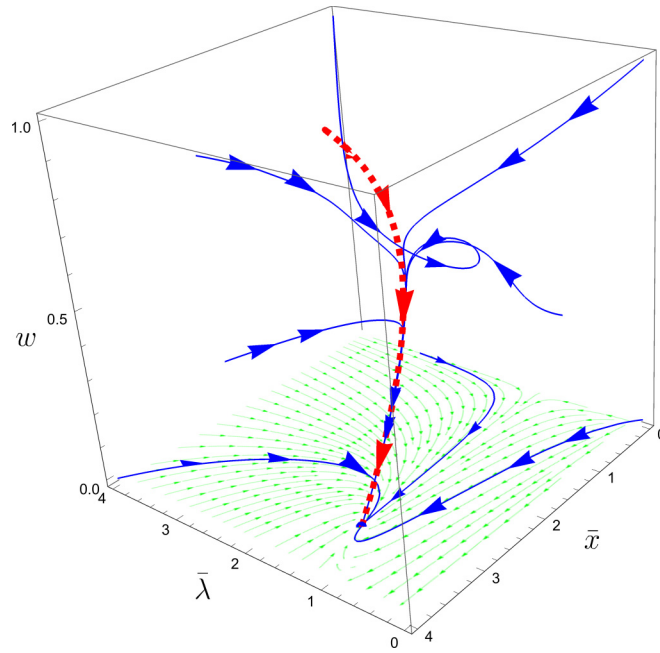

FIG. 5. RG flow projected in the space of $(\bar{\lambda}, \bar{x}, w)$ for $N_c = 2$, $N_f = 1$, and $\epsilon = 0.01$ with $\kappa_i = 0$. The axes are scaled as $\bar{\lambda} = 10\lambda$ and $\bar{x} = x/10$. The dashed (red) line corresponds to the one-dimensional manifold towards which the RG flow is rapidly attracted before a slow flow along the manifold takes the couplings to the low-energy fixed point located on the $w = 0$ plane. The three trajectories that do not seem to converge to the universal one-dimensional manifold lie on the $w = 0$ plane.

TABLE II. Comparison between the scaling dimensions of fields and couplings deduced from the Gaussian and interaction-driven (ID) scalings.

Quantity	Gaussian	ID
$[\Psi(k)]$	$-\left(\frac{d+2}{2}\right)$	$-\left(\frac{d+2}{2}\right)$
$[\Phi(k)]$	$-\left(\frac{d+3}{2}\right)$	$-d$
$[g]$	$\frac{3-d}{2}$	0
$[u_i]$	$3-d$	$-(3-d)$

are marginal while the boson kinetic term and the quartic coupling are irrelevant. A similar protection of the scaling exponents arises in the $1/N$ expansion for the nematic QCP in d-wave superconductors [73]. Physically, the collective mode is strongly dressed by particle-hole excitations, while its feedback to fermions remains small. This provides a crucial hint in constructing a nonperturbative ansatz for regions II and III.

B. Region II: $2 < d < 3$

As the dimension approaches two, quantum fluctuations become progressively stronger, and the perturbative expansion no longer works. In the following we describe a nonperturbative approach that captures the universal low-energy physics for any $0 < \epsilon \leqslant 1$ [72].

1. Tree level scaling: Gaussian vs interaction driven

Under the Gaussian scaling, which prioritizes the kinetic terms over the interactions in Eq. (2), the scaling dimensions of g and u_i are $\epsilon/2$ and ϵ, respectively. For $\epsilon \sim 1$, quantum corrections to the Gaussian scaling are expected to be $O(1)$ and the ϵ expansion breaks down. For strongly coupled theories, it is better to start with a scaling which takes into account the interaction upfront rather than perturbatively. The interaction-driven scaling [32] is a scaling that treats the interaction ahead of some kinetic terms. Here we use the information obtained from the ϵ expansion to construct a scaling ansatz for general ϵ. In particular, we choose a scaling in which the fermion kinetic term and the fermion-boson interaction are treated as marginal operators at the expense of treating the boson kinetic and quartic terms as irrelevant. This uniquely fixes the scaling dimensions of the fields as in Table II.

The ansatz is consistent with the result from the ϵ expansion which suggests that the collective mode is likely to acquire an $O(1)$ anomalous dimension near $d = 2$. Since the boson dynamics is dominated by particle-hole excitations, treating the boson kinetic term as an irrelevant operator is natural. Dropping those terms that are irrelevant under the interaction-driven scaling, we write down the minimal action as

$$\begin{aligned} S_d = &\sum_{n=1}^{4}\sum_{\sigma=1}^{N_c}\sum_{j=1}^{N_f}\int dk \overline{\Psi}_{n,\sigma,j}(k)[i\boldsymbol{\Gamma}\cdot\mathbf{K} + i\gamma_{d-1}\varepsilon_n(\vec{k};v)] \\ &\times \Psi_{n,\sigma,j}(k) \\ &+ \frac{i\beta_d\sqrt{v}}{\sqrt{N_f}}\sum_{n=1}^{4}\sum_{\sigma,\sigma'=1}^{N_c}\sum_{j=1}^{N_f}\int dk\int dq \overline{\Psi}_{\bar{n},\sigma,j}(k+q) \\ &\times \Phi_{\sigma\sigma'}(q)\gamma_{d-1}\Psi_{n,\sigma',j}(k), \end{aligned} \tag{12}$$

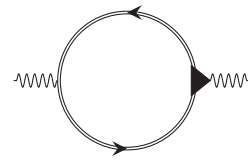

FIG. 6. Schwinger-Dyson (SD) equation for the exact boson self-energy. The double line represents the fully dressed fermion propagator and the triangle represents the fully dressed vertex.

where

$$\beta_d = \frac{\pi^{\frac{d-1}{4}}}{\Gamma\left(\frac{d}{2}\right)}\sqrt{\frac{\Gamma(d)\Gamma\left(\frac{d-1}{2}\right)\cos\left(\frac{\pi(d+2)}{2}\right)}{2^{3-d}}} \tag{13}$$

is a positive constant in $2 \leqslant d < 3$. The freedom in choosing the overall scale of the boson field is used to fix the Yukawa coupling in terms of v such that $g^2/v \sim (3-d)$. The choice of β_d is such that the one-loop boson self-energy becomes order of one. Roughly speaking, the fermion-boson coupling is replaced by $\sqrt{v}$ as the interaction is screened in such a way that g^2 and v balance with each other in the low-energy limit [34,53,72]. Since the ϵ expansion is organized in powers of g^2/v, the theory with $g^2/v \sim 1$ is a strongly coupled theory that cannot be accessed perturbatively in ϵ.

The five parameters (v, c, g, u_1, u_2) in the original theory are now reduced to one (v) in the minimal theory. The velocity v specifies the low-energy effective theory within the one-dimensional manifold shown in Fig. 5. The minimal theory is valid at energy scales low enough that the five parameters of the theory have already flown to the one-dimensional manifold, and all renormalized couplings are tied to one leading irrelevant parameter.

2. Schwinger-Dyson equation for the boson dynamics

In the absence of the bare kinetic term for the boson, its dynamics is entirely generated from the self-consistent Schwinger-Dyson (SD) equation shown in Fig. 6. The SD equation for the exact boson self-energy is given by

$$\begin{aligned} D(q)^{-1} = m_{\text{C.T.}} - 2\beta_d^2 v\sum_{n=1}^{4}\int dk \\ \times \mathrm{Tr}\left[\gamma_{d-1}G_{\bar{n}}(k+q)\Gamma_n^{(2,1)}(k,q)G_n(k)\right]. \end{aligned} \tag{14}$$

Here $m_{\text{C.T.}}$ is a counter term that tunes the mass to zero in order to keep the theory at criticality. $\Gamma_n^{(2,1)}(k,q)$ denotes the fully dressed vertex function. $D(q)$ and $G_n(k)$ denote the fully dressed boson and fermion propagators, respectively.

We proceed following the scheme used in Ref. [72]:

(1) We first assume that $v \ll 1$ and solve the SD equation in the small v limit to obtain the boson dynamics to the leading order in v.

(2) By using the dressed boson propagator obtained under the assumption that v is small, we show that v indeed flows to zero in the low-energy limit.

We start with an ansatz for the fully dressed boson propagator in the small v limit:

$$D(q)^{-1} = |\mathbf{Q}|^{d-1} + c(v)^{d-1}(|q_x|^{d-1} + |q_y|^{d-1}), \tag{15}$$

where $c(v)$ is the "velocity" of the damped AFM collective mode that is to be determined as a function of v from the SD equation. This ansatz is consistent with the interaction-driven scaling and the symmetries of the theory. However, the ultimate justification for the ansatz comes from the fact that Eq. (15) satisfies the SD equation as will be shown below.

Assuming that $v \ll c(v) \ll 1$, one can show that a general L-loop diagram with L_f fermion loops and E external legs scales at most as

$$\mathcal{G}(L, L_f, E) \sim v^{\frac{E-2}{2}} \left(\frac{v}{c(v)}\right)^{L-L_f} \tag{16}$$

up to logarithmic corrections. The proof closely follows the one given in Refs. [53,72]. In Appendix B we provide a brief review of the proof.

The magnitude of general diagrams is not determined solely by the number of interaction vertices since v appears not only in the interaction term, but also in the fermion kinetic term. In the presence of the assumed hierarchy between velocities $[v \ll c(v) \ll 1]$ there is a systematic suppression of diagrams with $L > L_f$.

To the zeroth order in v, only the one-loop diagram in Fig. 7(a) survives. However, the leading order graph is independent of the spatial momentum. To determine such a dependence of the boson propagator, one has to go to the next order in v shown in Figs. 7(b) and 7(c). Figure 7(c) is again independent of the spatial momentum, and only Fig. 7(b) remains important to the next leading order in v. This is shown in Appendix D. Figures 7(a) and 7(b) give rise to the SD equation:

$$\begin{aligned} D(q)^{-1} = m'_{\text{C.T.}} + |\mathbf{Q}|^{d-1} - \frac{4\beta_d^4 v^2}{N_c N_f} \sum_{n=1}^{4} \int dp \int dk \\ \times \text{Tr}\big[\gamma_{d-1} G_{\bar{n}}^{(0)}(k+p)\gamma_{d-1} G_n^{(0)}(k+q+p)\gamma_{d-1} \\ \times G_{\bar{n}}^{(0)}(k+q)\gamma_{d-1} G_n^{(0)}(k)\big] D(p), \end{aligned} \tag{17}$$

where

$$G_n^{(0)}(k) = \frac{1}{i}\left(\frac{\mathbf{\Gamma}\cdot\mathbf{K} + \gamma_{d-1}\varepsilon_n(\vec{k}; v)}{\mathbf{K}^2 + \varepsilon_n(\vec{k}; v)^2}\right) \tag{18}$$

denotes the bare fermion propagator and $m'_{\text{C.T.}}$ is a two-loop mass counter term. The term $|\mathbf{Q}|^{d-1}$ in Eq. (17) is the contribution from the one-loop self-energy. Explicit computation of the two-loop boson self-energy with Eq. (15) in the small v limit indeed yields the boson propagator of the form in Eq. (15) with a self-consistent equation for $c(v)$ (see Appendix D for details),

$$c(v)^{d-1} = \frac{4\beta_d^4 \mathfrak{B}(d)}{(3-d)N_c N_f} \frac{v}{c(v)} \mathfrak{S}\left(d-2; \frac{v}{c(v)}\right), \tag{19}$$

where $\mathfrak{S}[d-2; w(v)]$ is defined in Eq. (D13). It has the following limiting behaviors: $\lim_{w(v)\to 0} \mathfrak{S}[d-2; w(v)] = 1/(d-2)$ and $\lim_{d\to 2} \mathfrak{S}[d-2; w(v)] = \log[1/w(v)]$. $\mathfrak{B}(d)$, defined in Eq. (D21), is positive and finite in $2 \leqslant d \leqslant 3$. Here we consider the low-energy limit at a fixed $d > 2$. If $w(v) \ll 1$, an assumption that needs to be checked later, we can use $\lim_{w(v)\to 0} \mathfrak{S}[d-2; w(v)] = 1/(d-2)$ to solve Eq. (19) and obtain

$$c(v) = \left(\frac{4\beta_d^4 \mathfrak{B}(d)}{(3-d)(d-2)N_c N_f}\right)^{\frac{1}{d}} v^{\frac{1}{d}}. \tag{20}$$

This general expression reduces to $c(v)^3/v = 64\pi^2 \mathfrak{B}(3)\epsilon/N_c N_f$ near three dimensions, which matches the result from the ϵ expansion in Ref. [53]. Finally we note that $v \ll c(v) \ll 1$ and, thus, the assumed hierarchy of velocities $[w(v) \ll 1]$ is satisfied if $v \ll 1$. This gives the first consistency check of the scaling ansatz.

3. *Low-energy fixed point*

The remaining question is whether v flows to zero in the low-energy limit. The beta function for v is determined by the fermion self-energy, and the vertex correction determines the $O[w(v)]$ correction to the scaling dimension of the collective mode. Because the Yukawa coupling remains marginal in any $2 \leqslant d \leqslant 3$ according to the interaction-driven scaling, the quantum corrections are logarithmically divergent in all $2 \leqslant d \leqslant 3$. This is in contrast to the conventional perturbative approaches where logarithmic divergences arise only at the critical dimensions. We determine local counter terms by requiring that physical observables are independent of UV cutoff scales (see Appendix C for details on the RG scheme).

According to Eq. (16), the contribution of the diagrams in Fig. 8(a) to the beta function of v is at most $O[w(v)]v$. An explicit computation in Appendix D shows that the contribution is actually suppressed further by $c(v)$. The reason for the additional suppression by $c(v)$ is that the external momentum can be directed to flow only through the boson propagator. As a result, the self-energy depends on the external spatial momentum through $c(v)\vec{k}$. According to Eq. (16), higher order diagrams are suppressed by at least one more power of $w(v)$. Because

$$w(v) \sim v^{(d-1)/d} \ll c(v) \sim v^{1/d} \tag{21}$$

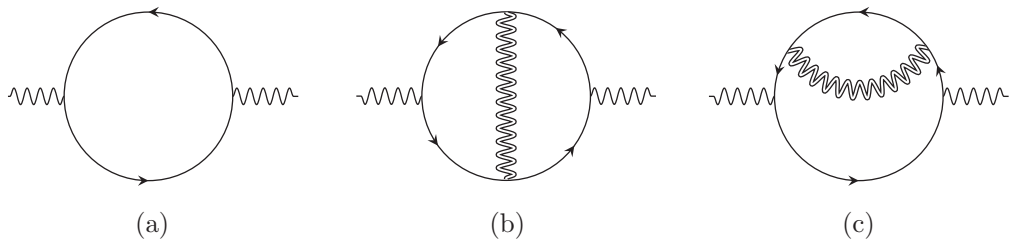

FIG. 7. Leading order corrections to the boson self-energy in the small v limit. The solid line represents the bare fermion propagator and the double wiggly line denotes the fully dressed self-consistent propagator in Eq. (15).

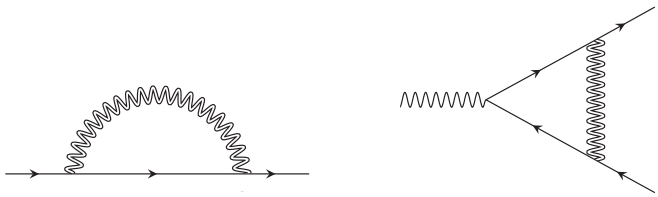

(a) (b)

FIG. 8. Leading order quantum corrections to the minimal local action. In $2 < d < 3$, all other diagrams are strictly subleading in v.

for $d > 2$, higher order diagrams remain smaller than Fig. 8(a) despite its additional suppression by $c(v)$. In the small v limit, Fig. 8(a) determines the beta function for v (see Appendix E for a derivation),

$$\beta_v \equiv \frac{dv}{d\log\mu} = \frac{4\left(N_c^2-1\right)}{\pi N_c N_f}\frac{(d-1)\zeta(d)}{d-2}v^2 \tag{22}$$

to the leading order in v in $2 < d < 3$, where

$$\zeta(d) = -\frac{\cos\left(\frac{\pi d}{2}\right)\Gamma\left(\frac{2d-3}{d-1}\right)\Gamma\left(\frac{1}{d-1}\right)\Gamma\left(\frac{d-1}{2}\right)}{2^{3-d}\pi^{3/2}\Gamma\left(\frac{d}{2}\right)} \tag{23}$$

is positive in $2 \leqslant d < 3$. The beta function indeed shows that v flows to zero at low energies in any $2 < d < 3$. This completes the proof that the theory flows to the fixed point described by the ansatz introduced in the previous section if the bare value of v is small.

At the low-energy fixed point with $v = 0$, the dynamical critical exponent (z) and the corrections to the interaction-driven scaling dimensions of the fields (η_Ψ and η_Φ) in Table II are given by

$$z = 1, \quad \eta_\Psi = 0, \quad \eta_\Phi = 0. \tag{24}$$

It is noted that $\eta_\Psi = \eta_\Phi = 0$ does not mean that the fixed point is the Gaussian fixed point because η_Ψ, η_Φ denote the correction to the interaction-driven scaling, which already includes the $O(1)$ anomalous dimension for the collective mode compared to the noninteracting theory.

4. Green's functions

Defining the logarithmic length scale $\ell = \log(\Lambda/\mu)$, Eqs. (20) and (22) imply that $w(v)$ flows to zero as

$$w(\ell) = \frac{\pi^{\frac{d-1}{d}} N_c N_f (d-2)}{4\left[(d-1)\zeta(d)\left(N_c^2-1\right)\right]^{\frac{d-1}{d}}}\left[\frac{(3-d)}{\beta_d^4\mathfrak{B}(d)}\right]^{\frac{1}{d}}\frac{1}{\ell^{\frac{d-1}{d}}} \tag{25}$$

for $\ell \gg \ell_0$ with $\ell_0 \equiv \frac{1}{v_0}\frac{N_c N_f}{N_c^2-1}\mathfrak{S}(d-2; v_0^{\frac{d-1}{d}})^{-1} \sim \frac{(d-2)}{v_0}\frac{N_c N_f}{N_c^2-1}$ and $v_0 \ll 1$ denoting the bare value of v (see Appendix E for details). Even though $w(\ell) = 0$ is a stable low-energy fixed point, $w(\ell)$ is nonzero at intermediate energy scales unless one starts with a fine tuned theory with a perfectly nested Fermi surface. This gives rise to corrections to the scaling form of physical observables. While critical exponents are well defined only at fixed points, it is useful to introduce "scale-dependent critical exponents" that determine the scaling forms of physical observables in the presence of a slowly running irrelevant coupling,

$$z(\ell) = 1 + \frac{\left(N_c^2-1\right)\zeta(d)}{N_c N_f}w(\ell), \tag{26}$$

$$\eta_\Psi(\ell) = -\frac{\left(N_c^2-1\right)(d-1)\zeta(d)}{2N_c N_f}w(\ell), \tag{27}$$

$$\eta_\Phi(\ell) = -\frac{\left[(d-2)N_c^2-d+1\right](d-1)\zeta(d)}{N_c N_f(d-2)}w(\ell). \tag{28}$$

Their derivation can be found in Appendix F. Had $w(\ell)$ flown to a nonzero value at the fixed point, the $O[w(\ell)]$ corrections would have modified the critical exponents in Eq. (24). Since $w(\ell)$ flows to zero, the exponents predicted by the interaction-driven scaling are exact, and the corrections introduce only subleading scalings in the physical observables.

The scaling form of the fermion Green's function is given by Eq. (3) with

$$F_z(|\mathbf{K}|) = \exp\left\{(d-2)\mathfrak{F}_z(d)\left(N_c^2-1\right)^{\frac{1}{d}}\left[\log\left(\frac{\Lambda}{|\mathbf{K}|}\right)\right]^{\frac{1}{d}}\right\}, \tag{29}$$

$$F_\Psi(|\mathbf{K}|) = \sqrt{\log\left[\frac{\Lambda}{|\mathbf{K}|}\right]}, \tag{30}$$

and

$$\mathfrak{F}_z(d) = \frac{\pi d}{4(d-1)}\left(\frac{(3-d)(d-1)\zeta(d)}{\pi\beta_d^4\mathfrak{B}(d)}\right)^{\frac{1}{d}}. \tag{31}$$

It is noted that $F_z(|\mathbf{K}|)$ and $F_\Psi(|\mathbf{K}|)$ introduce corrections that are not strong enough to modify the exponents in the power-law behavior, yet $F_z(|\mathbf{K}|)$ is stronger than logarithmic corrections of marginal Fermi liquids [74,75]. Similarly the crossover function for the bosonic Green's function in Eq. (4) is given by

$$F_\Phi(|\mathbf{Q}|) = \exp\left[\frac{\mathfrak{F}_\Phi(d)\left[\log\left(\frac{\Lambda}{|\mathbf{Q}|}\right)\right]^{\frac{1}{d}}}{2\left(N_c^2-1\right)^{\frac{d-1}{d}}}\left[d-(d-2)N_c^2\right]\right], \tag{32}$$

with

$$\mathfrak{F}_\Phi(d) = \frac{d\pi^{\frac{d-1}{d}}}{2}\left(\frac{(d-1)(3-d)\zeta(d)}{\beta_d^4\mathfrak{B}(d)}\right)^{\frac{1}{d}}. \tag{33}$$

In Appendix F we provide the derivation of these results. Compared to the bare boson propagator, the physical propagator describing the low-energy dynamics of the AFM collective mode is highly damped and incoherent. We note that the deviation of fermion Green's function from that of Fermi liquids as well as the incoherent nature of the AFM collective mode become stronger as d is lowered. This is expected because the effect of interactions is stronger in lower dimensions.

C. Region III: From $d > 2$ to $d = 2$

In this section we discuss how the results obtained in $2 < d < 3$ are connected to the solution in $d = 2$ [72]. We note that the expression in Eq. (20), which is divergent in $d = 2$, is valid only for $d > 2$. This is because the $d \to 2$ limit and the $w(v) \to 0$ limit do not commute in Eq. (19). In order to

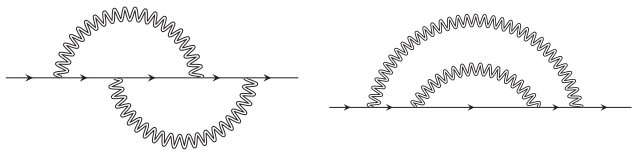

(a) (b)

FIG. 9. Two-loop fermion self-energies. As explained in the text, the two-loop diagram (a) is of the same order as the one-loop diagram in Fig. 8(a). The diagram in (b) is subleading due to an additional suppression by $c(v)$.

access the physics in $d = 2$, we have to take the $d \to 2$ limit before the low-energy limit is taken. In $d = 2$, the $1/(d-2)$ divergence in Eq. (20) is replaced by $\log[1/w(v)]$, and the solution to Eq. (19) is given by

$$c(v) = \sqrt{\frac{1}{8N_cN_f} v \log\left(\frac{1}{v}\right)} \tag{34}$$

to the leading order in v [72]. Notice that the hierarchy $v \ll c(v)$ still holds if $v \ll 1$, and general diagrams still obey Eq. (16) up to logarithmic corrections.

Another complication that arises in $d = 2$ is that the inequality in Eq. (21) no longer holds. This means that the two-loop fermion self-energies shown in Fig. 9 can be as important as the one-loop graph in Fig. 8(a). Figure 9(b) is also additionally suppressed by $c(v)$ for the same reason that Fig. 8(a) is further suppressed by $c(v)$. However, this extra suppression is absent in Fig. 9(a) because the external momentum cannot be directed to flow only through the boson lines. As a result, Fig. 9(a) is of the same order as the one-loop fermion self-energy in $d = 2$. Taking into account the contribution from Figs. 8(a) and 9(a), we obtain the beta function for v in $d = 2$ [72],

$$\beta_v = \frac{2}{\pi^2}\frac{(N_c^2-1)}{N_cN_f} v^2 \log\left(\frac{1}{v}\right). \tag{35}$$

It again predicts that v flows to zero if v is small to begin with.

In $d = 2$, the scale-dependent critical exponents are given by

$$z(\ell) = 1 + \frac{(N_c^2-1)}{2\pi N_cN_f} w(\ell), \tag{36}$$

$$\eta_\Psi(\ell) = -\frac{(N_c^2-1)}{4\pi N_cN_f} w(\ell), \tag{37}$$

$$\eta_\Phi(\ell) = \frac{1}{2\pi N_cN_f} w(\ell) \log\left(\frac{1}{w(\ell)}\right), \tag{38}$$

where $w(\ell)$ flows to zero as

$$w(\ell) = \frac{2\pi N_cN_f}{\sqrt{N_c^2-1}} \frac{1}{\sqrt{\ell}\log(\ell)} \tag{39}$$

for $\ell \gg \ell_0$ with $\ell_0 \equiv \lim_{d\to 2} \frac{1}{v_0}\frac{N_cN_f}{N_c^2-1} \mathfrak{S}(d-2; v_0^{\frac{d-1}{d}})^{-1} \sim \frac{2}{v_0 \log(1/v_0)}\frac{N_cN_f}{N_c^2-1}$ and $v_0 \ll 1$ denoting the bare value of v (see Appendix E for details).

Comparing Eq. (39) with the $d \to 2$ limit of Eq. (25) shows that the flow of $w(\ell)$ in $d > 2$ does not smoothly extend to $d = 2$. This is due to the existence of a crossover energy scale $E_2(d)$ that vanishes in the $d \to 2$ limit. As the energy scale is lowered, the crossover from region III to region II occurs at a scale where $\lim_{w(v)\to 0} \mathfrak{S}[d-2; w(v)] = 1/(d-2) \sim \lim_{d\to 2} \mathfrak{S}[d-2; w(v)] = \log[1/w(v)]$ in Eq. (19). From Eq. (39), the crossover energy scale is obtained to be $E_2(d) \sim \Lambda \exp[-(d-2)^2 \frac{(N_cN_f)^2}{(N_c^2-1)} e^{2/(d-2)}]$. The double exponential dependence originates from the fact that $w(v)$ needs to be exponentially small in $-(d-2)^{-1}$ for the crossover to happen, and, up to sublogarithmic corrections, $w(v)^2$ itself flows to zero logarithmically in two dimensions. The sublogarithmic correction to the flow of $w(\ell)$ is responsible for the extra factor of $(d-2)^2$ in the exponential. For $\mu > E_2(d)$ (region III), $w(\ell)$ flows to zero according to Eq. (39), while for $\mu < E_2(d)$ (region II), the flow is dictated by Eq. (25). Thus, unless $d = 2$, the theory will always flow into region II at sufficiently low energies.

Finally, the corrections to the exponents predicted by the interaction-driven scaling go to zero in the long distance limit because $w(\ell)$ flows to zero. The Green's functions at intermediate energy scales receive super-logarithmic corrections given by the crossover functions [72],

$$F_z(k_0) = \exp\left(2\sqrt{N_c^2-1}\frac{[\log(\Lambda/|k_0|)]^{1/2}}{\log[\log(\Lambda/|k_0|)]}\right), \tag{40}$$

$$F_\Psi(k_0) = [\log(\Lambda/|k_0|)]^{3/8}, \tag{41}$$

$$F_\Phi(k_0) = \exp\left(\frac{2[\log(\Lambda/|k_0|)]^{1/2}}{\sqrt{N_c^2-1}}\right). \tag{42}$$

The crossover functions in $d = 2$ are different from the $d \to 2$ limit of the crossover functions obtained in $d > 2$. This is due to the fact that the low-energy limit and the $d \to 2$ limit do not commute.

IV. SUMMARY

In this paper we solved the low-energy effective theory for the commensurate AFM quantum critical metal with a C_4-symmetric one-dimensional Fermi surface embedded in space dimensions between two and three. The exact critical exponents and the subleading corrections generated from the leading irrelevant perturbation are obtained by extending the nonperturbative approach based on an interaction-driven scaling [72]. The solution in $2 \leqslant d \leqslant 3$ provides an interpolation between the perturbative solution obtained based on the ϵ expansion near the upper critical dimension and the nonperturbative solution for the two-dimensional theory. The general solution exposes both merits and subtle issues of RG schemes based on dimensional regularization. On the one hand, the critical exponents that characterize the low-energy fixed point are smooth functions of the space dimension. This allows one to make an educated guess on the critical exponents in two dimensions from the solution obtained in higher dimensions. On the other hand, the full scaling behaviors in two dimensions are not correctly captured by the low-energy solutions obtained above two dimensions. A crossover scale that vanishes in the $d \to 2$ limit makes it difficult to access the full scaling forms of physical observables in $d = 2$ from solutions obtained in the low-energy limit in $d > 2$. These crossovers give rise to emergent

noncommutativities, where the low-energy limit and the limits in which physical dimensions are approached do not commute.

ACKNOWLEDGMENTS

The research was supported by the Natural Sciences and Engineering Research Council of Canada. Research at the Perimeter Institute is supported in part by the Government of Canada through Industry Canada, and by the Province of Ontario through the Ministry of Research and Information. The Flatiron Institute is a division of the Simons Foundation.

APPENDIX A: PHYSICAL OBSERVABLES IN THREE DIMENSIONS

Here we derive the scaling form of the Green's functions in $d = 3$. We first summarize the regularization and renormalization group (RG) prescription [34], and proceed to compute the scaling form of the low-energy Green's functions.

1. Regularization and RG scheme in $d = 3$

Since $d = 3$ is the upper critical dimension of the theory, every term in Eq. (2) is marginal under the Gaussian scaling, and quantum corrections are expected to be logarithmically divergent. We regulate the theory by introducing two UV cutoffs: Λ in the frequency and codimensional momentum space that is SO$(d-1)$ symmetric, and $\widetilde{\Lambda}$ in the original two-dimensional momentum subspace. We assume that they are comparable in magnitude. To make sure that physical observables are independent of the UV energy scales, we add the following counter terms to the action:

$$
\begin{aligned}
S^{\mathrm{C.T}}_{d=3} = &\sum_{n=1}^{4}\sum_{\sigma=1}^{N_c}\sum_{j=1}^{N_f}\int dk\overline{\Psi}_{n,\sigma,j}(k)[i\mathcal{A}_1\mathbf{\Gamma}\cdot\mathbf{K} + i\gamma_2\widetilde{\varepsilon}_n(\vec{k};v)]\Psi_{n,\sigma,j}(k) + \frac{1}{4}\int dq(\mathcal{A}_4|\mathbf{Q}|^2 + \mathcal{A}_5c^2|\vec{q}|^2)\mathrm{Tr}[\Phi(-q)\Phi(q)]\\
&+\frac{ig\mathcal{A}_6}{\sqrt{N_f}}\sum_{n=1}^{4}\sum_{\sigma,\sigma'=1}^{N_c}\sum_{j=1}^{N_f}\int dk\int dq\overline{\Psi}_{\bar{n},\sigma,j}(k+q)\Phi_{\sigma\sigma'}(q)\gamma_2\Psi_{n,\sigma',j}(k)\\
&+\frac{1}{4}\left[\prod_{i=1}^{3}\int dq_i\right]\{\mathcal{A}_7u_1\mathrm{Tr}[\Phi(q_1+q_3)\Phi(q_2-q_3)]\mathrm{Tr}[\Phi(-q_1)\Phi(-q_2)]\\
&+\mathcal{A}_8u_2\mathrm{Tr}[\Phi(q_1+q_3)\Phi(q_2-q_3)\Phi(-q_1)\Phi(-q_2)]\}. \qquad \text{(A1)}
\end{aligned}
$$

Here $\gamma_2 = \sigma_x$ is the first Pauli matrix, $\widetilde{\varepsilon}_1(\vec{k};v) = \mathcal{A}_2vk_x + \mathcal{A}_3k_y$, $\widetilde{\varepsilon}_2(\vec{k};v) = -\mathcal{A}_3k_x + \mathcal{A}_2vk_y$, $\widetilde{\varepsilon}_3(\vec{k};v) = \mathcal{A}_2vk_x - \mathcal{A}_3k_y$, and $\widetilde{\varepsilon}_4(\vec{k};v) = \mathcal{A}_3k_x + \mathcal{A}_2vk_y$. The $\mathcal{A}_i$'s are momentum-independent counter term coefficients. Adding this counter term action to Eq. (2) in $d = 3$ yields the renormalized action:

$$
\begin{aligned}
S^{\mathrm{Ren}}_{d=3} = &\sum_{n=1}^{4}\sum_{\sigma=1}^{N_c}\sum_{j=1}^{N_f}\int dk_B\overline{\Psi}_{n,\sigma,j;B}(k_B)[i\mathbf{\Gamma}\cdot\mathbf{K}_B + i\gamma_2\varepsilon_n(\vec{k}_B;v_B)]\Psi_{n,\sigma,j;B}(k_B)\\
&+\frac{1}{4}\int dq_B\left(|\mathbf{Q}_B|^2 + c_B^2|\vec{q}_B|^2\right)\mathrm{Tr}[\Phi_B(-q_B)\Phi_B(q_B)]\\
&+\frac{ig_B}{\sqrt{N_f}}\sum_{n=1}^{4}\sum_{\sigma,\sigma'=1}^{N_c}\sum_{j=1}^{N_f}\int dk_B\int dq_B\overline{\Psi}_{\bar{n},\sigma,j;B}(k_B+q_B)\Phi_{B;\sigma\sigma'}(q_B)\gamma_2\Psi_{n,\sigma',j;B}(k_B)\\
&+\frac{1}{4}\left[\prod_{i=1}^{3}\int dq_{i;B}\right]\{u_{1;B}\mathrm{Tr}[\Phi_B(q_{1;B}+q_{3;B})\Phi_B(q_{2;B}-q_{3;B})]\mathrm{Tr}[\Phi_B(-q_{1;B})\Phi_B(-q_{2;B})]\\
&+u_{2;B}\mathrm{Tr}[\Phi(q_{1;B}+q_{3;B})\Phi_B(q_{2;B}-q_{3;B})\Phi_B(-q_{1;B})\Phi_B(-q_{2;B})]\}. \qquad \text{(A2)}
\end{aligned}
$$

The renormalized frequency, momenta, fields, velocities, and couplings are related to the bare ones through

$$\mathbf{K}_B = \frac{\mathcal{Z}_1}{\mathcal{Z}_3}\mathbf{K}, \quad \vec{k}_B = \vec{k}, \quad v_B = \frac{\mathcal{Z}_2}{\mathcal{Z}_3}v, \quad c_B = \sqrt{\frac{\mathcal{Z}_5}{\mathcal{Z}_4}}\left(\frac{\mathcal{Z}_1}{\mathcal{Z}_3}\right)c, \qquad \text{(A3)}$$

$$g_B = \frac{\mathcal{Z}_6}{\mathcal{Z}_3\sqrt{\mathcal{Z}_4}}g, \quad u_{1;B} = \frac{\mathcal{Z}_7}{\mathcal{Z}_4^2}\left(\frac{\mathcal{Z}_1}{\mathcal{Z}_3}\right)^2u_1, \quad u_{2;B} = \frac{\mathcal{Z}_8}{\mathcal{Z}_4^2}\left(\frac{\mathcal{Z}_1}{\mathcal{Z}_3}\right)^2u_2, \qquad \text{(A4)}$$

$$\Psi_B(k_B) = \mathcal{Z}_\Psi^{1/2}\Psi(k), \quad \text{and} \quad \Phi_B(k_B) = \mathcal{Z}_\Phi^{1/2}\Phi(k), \qquad \text{(A5)}$$

where $\mathcal{Z}_i = 1 + \mathcal{A}_i$, $\mathcal{Z}_\Psi = \mathcal{Z}_3(\mathcal{Z}_3/\mathcal{Z}_1)^2$, $\mathcal{Z}_\Phi = \mathcal{Z}_4(\mathcal{Z}_3/\mathcal{Z}_1)^4$, and the field indices have been suppressed. The renormalized action gives rise to the quantum effective action that can be expanded as

$$\mathbf{\Gamma}[\{\overline{\Psi}, \Psi, \Phi\}, v, c, g, u_i; \mu] = \sum_{m=0}^{\infty}\sum_{n=0}^{\infty} \mathbf{\Gamma}^{(2m,n)}[\{\overline{\Psi}, \Psi, \Phi\}, v, c, g, u_i; \mu],$$

where

$$\begin{aligned}
&\mathbf{\Gamma}^{(2m,n)}[\{\overline{\Psi}, \Psi, \Phi\}, v, c, g, u_i; \mu] \\
&= \left(\prod_{j=1}^{2m+n}\int dk_j\right)(2\pi)^{d+1}\delta\left(\sum_{j=1}^{m} k_j - \sum_{j=1+m}^{2m+n} k_j\right) \\
&\quad\times \Gamma^{(2m,n)}(k_1, \ldots, k_{2m+n-1}, v, c, g, u_i; \mu)\overline{\Psi}(k_1)\cdots\overline{\Psi}(k_m)\Psi(k_{1+m})\cdots\Psi(k_{2m})\Phi(k_{1+2m})\cdots\Phi(k_{n+2m}).
\end{aligned} \tag{A6}$$

Here $\Gamma^{(2m,n)}(k_1, \ldots, k_{2m+n-1}, v, c, g, u_i; \mu)$ denote the one-particle irreducible (1PI) vertex functions that implicitly depend on all discrete indices. The summation over these indices has been left implicit. The counter term coefficients in Eq. (A1) are determined according to a minimal subtraction scheme which imposes the following renormalization conditions on the vertex functions:

$$\lim_{\tilde{\Lambda}\to\infty}\lim_{\Lambda\to\infty}\frac{1}{2i}\frac{\partial}{\partial\mathbf{K}^2}\mathrm{Tr}\left[(\mathbf{K}\cdot\mathbf{\Gamma})\Gamma_n^{(2,0)}(k)\right]\big|_{|\mathbf{K}|=\mu,\vec{k}=0} = 1 + E_1(v, c, g, u_i), \quad n = 1, 2, 3, 4, \tag{A7}$$

$$\lim_{\tilde{\Lambda}\to\infty}\lim_{\Lambda\to\infty}\frac{1}{2i}\frac{\partial}{\partial k_x}\mathrm{Tr}\left[\gamma_2\Gamma_{n=1}^{(2,0)}(k)\right]\big|_{|\mathbf{K}|=0,k_x=\mu,k_y=0} = v[1 + E_2(v, c, g, u_i)], \tag{A8}$$

$$\lim_{\tilde{\Lambda}\to\infty}\lim_{\Lambda\to\infty}\frac{1}{2i}\frac{\partial}{\partial k_y}\mathrm{Tr}\left[\gamma_2\Gamma_{n=1}^{(2,0)}(k)\right]\big|_{|\mathbf{K}|=0,k_x=0,k_y=\mu} = 1 + E_3(v, c, g, u_i), \tag{A9}$$

$$\lim_{\tilde{\Lambda}\to\infty}\lim_{\Lambda\to\infty}\frac{\partial}{\partial\mathbf{Q}^2}[\Gamma^{(0,2)}(q)]|_{|\mathbf{Q}|=\mu,\vec{q}=0} = 1 + E_4(v, c, g, u_i), \tag{A10}$$

$$\lim_{\tilde{\Lambda}\to\infty}\lim_{\Lambda\to\infty}\left[\frac{\partial}{\partial q_j^2}\Gamma^{(0,2)}(q)\right]\Bigg|_{|\mathbf{Q}|=0,\vec{q}=(\mu,\mu)} = c^2[1 + E_5(v, c, g, u_i)], \quad j = x, y, \tag{A11}$$

$$\lim_{\tilde{\Lambda}\to\infty}\lim_{\Lambda\to\infty}\tfrac{1}{2}\mathrm{Tr}\left[\gamma_2\Gamma_n^{(2,1)}(k, q)\right]\big|_{q=0,|\mathbf{K}|=\mu,\vec{k}=0} = 1 + E_6(v, c, g, u_i), \quad n = 1, 2, 3, 4, \tag{A12}$$

$$\lim_{\tilde{\Lambda}\to\infty}\lim_{\Lambda\to\infty}\Gamma_{abcd}^{(0,4)}(k_1, k_2, k_3)|_{|\mathbf{K}_i|=\mu,\vec{k}_i=\vec{0}} = \tfrac{1}{4}(u_1\mathrm{Tr}[\tau^a\tau^b]\mathrm{Tr}[\tau^c\tau^d] + u_2\mathrm{Tr}[\tau^a\tau^b\tau^c\tau^d]) + E_7(v, c, g, u_i). \tag{A13}$$

Here μ is an energy scale at which the physical observables are measured. $E_i(v, c, g, u_i)$'s are finite functions of the renormalized couplings. They vanish in the $u_i \to 0$ and $g \to 0$ limits. τ^a denote the generators of SU(N_c) with $a = 1, 2, \ldots, N_c^2 - 1$. The conditions in Eqs. (A7) to (A9) fix the fermion two-point function at the $n = 1$ hot spot and, by virtue of the C_4 symmetry of the theory, they also fix the two-point function at the other three hot spots. The renormalization conditions in Eqs. (A10) and (A11) fix the bosonic two-point function. Equations (A12) and (A13) fix the Yukawa vertex and the bosonic four-point function, respectively.

Under the Gaussian scaling, the 1PI vertex functions have scaling dimension $[\Gamma^{(2m,n)}(\{k_i\}, v, c, g, u_i; \mu)] = 4 - n - 3m$ and the renormalized vertex functions are related to the bare ones via

$$\Gamma_B^{(2m,n)}(\{k_{i;B}\}, v_B, c_B, g_B, u_{i;B}; \Lambda; \tilde{\Lambda}) = \left(\frac{\mathcal{Z}_3}{\mathcal{Z}_1}\right)^{2(2m+n-1)}\mathcal{Z}_\Psi^{-m}\mathcal{Z}_\Phi^{-\frac{n}{2}}\Gamma^{(2m,n)}(\{k_i\}, v, c, g, u_i; \mu). \tag{A14}$$

Since the bare vertex functions are independent of the running energy scale μ, the vertex functions satisfy the RG equation,

$$\begin{aligned}
&\Bigg[\sum_{i=1}^{2m+n-1}\left(z\mathbf{K}_i\cdot\nabla_{\mathbf{K}_i} + \vec{k}_i\cdot\nabla_{\vec{k}_i}\right) - \beta_v\frac{\partial}{\partial v} - \beta_c\frac{\partial}{\partial c} - \beta_g\frac{\partial}{\partial g} - \beta_{u_1}\frac{\partial}{\partial u_1} - \beta_{u_2}\frac{\partial}{\partial u_2} \\
&\quad + 2m\left(\eta_\Psi - \frac{5}{2}\right) + n(\eta_\Phi - 3) + 2(2m + n - 1)(z + 1)\Bigg]\Gamma^{(2m,n)}(\{k_i\}, v, c, g, u_i; \mu) = 0,
\end{aligned} \tag{A15}$$

where the critical exponents and beta functions of the velocities and couplings are given by

$$z = 1 - \frac{d}{d\log\mu}\log\left(\frac{\mathcal{Z}_3}{\mathcal{Z}_1}\right), \tag{A16}$$

$$\eta_{\Psi(\Phi)} = \frac{1}{2}\frac{d}{d\log\mu}\log\mathcal{Z}_{\Psi(\Phi)}, \tag{A17}$$

$$\beta_{\mathsf{A}} = \frac{d\mathsf{A}}{d\log\mu}, \quad \mathsf{A} = v, c, g, u_1, u_2. \tag{A18}$$

Here z denotes the dynamical critical exponent and η_Ψ (η_Φ) denotes the anomalous scaling dimension of the fermion (boson) field with respect to the Gaussian scaling.

The one-loop counter term coefficients in $d = 3$ are given by [34]

$$\mathcal{Z}_1 = 1 - \frac{(N_c^2-1)}{4\pi^2 N_c N_f}\frac{g^2}{c}h_1(v,c)\log\left(\frac{\Lambda}{\mu}\right), \tag{A19}$$

$$\mathcal{Z}_2 = 1 + \frac{(N_c^2-1)}{4\pi^2 N_c N_f}\frac{g^2}{c}h_2(v,c)\log\left(\frac{\Lambda}{\mu}\right), \tag{A20}$$

$$\mathcal{Z}_3 = 1 - \frac{(N_c^2-1)}{4\pi^2 N_c N_f}\frac{g^2}{c}h_2(v,c)\log\left(\frac{\Lambda}{\mu}\right), \tag{A21}$$

$$\mathcal{Z}_4 = 1 - \frac{1}{4\pi}\frac{g^2}{v}\log\left(\frac{\Lambda}{\mu}\right), \tag{A22}$$

$$\mathcal{Z}_5 = 0, \tag{A23}$$

$$\mathcal{Z}_6 = 1 - \frac{1}{8\pi^3 N_c N_f}\frac{g^2}{c}h_3(v,c)\log\left(\frac{\Lambda}{\mu}\right), \tag{A24}$$

$$\mathcal{Z}_7 = 1 + \frac{1}{2\pi^2 c^2}\left[(N_c^2+7)u_1 + 2\left(\frac{2N_c^2-3}{N_c}\right)u_2 + 3\left(\frac{N_c^2+3}{N_c^2}\right)\frac{u_2^2}{u_1}\right]\log\left(\frac{\Lambda}{\mu}\right), \tag{A25}$$

$$\mathcal{Z}_8 = 1 + \frac{1}{2\pi^2 c^2}\left[12u_1 + 2\left(\frac{N_c^2-9}{N_c}\right)u_2\right]\log\left(\frac{\Lambda}{\mu}\right). \tag{A26}$$

Here $h_i(v,c)$ are finite functions of v and c defined in Ref. [34]. They have the following limiting behaviors: $\lim_{c\to 0} h_1(wc,c) = \frac{\pi}{2}$, $\lim_{c\to 0} h_2(wc,c) = 2c$, and $\lim_{c\to 0} h_3(wc,c) = 2\pi^2/(1+w)$, with $w = v/c$ fixed. In the low-energy limit, all g, v, c, u_i flow to zero such that $\lambda \equiv g^2/v \sim 1/l$, $\kappa_i \equiv u_i/c^2 \sim 1/l$, $v \sim c \sim 1/\log(l)$, where l is the logarithmic length scale [34]. The quasilocal marginal Fermi liquid fixed point is stable. While the leading scaling behaviors are characterized by the Gaussian critical exponents, there exist logarithmic corrections generated from the marginally irrelevant couplings. Below we discuss those corrections in the two-point functions. For simplicity, we set $u_i = 0$, and focus on the corrections from the Yukawa coupling.

2. Fermionic and Bosonic Green's functions

The scaling form of the two-point functions is governed by

$$\left[z\mathbf{K}\cdot\boldsymbol{\nabla}_{\mathbf{K}} + \vec{k}\cdot\boldsymbol{\nabla}_{\vec{k}} - \beta_w\frac{\partial}{\partial w} - \beta_\lambda\frac{\partial}{\partial\lambda} - \beta_c\frac{\partial}{\partial c} + \widetilde{D}_{\mathsf{a}}\right] \times \Gamma^{(2)}_{\mathsf{a}}(k,\lambda,w,c;\mu) = 0. \tag{A27}$$

Here $\mathsf{a} = \mathsf{b}, \mathsf{f}$ labels the bosonic and fermionic two-point functions, respectively. We write the RG equation in terms of c, $\lambda \equiv g^2/v$ and $w \equiv v/c$. In particular, λ controls the perturbative expansion in three dimensions [34]. $\widetilde{D}_{\mathsf{a}}$ denotes the total scaling dimension of the two-point vertex functions,

$$\widetilde{D}_{\mathsf{f}} = 2(\eta_\Psi + z) - 3, \tag{A28}$$

$$\widetilde{D}_{\mathsf{b}} = 2(\eta_\Phi + z - 2), \tag{A29}$$

where the dynamical critical exponent and the anomalous dimensions of the fields are defined in Eqs. (A16) and (A17), respectively.

Equation (A27) can be rewritten as

$$\left[\mathbf{K}\cdot\boldsymbol{\nabla}_{\mathbf{K}} + \frac{\vec{k}}{z(l)}\cdot\boldsymbol{\nabla}_{\vec{k}} + \frac{d}{dl} + \frac{\widetilde{D}_{\mathsf{a}}(l)}{z(l)}\right] \times \Gamma^{(2)}_{\mathsf{a}}[k,\lambda(l),w(l),c(l)] = 0, \tag{A30}$$

where the scale-dependent couplings obey

$$\frac{dw(l)}{dl} = -\frac{\beta_w}{z(l)}, \quad \frac{d\lambda(l)}{dl} = -\frac{\beta_\lambda}{z(l)}, \quad \frac{dc(l)}{dl} = -\frac{\beta_c}{z(l)}, \quad \text{with} \quad [w(0),\lambda(0),c(0)] = (w_0,\lambda_0,c_0), \tag{A31}$$

and l is the logarithmic length scale.

The solution to Eq. (A30) is given by

$$\Gamma^{(2)}_{\mathsf{a}}(\mathbf{K},\vec{k},\lambda_0,w_0,c_0) = \exp\left(\int_0^l d\ell\frac{\widetilde{D}_{\mathsf{a}}(\ell)}{z(\ell)}\right) \times \Gamma^{(2)}_{\mathsf{a}}\left[e^l\mathbf{K}, \exp\left(\int_0^l\frac{d\ell}{z(\ell)}\right)\vec{k},\lambda(l),w(l),c(l)\right]. \tag{A32}$$

The boundary problems in Eq. (A31) are solved by following the results of Ref. [34]:

$$\lambda(l) = \frac{4\pi\left(N_c^2-1+N_cN_f\right)}{N_c^2+N_cN_f-3}\frac{1}{l}, \tag{A33}$$

$$w(l) = \frac{N_cN_f}{N_c^2-1} + O\left(\frac{1}{\log(l)}\right), \tag{A34}$$

$$c(l) = \frac{\pi\left(N_c^2+N_cN_f-3\right)}{4\left(N_c^2-1+N_cN_f\right)}\frac{1}{\log l}, \tag{A35}$$

in the large l limit.

The integrations over the length scale in Eq. (A32) are straightforward to perform in both the bosonic and fermionic cases after separating the contributions from the dynamical critical exponent and the net anomalous dimension of the fields. Setting $l = \log(\Lambda/|\mathbf{K}|)$ in Eq. (A32) for the fermion two-point function, we obtain the scaling form,

$$\Gamma^{(2,0)}_n(\mathbf{K},\vec{k}) = \Gamma^{(2)}_f(\mathbf{K},\vec{k}) = F_\Psi(|\mathbf{K}|)[iF_z(|\mathbf{K}|)\boldsymbol{\Gamma}\cdot\mathbf{K} + i\gamma_2\varepsilon_n(\vec{k};v_{|\mathbf{K}|})], \tag{A36}$$

where

$$F_z(|\mathbf{K}|) = \exp\left(\frac{\left(N_c^2 + N_c N_f - 1\right)}{2\left(N_c^2 + N_c N_f - 3\right)} \log[\log(\Lambda/|\mathbf{K}|)]\right), \tag{A37}$$

$$F_\Psi(|\mathbf{K}|) = \sqrt{\log[\log(\Lambda/|\mathbf{K}|)]}. \tag{A38}$$

Moreover, $v_{|\mathbf{K}|} = v(\log[\Lambda/|\mathbf{K}|])$ with

$$v(l) = w(l)c(l) \approx \frac{\pi N_c N_f \left(N_c^2 + N_c N_f - 3\right)}{4\left(N_c^2 - 1\right)\left(N_c^2 + N_c N_f - 1\right)} \frac{1}{\log l} \tag{A39}$$

in the low-energy limit and Eq. (A36) is obtained by keeping $\frac{\vec{k}}{[|\mathbf{K}|F_z(|\mathbf{K}|)]} \sim 1$ fixed.

Similarly, the boson two-point function takes the form

$$\Gamma^{(0,2)}(\mathbf{Q}, \vec{q}) = \Gamma_b^{(2)}(\mathbf{Q}, \vec{q}) = F_\Phi(|\mathbf{Q}|)[F_z(|\mathbf{Q}|)^2|\mathbf{Q}|^2 + c_{|\mathbf{Q}|}^2|\vec{q}|^2], \tag{A40}$$

where

$$F_\Phi(|\mathbf{Q}|) = \log[\log(\Lambda/|\mathbf{Q}|)], \tag{A41}$$

and $c_{|\mathbf{Q}|} = c(\log[\Lambda/|\mathbf{Q}|])$. Equation (A40) is obtained by setting $l = \log(\Lambda/|\mathbf{Q}|)$ while keeping $\frac{\vec{q}}{[|\mathbf{Q}|F_z(|\mathbf{Q}|)]} \sim 1$ fixed and $c(l)$ is given by Eq. (A35).

APPENDIX B: UPPER BOUND FOR HIGHER-LOOP DIAGRAMS IN $d < 3$

Here we sketch the proof of the upper bound in Eq. (16). Since the proof is essentially identical to the one given in Ref. [72], here we only highlight the important steps without a full derivation. We assume that the completely dressed boson propagator is given by Eq. (15) in the limit in which the hierarchy of velocities $v \ll c(v) \ll 1$ is satisfied. A general diagram with L loops, L_f fermion loops, E external legs, and $V = 2L - 2 + E$ vertices is given by

$$\mathcal{G}(L, L_f, E) \sim v^{\frac{V}{2}} \int \prod_{r=1}^{L} dp_r \left[\prod_{l=1}^{I_f} \frac{1}{\mathbf{\Gamma} \cdot \mathbf{K}_l + \gamma_{d-1}\varepsilon_{n_l}(\vec{k}_l; v)}\right] \times \left[\prod_{s=1}^{I_b} \frac{1}{|\mathbf{Q}_s|^{d-1} + c(v)^{d-1}(|q_{s,x}|^{d-1} + |q_{s,y}|^{d-1})}\right]. \tag{B1}$$

Here $p_r = (\mathbf{P}_r, \vec{p}_r)$ denotes the $(d+1)$-dimensional frequency and momentum that runs in the rth loop. $k_l = (\mathbf{K}_l, \vec{k}_l)$ $[q_s = (\mathbf{Q}_s, \vec{q}_s)]$, which is a linear combination of the loop momenta and external momenta, denotes the frequency and momentum vector of the lth fermion (sth boson) propagator. I_f (I_b) denotes the number of internal fermion (boson) propagators and n_l symbolizes the hot spot index for the lth fermion propagator.

In the small v limit, patches of the Fermi surface become locally nested, and the AFM collective mode becomes dispersionless. For a small but finite v, the integrations over internal fermion (boson) spatial momenta are cut off at momentum scales proportional to $1/v$ $[1/c(v)]$. This gives rise to enhancement factors of $1/v$ $[1/c(v)]$. The enhancement of a diagram becomes maximal when the diagram contains only fermions belonging to patches of the Fermi surface that become locally nested in the small v limit. Because of this we consider Eq. (B1) for $n_l = 1, 3$, without loss of generality.

Since the enhancement factor comes from the integrations over the x and y components of the momenta, we focus on the $2L$-dimensional integration over those components. Through a change of variables of the $2L$ spatial loop momenta described in Ref. [72], Eq. (B1) can be rewritten as

$$\mathcal{G}(L, L_f, E) \sim v^{\frac{V}{2}-L_f} c(v)^{-(L-L_f)} \int \prod_{r=1}^{2L} dp_i' \times \left[\prod_{l=L-L_f+1}^{2L} \frac{1}{\cdots + \gamma_{d-1} p_l'}\right] \times \left[\prod_{s=1}^{L-L_f} \frac{1}{\cdots + |p_s'|^{d-1} + O[c(v)^{d-1}]}\right] R(p'). \tag{B2}$$

Here p_i' denotes the new $2L$ variables for the x and y components of the internal momenta. The ellipsis denote the frequency and codimensional momenta that play no role in determining the enhancement factor. $R(p')$ denotes the product of all the remaining propagators. The point of the change of basis is to make it manifest that there is at least one propagator that guarantees that the integrand decays in the UV at least as $1/p_i'$ in each of the internal momenta once a factor of v^{-1} or $c(v)^{-1}$ is scaled out from each loop. Each fermion loop contributes v^{-1} because the x-momentum component becomes unbounded in the small v limit. Each of the remaining $L - L_f$ loops contribute a factor of $c(v)^{-1}$ because the x-momentum component in the loop necessarily runs through a boson propagator and is cut off at a scale proportional to $1/c(v)$, since $c(v) \gg v$. It follows from this that the magnitude of a generic L-loop diagram with L_f fermionic loops is at most

$$\mathcal{G}(L, L_f, E) \sim v^{\frac{E-2}{2}} \left(\frac{v}{c(v)}\right)^{L-L_f} \tag{B3}$$

up to a potential logarithmic correction in the small v limit. We note that Eq. (B3) is independent of the space dimension because the fully dressed boson propagator in Eq. (15) depends on q_x and q_y only through $c(v)\vec{q}$ and the velocities along the extra codimensions are fixed to be one.

APPENDIX C: REGULARIZATION AND RG SCHEME

Here we briefly explain the RG scheme used in $d < 3$. The main difference from the case with $d = 3$ is that we start with the interaction-driven scaling in $d < 3$. As a result, the minimal action only includes the fermion kinetic term and the Yukawa interaction. Quantum corrections are computed with the self-consistent boson propagator in Eq. (15). Under the interaction-driven scaling, the Yukawa vertex is marginal in any dimension between two and three. As a result, we expect logarithmic divergences in this dimensional range. We regularize the theory with the same prescription as the one given in Appendix A1 and follow a similar RG scheme. We add the following local counter term to the action in Eq. (12) such that low-energy physical observables are independent of the UV cutoff

scales:

$$S_d^{\text{C.T.}} = \sum_{n=1}^{4}\sum_{\sigma=1}^{N_c}\sum_{j=1}^{N_f}\int dk\,\overline{\Psi}_{n,\sigma,j}(k)[iA_1\mathbf{\Gamma}\cdot\mathbf{K} + i\gamma_{d-1}\widetilde{\varepsilon}_n(\vec{k};v)]\Psi_{n,\sigma,j}(k)$$
$$+ A_6\frac{i\beta_d\sqrt{v}}{\sqrt{N_f}}\sum_{n=1}^{4}\sum_{\sigma,\sigma'=1}^{N_c}\sum_{j=1}^{N_f}\int dk\int dq\,\overline{\Psi}_{\bar{n},\sigma,j}(k+q)\Phi_{\sigma\sigma'}(q)\gamma_{d-1}\Psi_{n,\sigma',j}(k). \tag{C1}$$

Here $\widetilde{\varepsilon}_1(\vec{k};v) = A_2vk_x + A_3k_y$, $\widetilde{\varepsilon}_2(\vec{k};v) = -A_3k_x + A_2vk_y$, $\widetilde{\varepsilon}_3(\vec{k};v) = A_2vk_x - A_3k_y$, and $\widetilde{\varepsilon}_4(\vec{k};v) = A_3k_x + A_2vk_y$. The A_i's are momentum-independent counter term coefficients. Adding this counter term action to Eq. (12) yields the renormalized action,

$$S_d^{\text{Ren}} = \sum_{n=1}^{4}\sum_{\sigma=1}^{N_c}\sum_{j=1}^{N_f}\int dk_B\,\overline{\Psi}_{n,\sigma,j;B}(k_B)[i\mathbf{\Gamma}\cdot\mathbf{K}_B + i\gamma_{d-1}\varepsilon_n(\vec{k}_B;v_B)]\Psi_{n,\sigma,j,B}(k_B)$$
$$+ \frac{i\beta_d\sqrt{v_B}}{\sqrt{N_f}}\sum_{n=1}^{4}\sum_{\sigma,\sigma'=1}^{N_c}\sum_{j=1}^{N_f}\int dk_B\int dq_B\,\overline{\Psi}_{\bar{n},\sigma,j;B}(k_B+q_B)\Phi_{B;\sigma\sigma'}(q_B)\gamma_{d-1}\Psi_{n,\sigma',j;B}(k_B). \tag{C2}$$

The renormalized frequency, momenta, fields, and velocity are related to the bare ones via the multiplicative relations:

$$\mathbf{K}_B = \frac{Z_1}{Z_3}\mathbf{K},\quad \vec{k}_B = \vec{k},\quad v_B = \frac{Z_2}{Z_3}v,\quad \Psi_B(k_B) = Z_\Psi^{1/2}\Psi(k),\quad \text{and}\quad \Phi_B(k_B) = Z_\Phi^{1/2}\Phi(k), \tag{C3}$$

where $Z_i = 1 + A_i$, $Z_\Psi = Z_3(Z_3/Z_1)^{d-1}$, $Z_\Phi = \frac{Z_6^2}{Z_3Z_2}(Z_3/Z_1)^{2(d-1)}$, and the field indices are suppressed. It is noted that the expression for Z_Φ is different from the one used in $d = 3$ because here we are using the interaction-driven scaling. The renormalized action gives rise to the quantum effective action in Eq. (A6). However, the dependencies on v, c, g, u_1, and u_2 of the latter and the 1PI vertex functions are now replaced by a single parameter: v. The counter term coefficients in Eq. (C1) are fixed by the renormalization conditions imposed over the vertex functions:

$$\lim_{\widetilde{\Lambda}\to\infty}\lim_{\Lambda\to\infty}\frac{1}{2i}\frac{\partial}{\partial\mathbf{K}^2}\text{Tr}\big[(\mathbf{K}\cdot\mathbf{\Gamma})\Gamma_n^{(2,0)}(k)\big]\big|_{|\mathbf{K}|=\mu,\vec{k}=0} = 1 + F_1(v),\quad n = 1,2,3,4, \tag{C4}$$
$$\lim_{\widetilde{\Lambda}\to\infty}\lim_{\Lambda\to\infty}\frac{1}{2i}\frac{\partial}{\partial k_x}\text{Tr}\big[\gamma_{d-1}\Gamma_{n=1}^{(2,0)}(k)\big]\big|_{|\mathbf{K}|=0,k_x=\mu,k_y=0} = v[1 + F_2(v)], \tag{C5}$$
$$\lim_{\widetilde{\Lambda}\to\infty}\lim_{\Lambda\to\infty}\frac{1}{2i}\frac{\partial}{\partial k_y}\text{Tr}\big[\gamma_{d-1}\Gamma_{n=1}^{(2,0)}(k)\big]\big|_{|\mathbf{K}|=0,k_x=0,k_y=\mu} = 1 + F_3(v), \tag{C6}$$
$$\lim_{\widetilde{\Lambda}\to\infty}\lim_{\Lambda\to\infty}\frac{1}{2}\text{Tr}\big[\gamma_{d-1}\Gamma_n^{(2,1)}(k,q)\big]\big|_{q=0,|\mathbf{K}|=\mu,\vec{k}=0} = 1 + F_4(v),\quad n = 1,2,3,4, \tag{C7}$$

which follow from a minimal subtraction scheme. Here we have left implicit the dependence of the vertex function on v. μ is an energy scale at which the physical observables are measured and $F_i(v)$ are functions that vanish in the small v limit.

Since the bare quantities are independent of the running energy scale μ, the 1PI vertex functions obey the RG equation:

$$\Bigg[\sum_{i=1}^{2m+n-1}\big(z\mathbf{K}_i\cdot\nabla_{\mathbf{K}_i} + \vec{k}_i\cdot\nabla_{\vec{k}_i}\big) - \beta_v\frac{\partial}{\partial v} + m[2\eta_\Psi - (d+2)] + n(\eta_\Phi - d)$$
$$+ (2m+n-1)[2 + z(d-1)]\Bigg]\Gamma^{(2m,n)}(\{k_i\},v;\mu) = 0, \tag{C8}$$

which is obtained by combining the fact that, under the interaction-driven scaling, the vertex functions have engineering scaling dimension $[\Gamma^{(2m,n)}(\{k_i\},v;\mu)] = -md - n + d + 1$ and that the bare vertex functions are related to the renormalized ones via

$$\Gamma_B^{(2m,n)}[\{k_{i,B}\},v_B;\Lambda;\widetilde{\Lambda}]$$
$$= \left(\frac{Z_3}{Z_1}\right)^{(d-1)(2m+n-1)} Z_\Psi^{-m}Z_\Phi^{-\frac{n}{2}}\Gamma^{(2m,n)}(\{k_i\},v;\mu). \tag{C9}$$

The dynamical critical exponent, the beta function for v, and the anomalous scaling dimensions of the fields are given by

$$z = 1 - \frac{d}{d\log\mu}\log\left(\frac{Z_3}{Z_1}\right), \tag{C10}$$
$$\beta_v = \frac{dv}{d\log\mu}, \tag{C11}$$
$$\eta_{\Psi(\Phi)} = \frac{1}{2}\frac{d\log Z_{\Psi(\Phi)}}{d\log\mu}, \tag{C12}$$

respectively. Here η_Ψ and η_Φ denote the deviations of the scaling dimensions of the fields from the ones predicted by the interaction-driven scaling (not the Gaussian scaling).

APPENDIX D: QUANTUM CORRECTIONS

Here we provide details on the computations of the quantum corrections to the minimal local action depicted in Figs. 7(a), 7(b) 7(c), 8(a), 8(b), and 8(c).

1. One-loop boson self-energy

The one-loop correction that generates dynamics of the boson is shown in Fig. 7(a). Its contribution to the quantum effective action reads

$$\delta\mathbf{\Gamma}^{(0,2)}_{1\mathrm{L}} = \frac{1}{4}\int dq\,\Pi^{1\mathrm{L}}(q)\mathrm{Tr}[\Phi(-q)\Phi(q)], \tag{D1}$$

where the one-loop boson self-energy is given by

$$\Pi^{1\mathrm{L}}(q) = -2v\beta_d^2\sum_{n=1}^{4}\int dk\mathrm{Tr}\big[\gamma_{d-1}G^{(0)}_{\bar{n}}(k+q)\gamma_{d-1}G^{(0)}_{n}(k)\big]. \tag{D2}$$

Here $G^{(0)}_n(k)$ is the bare fermion propagator given in Eq. (18) and β_d is defined in Eq. (13). Taking the trace over the spinor indices and integrating over the spatial momenta $\vec{k}$, yields

$$\Pi^{1\mathrm{L}}(q) = -2\beta_d^2\int_{\mathbb{R}^{d-1}}\frac{d\mathbf{K}}{(2\pi)^{d-1}}\frac{\mathbf{K}\cdot(\mathbf{K}+\mathbf{Q})}{|\mathbf{K}||\mathbf{K}+\mathbf{Q}|}. \tag{D3}$$

Subtracting the mass renormalization, we focus on the momentum dependent self-energy: $\Delta\Pi^{1\mathrm{L}}(q) = \Pi^{1\mathrm{L}}(q) - \Pi^{1\mathrm{L}}(0)$. Integration over $\mathbf{K}$ is done after imposing a cutoff Λ in the UV. In the $\Lambda/|\mathbf{Q}| \gg 1$ limit this becomes

$$\Delta\Pi^{1\mathrm{L}}(q) = \frac{\beta_d^2\Gamma\left(\frac{5-d}{2}\right)\Gamma\left(\frac{d}{2}\right)}{2^{2d-5}\pi^{\frac{d}{2}}\Gamma\left(\frac{d+1}{2}\right)}|\mathbf{Q}|^{d-1} \times\left(\frac{1}{3-d}-\frac{1}{3-d}\left[\frac{2\cos\left(\frac{\pi d}{2}\right)}{\pi(d-3)}\right]\left(\frac{\Lambda}{|\mathbf{Q}|}\right)^{d-3}\right). \tag{D4}$$

While the expression is logarithmically divergent in $d = 3$, it is UV finite for $d < 3$. In $d < 3$, the one-loop boson self-energy is given by

$$\Delta\Pi^{1\mathrm{L}}(q) = |\mathbf{Q}|^{d-1}. \tag{D5}$$

2. Two-loop boson self-energy

We first compute the two-loop boson self-energy shown in Fig. 7(b), and then comment on the contribution arising from Fig. 7(c). The contribution of Fig. 7(b) to the quantum effective action is given by

$$\delta\mathbf{\Gamma}^{(0,2)}_{2\mathrm{L}} = \frac{1}{4}\int dq\,\Pi^{2\mathrm{L}}(q)\mathrm{Tr}[\Phi(q)\Phi(-q)], \tag{D6}$$

with

$$\Pi^{2\mathrm{L}}(q) = -\frac{4\beta_d^4v^2}{N_cN_f}\sum_{n=1}^{4}\int dk\int dp\mathrm{Tr}\big[\gamma_{d-1}G^{(0)}_{\bar{n}}(k+p)\gamma_{d-1}G^{(0)}_{n}(k+q+p)\gamma_{d-1}G^{(0)}_{\bar{n}}(k+q)\gamma_{d-1}G^{(0)}_{n}(k)]D(p). \tag{D7}$$

Here β_d is defined in Eq. (13) and $D(p)$ is given by the self-consistent propagator in Eq. (15). The frequency-dependent part of the two-loop self-energy is subleading with respect to the one-loop boson self-energy by a factor of $w(v) = v/c(v)$. Therefore, we focus on the momentum dependent part by setting $\mathbf{Q} = \mathbf{0}$. Taking the trace over the spinor indices, changing variables to $k_+ = \varepsilon_n(\vec{k}; v)$ and $k_- = \varepsilon_{\bar{n}}(\vec{k}+\vec{q}; v)$, and noting that the latter has a Jacobian of $1/(2v)$, the spatial part of the two-loop boson self-energy takes the form

$$\Pi^{2\mathrm{L}}(\mathbf{0},\vec{q}) = -\frac{4v\beta_d^4}{N_cN_f}\sum_{n=1}^{4}\int dk\int dp\Bigg(\frac{1}{(\mathbf{K}^2+k_+^2)(\mathbf{K}^2+k_-^2)\{(\mathbf{K}+\mathbf{P})^2+[k_+ + \varepsilon_n(\vec{p}+\vec{q}; v)]^2\}} \times\frac{1}{\{(\mathbf{K}+\mathbf{P})^2+[k_- + \varepsilon_{\bar{n}}(\vec{p}-\vec{q}; v)]^2\}}[(\mathbf{K}^2-k_+k_-)\{(\mathbf{K}+\mathbf{P})^2-[k_+ + \varepsilon_n(\vec{p}+\vec{q}; v)][k_- + \varepsilon_{\bar{n}}(\vec{p}-\vec{q}; v)]\} - \mathbf{K}\cdot(\mathbf{K}+\mathbf{P})[k_+ + k_- + \varepsilon_n(\vec{p}+\vec{q}; v) + \varepsilon_{\bar{n}}(\vec{p}-\vec{q}; v)](k_+ + k_-)]\Bigg)D(p). \tag{D8}$$

This expression can be written as a sum of the contributions from the four hot spots,

$$\Pi^{2\mathrm{L}}(\mathbf{0},\vec{q}) = \sum_{n=1}^{4}\Pi^{2\mathrm{L}}_n(\vec{q}). \tag{D9}$$

Let us first consider the contribution from the $n = 1$ hot spot. Since the self-energy depends on the external momentum component q_x only through vq_x, the first hot spot gives rise to the self-energy that depends on q_y to the leading order in the small v limit.

After setting $q_x = 0$, we perform a change of variables $p_x \to p_x/v$ to write the the two-loop boson self-energy as

$$\Pi_1^{2L}(\vec{q}) = -\frac{4w(v)^{d-1}\beta_d^4}{N_c N_f}\int dk \int dp \Bigg\{ \frac{1}{(\mathbf{K}^2+k_+^2)(\mathbf{K}^2+k_-^2)[(\mathbf{K}+\mathbf{P})^2+(k_+ + p_x + p_y + q_y)^2]} \times \frac{1}{[(\mathbf{K}+\mathbf{P})^2+(k_- + p_x - p_y + q_y)^2]} \{(\mathbf{K}^2 - k_+k_-)[(\mathbf{K}+\mathbf{P})^2 - (k_+ + p_x + p_y + q_y)(k_- + p_x - p_y + q_y)] - \mathbf{K}\cdot(\mathbf{K}+\mathbf{P})(k_+ + k_- + 2p_x + 2q_y)(k_+ + k_-)\} \left(\frac{1}{w(v)^{d-1}|\mathbf{P}|^{d-1} + |p_x|^{d-1} + v^{d-1}|p_y|^{d-1}} \right) \Bigg\}. \tag{D10}$$

We can neglect $|vp_y|^{d-1}$ in the boson propagator in the small v limit. The integration over p_x is divided into two regimes: $p_x \in (-\lambda, \lambda)$ and $p_x \in \mathbb{R} \setminus (-\lambda, \lambda)$ where $\lambda \sim \min(k_+, k_-, \mathbf{P}, \mathbf{K}, p_y)$ is a momentum scale below which the p_x dependence in the fermion propagators can be ignored. The exact form of λ is unimportant in the small $w(v)$ limit. The integration over the first regime is divergent in the small $w(v)$ limit due to the infrared singularity that is cut off by $w(v)|\mathbf{P}|$. On the other hand, the contribution from the second regime is regular. To the leading order in $w(v) \ll 1$, we can keep only the first contribution to write the p_x integration as

$$|\mathbf{P}|^{2-d}\overline{\mathfrak{S}}\left(d-2; w(v); \frac{\lambda}{|\mathbf{P}|}\right) \equiv \frac{\pi}{(d-2)}\frac{1}{\Gamma\left(\frac{d-2}{d-1}\right)\Gamma\left(\frac{d}{d-1}\right)}\int_{-\lambda}^{\lambda}\frac{dp_x}{(2\pi)}\left(\frac{w(v)^{d-2}}{w(v)^{d-1}|\mathbf{P}|^{d-1}+|p_x|^{d-1}}\right). \tag{D11}$$

In the $w(v) \to 0$ and in the $d \to 2$ limits, $\overline{\mathfrak{S}}[d-2; w(v); \lambda/|\mathbf{P}|]$ becomes independent of $\lambda/|\mathbf{P}|$ because it has the following limiting behaviors:

$$\lim_{d\to 2}\overline{\mathfrak{S}}\left(d-2; w(v); \frac{\lambda}{|\mathbf{P}|}\right) = -\log[w(v)], \quad \lim_{w(v)\to 0}\overline{\mathfrak{S}}\left(d-2; w(v); \frac{\lambda}{|\mathbf{P}|}\right) = \frac{1}{d-2}. \tag{D12}$$

Since we are mainly interested in these limits, we can replace $\overline{\mathfrak{S}}[d-2; w(v); \lambda/|\mathbf{P}|]$ with

$$\mathfrak{S}[d-2; w(v)] \equiv \overline{\mathfrak{S}}[d-2; w(v); 1] = \frac{1}{d-2}[1 - w(v)^{d-2}], \tag{D13}$$

where the last equality comes from explicitly computing Eq. (D11) at $\lambda/|\mathbf{P}| = 1$ in the small $w(v)$ limit. In the rest of the paper, $\mathfrak{S}[d-2; w]$ and $\mathfrak{S}(d-2; w)$ will be used interchangeably. The p_x, p_y, and k_+ integrations in Eq. (D10) result in

$$\Pi_1^{2L}(\vec{q}) = -\frac{4(d-2)\beta_d^4 w(v)}{\pi N_c N_f}\Gamma\left(\frac{d-2}{d-1}\right)\Gamma\left(\frac{d}{d-1}\right)\mathfrak{S}[d-2; w(v)]\int_{\mathbb{R}^{d-1}}\frac{d\mathbf{K}}{(2\pi)^{d-1}}\int_{\mathbb{R}}\frac{dk_-}{(2\pi)}\int_{\mathbb{R}^{d-1}}\frac{d\mathbf{P}}{(2\pi)^{d-1}} \times \frac{|\mathbf{P}|^{2-d}}{|\mathbf{K}||\mathbf{K}+\mathbf{P}|}\left[\frac{4\mathbf{K}^2(\mathbf{K}+\mathbf{P})^2 - 2q_y k_- \mathbf{K}\cdot(\mathbf{K}+\mathbf{P}) - \mathbf{K}\cdot(\mathbf{K}+\mathbf{P})k_-^2}{(4\mathbf{K}^2+k_-^2)[4(\mathbf{K}+\mathbf{P})^2+(k_- + 2q_y)^2]}\right], \tag{D14}$$

to leading order in $v \ll 1$. Subtracting the mass renormalization, the momentum dependent self-energy [defined as $\Delta\Pi_1^{2L}(\vec{q}) \equiv \Pi_1^{2L}(\vec{q}) - \Pi_1^{2L}(\vec{0})$] is obtained to be

$$\Delta\Pi_1^{2L}(\vec{q}) = -\frac{4(d-2)\beta_d^4 w(v)}{\pi N_c N_f}\Gamma\left(\frac{d-2}{d-1}\right)\Gamma\left(\frac{d}{d-1}\right)\mathfrak{S}[d-2; w(v)]\int_{\mathbb{R}^{d-1}}\frac{d\mathbf{K}}{(2\pi)^{d-1}}\int_{\mathbb{R}}\frac{dk_-}{(2\pi)}\int_{\mathbb{R}^{d-1}}\frac{d\mathbf{P}}{(2\pi)^{d-1}} \times \frac{|\mathbf{P}|^{2-d}}{|\mathbf{K}||\mathbf{K}+\mathbf{P}|}\left[\frac{\mathcal{F}(\mathbf{P}, \mathbf{K}, k_-, q_y)}{(4\mathbf{K}^2+k_-^2)[4(\mathbf{K}+\mathbf{P})^2+(k_- + 2q_y)^2][4(\mathbf{K}+\mathbf{P})^2+k_-^2]}\right], \tag{D15}$$

where

$$\mathcal{F}(\mathbf{P}, \mathbf{K}, k_-, q_y) = [4\mathbf{K}^2(\mathbf{K}+\mathbf{P})^2 - 2q_y k_- \mathbf{K}\cdot(\mathbf{K}+\mathbf{P}) - \mathbf{K}\cdot(\mathbf{K}+\mathbf{P})k_-^2][4(\mathbf{K}+\mathbf{P})^2+k_-^2] - [4\mathbf{K}^2(\mathbf{K}+\mathbf{P})^2 - \mathbf{K}\cdot(\mathbf{K}+\mathbf{P})k_-^2][4(\mathbf{K}+\mathbf{P})^2+(k_- + 2q_y)^2]. \tag{D16}$$

We proceed by scaling out q_y from the above integral and introduce a two-variable Feynman parametrization that allows the explicit computation of the k_- integration. Performing this integration yields

$$\Delta\Pi_1^{2L}(\vec{q}) = -\frac{\beta_d^4(d-2)|q_y|^{d-1}w(v)}{64\pi N_c N_f}\Gamma\left(\frac{d-2}{d-1}\right)\Gamma\left(\frac{d}{d-1}\right)\mathfrak{S}[d-2; w(v)]\int_{\mathbb{R}^{d-1}}\frac{d\mathbf{K}}{(2\pi)^{d-1}}\int_{\mathbb{R}^{d-1}}\frac{d\mathbf{P}}{(2\pi)^{d-1}} \times \int_0^1 dx_1\int_0^{1-x_1}dx_2\frac{|\mathbf{P}|^{2-d}}{|\mathbf{K}||\mathbf{K}+\mathbf{P}|}\left[\frac{3A + 4B[\mathbf{K}\cdot(\mathbf{K}+\mathbf{P})(3x_1+3x_2-2)]}{[\mathbf{K}^2 - 2\mathbf{K}\cdot\mathbf{P}(x_1-1) - \mathbf{P}^2(x_1-1) - (x_1+x_2)^2 + x_1 + x_2]^{5/2}}\right], \tag{D17}$$

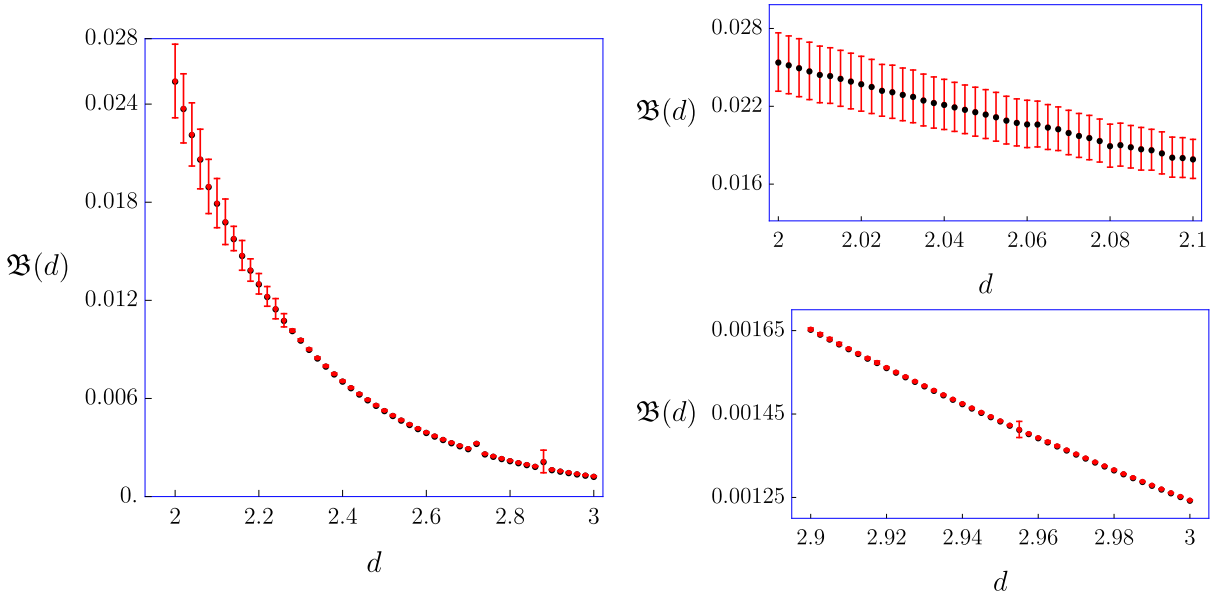

(a) $\mathfrak{B}(d)$ for $2 \le d \le 3$.

(b) $\mathfrak{B}(d)$ near $d = 2$ (top) and $d = 3$ (bottom).

FIG. 10. (a) The function $\mathfrak{B}(d)$. The (black) dots correspond to the value of the numerical integration and the (red) error bars represent the numerical error in the computation. (b) Numerical evaluation near $d = 2$ (top) and $d = 3$ (bottom).

where

$$A = -16\{\mathbf{K}^2(2x_1 + 2x_2 - 1)(\mathbf{K} + \mathbf{P})^2 + (x_1 + x_2 - 1)\mathbf{K} \cdot (\mathbf{K} + \mathbf{P})[(\mathbf{K} + \mathbf{P})^2 - (x_1 + x_2 - 1)(x_1 + x_2)]\}, \tag{D18}$$

$$B = 4[\mathbf{K}^2 - 2\mathbf{K} \cdot \mathbf{P}(x_1 - 1) - \mathbf{P}^2(x_1 - 1) - (x_1 + x_2)^2 + x_1 + x_2]. \tag{D19}$$

Integrations over the remaining frequency and codimensional momentum components are done by introducing another two-variable Feynman parametrization. This yields the contribution from the $n = 1$ hot spot to the two-loop boson self-energy

$$\Delta\Pi_1^{2L}(\vec{q}) = \frac{2\beta_d^4 |q_y|^{d-1}}{N_c N_f} w(v)\mathfrak{B}(d)\mathfrak{S}[d-2; w(v)]\tilde{\mathfrak{S}}\left(3-d; \frac{|q_y|}{\Lambda}\right), \tag{D20}$$

where $\mathfrak{B}(d)$ is a smooth function of d (see Fig. 10) defined by

$$\mathfrak{B}(d) = \frac{(d-2)\Gamma(3-d)}{3\times 2^{d+4}\pi^{\frac{2d+3}{2}}} \frac{\cos\left(\frac{\pi d}{2}\right)\Gamma\left(\frac{d-2}{d-1}\right)\Gamma\left(\frac{d}{d-1}\right)\Gamma\left(\frac{5-d}{2}\right)}{\Gamma\left(\frac{8-d}{2}\right)} \int_0^1 dx_1 \int_0^{1-x_1} dx_2 \int_0^1 dy_1 \int_0^{1-y_1} dy_2$$
$$\times \left[\frac{(1-y_1-y_2)^{3/2}}{\sqrt{y_1}\sqrt{y_2}} \frac{(d-5)(d-3)C_3 D_1^2 + D_2[(3-d)C_2 D_1 + 3C_1 D_2]}{D_1^{5/2} D_2^{\frac{7-d}{2}}}\right], \tag{D21}$$

with

$$D_1 = -[x_1(y_1 + y_2 - 1) - y_1][x_1(y_1 + y_2 - 1) - y_1 + 1], \tag{D22}$$

$$D_2 = (x_1 + x_2 - 1)(x_1 + x_2)(y_1 + y_2 - 1), \tag{D23}$$

$$\begin{aligned} C_1 = {} & \left[-x_1^2(y_1 + y_2 - 1)^2 + x_1(2y_1 - 1)(y_1 + y_2 - 1) - (y_1 - 1)y_1\right]\{(d^2 - 1)(-6x_1 - 6x_2 + 4) \\ & \times \left(-x_1^2(y_1 + y_2 - 1)^2 + x_1(2y_1 - 1)(y_1 + y_2 - 1) - (y_1 - 1)y_1\right) + (4 - d)\big[(d - 1)\big(-6x_1^3(y_1 + y_2 - 1) \\ & \times (2y_1 + 2y_2 - 3) + x_1^2(2(4(y_1 + y_2)(4y_1 + y_2) - 3x_2(y_1 + y_2 - 1)(2y_1 + 2y_2 - 3)) - 62y_1 - 32y_2 \\ & + 27) + x_1(3x_2(2y_1 - 1)(4y_1 + 4y_2 - 5) + y_1(-28y_1 - 16y_2 + 39) + 7y_2 - 15) - 6x_2(2(y_1 - 1)y_1 + 1) \\ & + y_1(8y_1 - 7) + 3) - 2\big(6x_1^3(y_1 + y_2 - 1)(2y_1 + 2y_2 - 3) + x_1^2(2(3x_2(y_1 + y_2 - 1)(2y_1 + 2y_2 - 3) \\ & - 4(y_1 + y_2)(4y_1 + y_2)) + 62y_1 + 32y_2 - 27) + x_1\big(-3x_2(2y_1 - 1)(4y_1 + 4y_2 - 5) - 7y_2 \\ & + y_1(28y_1 + 16y_2 - 39) + 9\big) + y_1(12x_2(y_1 - 1) - 8y_1 + 7)\big)\big]\} - (d - 6)(d - 4)(x_1(y_1 + y_2 - 1) - y_1) \end{aligned}$$

$$\times(x_1(y_1+y_2-1)-y_1+1)\{6x_1^3(y_1+y_2-2)(y_1+y_2-1)+x_1^2(2(3x_2(y_1+y_2-2)(y_1+y_2-1)$$
$$-2(y_1+y_2)(4y_1+y_2))+36y_1+18y_2-17)+x_1(-3x_2(2y_1-1)(2y_1+2y_2-3)-3y_2$$
$$+y_1(14y_1+8y_2-21)+5)+6x_2(y_1-1)y_1+(3-4y_1)y_1\}, \tag{D24}$$

$$C_2=\left(-x_1^2(y_1+y_2-1)^2+x_1(2y_1-1)(y_1+y_2-1)-(y_1-1)y_1\right)\left[(d^2-1)(-6x_1-6x_2+4)\right.$$
$$\times\left(x_1^2+(2x_2-1)x_1+(x_2-1)x_2\right)(y_1+y_2-1)+(4-d)(d-1)(-(x_1+x_2)^2+x_1+x_2)\left.\right]$$
$$+\left(x_1^2+(2x_2-1)x_1+(x_2-1)x_2\right)(y_1+y_2-1)\{(d^2-1)(-6x_1-6x_2+4)\left(-x_1^2(y_1+y_2-1)^2\right.$$
$$+x_1(2y_1-1)(y_1+y_2-1)-(y_1-1)y_1\left.\right)+(4-d)\left[(d-1)\left(-6x_1^3(y_1+y_2-1)(2y_1+2y_2-3)\right.\right.$$
$$+x_1^2(2(4(y_1+y_2)(4y_1+y_2)-3x_2(y_1+y_2-1)(2y_1+2y_2-3))-62y_1-32y_2+27)$$
$$+x_1(3x_2(2y_1-1)(4y_1+4y_2-5)+y_1(-28y_1-16y_2+39)+7y_2-15)-6x_2(2(y_1-1)y_1+1)$$
$$+y_1(8y_1-7)+3)-2\{6x_1^3(y_1+y_2-1)(2y_1+2y_2-3)+x_1^2(2(3x_2(y_1+y_2-1)(2y_1+2y_2-3)$$
$$-4(y_1+y_2)(4y_1+y_2))+62y_1+32y_2-27)+x_1(-3x_2(2y_1-1)(4y_1+4y_2-5)-7y_2$$
$$+y_1(28y_1+16y_2-39)+9)+y_1(12x_2(y_1-1)-8y_1+7)\}\left.\right]\}-(d-6)(d-4)\left(x_1^2+(2x_2-1)x_1\right.$$
$$+(x_2-1)x_2)(x_1(y_1+y_2-1)-y_1)(x_1(y_1+y_2-1)-y_1+1), \tag{D25}$$

$$C_3=\left(x_1^2+(2x_2-1)x_1+(x_2-1)x_2\right)(y_1+y_2-1)\{(d^2-1)(-6x_1-6x_2+4)\left(x_1^2+(2x_2-1)x_1\right.$$
$$\left.+(x_2-1)x_2\right)(y_1+y_2-1)+(4-d)(d-1)\left(-(x_1+x_2)^2+x_1+x_2\right)\}, \tag{D26}$$

and

$$\widetilde{\mathfrak{S}}\left(3-d;\frac{|q_y|}{\Lambda}\right)\equiv-\frac{(d-2)\Gamma(3-d)\sin(\pi d)\csc\left(\frac{\pi d}{2}\right)}{6(2\pi)^{d+2}\mathfrak{B}(d)}\Gamma\left(\frac{d-2}{d-1}\right)\Gamma\left(\frac{d}{d-1}\right)$$
$$\times\int_0^1 dx_1\int_0^{1-x_1}dx_2\int_0^1 dy_1\int_0^{1-y_1}dy_2\frac{(1-y_1-y_2)^{3/2}}{\sqrt{y_1}\sqrt{y_2}}\int_0^{\frac{\Lambda}{|q_y|}}dP\left[\frac{C_1P^4+C_2P^2+C_3}{(D_1P^2+D_2)^{\frac{8-d}{2}}}\right]. \tag{D27}$$

$\widetilde{\mathfrak{S}}(3-d;\frac{|q_y|}{\Lambda})$ singles out the contribution that is divergent in the $d\to 3$ limit. In the large $\Lambda/|q_y|$ limit, it satisfies the limits

$$\lim_{d\to 3}\widetilde{\mathfrak{S}}\left(3-d;\frac{|q_y|}{\Lambda}\right)=-\log\left(\frac{|q_y|}{\Lambda}\right),\quad\lim_{\frac{|q_y|}{\Lambda}\to 0}\widetilde{\mathfrak{S}}\left(3-d;\frac{|q_y|}{\Lambda}\right)=\frac{1}{3-d}. \tag{D28}$$

The contribution from the remaining hot spots are obtained by performing a C_4 transformation on the $n=1$ hot spot contribution. Taking the contributions from all hot spots into account, Eq. (D9) leads to

$$\Delta\Pi^{2L}(\mathbf{0},\vec{q})=\frac{4\beta_d^4}{N_cN_f}w(v)\mathfrak{B}(d)\mathfrak{S}[d-2;w(v)]\left[|q_y|^{d-1}\widetilde{\mathfrak{S}}\left(3-d;\frac{|q_y|}{\Lambda}\right)+|q_x|^{d-1}\widetilde{\mathfrak{S}}\left(3-d;\frac{|q_x|}{\Lambda}\right)\right]. \tag{D29}$$

According to Eq. (D28), the UV cutoff drops out in $d<3$ and we have

$$\Delta\Pi^{2L}(\mathbf{0},\vec{q})=\frac{4\beta_d^4}{(3-d)N_cN_f}w(v)\mathfrak{B}(d)\mathfrak{S}[d-2;w(v)][|q_y|^{d-1}+|q_x|^{d-1}]. \tag{D30}$$

We note that Eq. (D21) reproduces the result obtained in Ref. [72] in the $d\to 2$ limit and is consistent with the findings of Ref. [53] close to three dimensions.

Now we show that Fig. 7(c) does not contribute to the momentum dependent self-energy. Figure 7(c) is written as

$$\Upsilon^{2L}(q)\sim\frac{4\left(N_c^2-1\right)\beta_d^4v^2}{N_cN_f}\sum_{n=1}^4\int dk\int dp\mathrm{Tr}\left[G_{\bar{n}}^{(0)}(k+q)\gamma_{d-1}G_n^{(0)}(k)\gamma_{d-1}G_{\bar{n}}^{(0)}(k+p)\gamma_{d-1}G_n^{(0)}(k)\gamma_{d-1}\right]D(p). \tag{D31}$$

Taking the trace over the spinor indices, making the change of variables $k_+=\varepsilon_n(\vec{k};v)$, and $k_-=\varepsilon_{\bar{n}}(\vec{k}+\vec{p};v)$ and integrating over k_+ results in

$$\Upsilon^{2L}(q)=\frac{2\left(N_c^2-1\right)\beta_d^4v}{N_cN_f}\sum_{n=1}^4\int dp\int_{\mathbb{R}^{d-1}}\frac{d\mathbf{K}}{(2\pi)^{d-1}}\int_{\mathbb{R}}\frac{dk_-}{(2\pi)}\left[\frac{[(\mathbf{K}\cdot\mathbf{P})(\mathbf{K}\cdot\mathbf{Q})-\mathbf{K}^2(\mathbf{P}\cdot\mathbf{Q})]D(p)}{|\mathbf{K}|^3[(\mathbf{K}+\mathbf{P})^2+k_-^2]\{(\mathbf{K}+\mathbf{Q})^2+[k_--\varepsilon_{\bar{n}}(\vec{p}-\vec{q};v)]^2\}}\right]. \tag{D32}$$

This expression vanishes when $\mathbf{Q} = \mathbf{0}$ for any v, and there is no spatial momentum dependent contribution in $d > 2$. We note that this diagram is exactly zero in $d = 2$ [15,18,62,72].

3. One-loop fermion self-energy

The quantum correction in Fig. 8(a) reads

$$\delta\mathbf{\Gamma}^{(2,0)}_{1\mathrm{L}} = \sum_{n=1}^{4}\sum_{\sigma=1}^{N_c}\sum_{j=1}^{N_f}\int dq\,\overline{\Psi}_{n,\sigma,j}(q)\Sigma^{1\mathrm{L}}_{n}(q)\Psi_{n,\sigma,j}(q), \tag{D33}$$

where the one-loop fermion self-energy is given by

$$\Sigma^{1\mathrm{L}}_{n}(q) = \frac{2\beta_d^2\left(N_c^2-1\right)v}{N_cN_f}\int dk\gamma_{d-1}G^{(0)}_{\overline{n}}(k+q)\gamma_{d-1}D(k). \tag{D34}$$

Here $G^{(0)}_n(k)$, β_d, and $D(k)$ are defined in Eqs. (18), (13), and (15), respectively. We will consider the part of the self-energy that depends on the spatial momentum and the one that depends on the frequency and codimensional momentum, separately. For this purpose we write

$$\Sigma_n(\mathbf{Q},\vec{q}) = (\mathbf{\Gamma}\cdot\mathbf{Q})\overline{\Sigma}_{n,\mathrm{f}}(\mathbf{Q}) + \gamma_{d-1}\Sigma_{n,\mathrm{s}}(\vec{q}), \tag{D35}$$

with

$$\overline{\Sigma}_{n,\mathrm{f}}(\mathbf{Q}) = \frac{1}{2}\mathrm{Tr}\left[\frac{(\mathbf{\Gamma}\cdot\mathbf{Q})}{\mathbf{Q}^2}\Sigma_n(\mathbf{Q},\vec{0})\right],\quad \Sigma_{n,\mathrm{s}}(\vec{q}) = \frac{1}{2}\mathrm{Tr}[\gamma_{d-1}\Sigma_n(\mathbf{0},\vec{q})]. \tag{D36}$$

a. $\overline{\Sigma}_{n,\mathrm{f}}(\mathbf{Q})$

We focus on the frequency and codimensional momentum component first,

$$\overline{\Sigma}^{1\mathrm{L}}_{n,\mathrm{f}}(\mathbf{Q}) = \frac{2i\beta_d^2\left(N_c^2-1\right)v}{N_cN_f}\frac{1}{\mathbf{Q}^2}\int dk\left(\frac{\mathbf{Q}\cdot(\mathbf{K}+\mathbf{Q})}{(\mathbf{K}+\mathbf{Q})^2+\varepsilon_{\overline{n}}(\vec{k};v)^2}\right)D(k). \tag{D37}$$

For concreteness we consider the $n = 1$ hot spot in the small v limit. Performing the scaling $k_x \to k_x/c(v)$ yields

$$\overline{\Sigma}^{1\mathrm{L}}_{1,\mathrm{f}}(\mathbf{Q}) = \frac{2i\beta_d^2\left(N_c^2-1\right)w(v)}{N_cN_f}\frac{1}{\mathbf{Q}^2}\int dk\left(\frac{\mathbf{Q}\cdot(\mathbf{K}+\mathbf{Q})}{(\mathbf{K}+\mathbf{Q})^2+[w(v)k_x-k_y]^2}\right)\frac{1}{|\mathbf{K}|^{d-1}+|k_x|^{d-1}+c(v)^{d-1}|k_y|^{d-1}}, \tag{D38}$$

where $w(v) = v/c(v)$. The integration over $\vec{k}$ gives

$$\overline{\Sigma}^{1\mathrm{L}}_{1,\mathrm{f}}(\mathbf{Q}) = \frac{i\beta_d^2\left(N_c^2-1\right)w(v)}{N_cN_f\pi\mathbf{Q}^2}\Gamma\left(\frac{d}{d-1}\right)\int_{\mathbb{R}^{d-1}}\frac{d\mathbf{K}}{(2\pi)^{d-1}}\left(\frac{\mathbf{Q}\cdot(\mathbf{K}+\mathbf{Q})}{|\mathbf{K}+\mathbf{Q}|}\right)\left[|\mathbf{K}|^{2-d}\Gamma\left(\frac{d-2}{d-1}\right)-\frac{[c(v)\widetilde{\Lambda}]^{2-d}(d-1)}{(d-2)\Gamma\left(\frac{1}{d-1}\right)}\right] \tag{D39}$$

in the small $c(v)$ limit.

In $d > 2$, the second term in the square brackets of Eq. (D39) can be dropped, and the first term gives rise to a logarithmically divergent contribution. In $d = 2$, the two terms in the square brackets combine to become a logarithm, and the integration over $\mathbf{K}$ is finite. In all cases, the logarithmically divergent contribution can be written as

$$\overline{\Sigma}^{1\mathrm{L}}_{1,\mathrm{f}}(\mathbf{Q}) = -\frac{\left(N_c^2-1\right)\cos\left(\frac{\pi d}{2}\right)\Gamma\left(\frac{2d-3}{d-1}\right)\Gamma\left(\frac{1}{d-1}\right)\Gamma\left(\frac{d-1}{2}\right)}{2^{3-d}N_cN_f\pi^{3/2}\Gamma\left(\frac{d}{2}\right)}iw(v)\log\left(\frac{\Lambda}{|\mathbf{Q}|}\right). \tag{D40}$$

Here we have used the fact that $\Lambda \approx \widetilde{\Lambda}$ and the definition of β_d in Eq. (13). Combining this result with the renormalization condition in Eq. (C4) and the fact that the other three hot spots give the same contribution, Z_1 is fixed to be

$$Z_1 = 1 - \frac{\left(N_c^2-1\right)\zeta(d)}{N_cN_f}w(v)\log\left(\frac{\Lambda}{\mu}\right), \tag{D41}$$

with $\zeta(d)$ defined in Eq. (23).

b. $\Sigma_{n,\mathrm{s}}(\vec{q})$

Now we turn our attention to the spatial part of the self-energy defined in Eq. (D36):

$$\Sigma^{1\mathrm{L}}_{n,\mathrm{s}}(\vec{q}) = -\frac{2\left(N_c^2-1\right)i\beta_d^2v}{N_cN_f}\int dk\left(\frac{\varepsilon_{\overline{n}}(\vec{k}+\vec{q};v)}{\varepsilon_{\overline{n}}(\vec{k}+\vec{q};v)^2+\mathbf{K}^2}\right)D(k). \tag{D42}$$

Without loss of generality we consider the contribution from the $n = 1$ hot spot,

$$\Sigma^{\rm 1L}_{\rm 1,s}(\vec{q}) = -\frac{2i\left(N_c^2-1\right)\beta_d^2 v}{N_c N_f}\int dk\left(\frac{[vk_x - k_y + \varepsilon_3(\vec{q};v)]}{[vk_x - k_y + \varepsilon_3(\vec{q};v)]^2 + \mathbf{K}^2}\right)\frac{1}{|\mathbf{K}|^{d-1} + c(v)^{d-1}(|k_x|^{d-1} + |k_y|^{d-1})}. \tag{D43}$$

When v and $c(v)$ are small, the integration over k_x yields

$$\Sigma^{\rm 1L}_{\rm 1,s}(\vec{q}) = -\frac{2i\left(N_c^2-1\right)\beta_d^2}{(d-1)\pi N_c N_f} w(v)\int_{\mathbb{R}^{d-1}}\frac{d\mathbf{K}}{(2\pi)^{d-1}}\int_{\mathbb{R}}\frac{dk_y}{(2\pi)}\left[\left(\frac{[\varepsilon_3(\vec{q};v) - k_y]}{[\varepsilon_3(\vec{q};v) - k_y]^2 + \mathbf{K}^2}\right)\right.$$
$$\left.\times\left[\Gamma\left(\frac{d-2}{d-1}\right)\Gamma\left(\frac{1}{d-1}\right)\frac{1}{\left[|\mathbf{K}|^{d-1} + c(v)^{d-1}|k_y|^{d-1}\right]^{\frac{d-2}{d-1}}} - \frac{c(v)^{2-d}\widetilde{\Lambda}^{2-d}(d-1)}{(d-2)}\right]\right]. \tag{D44}$$

We drop the second term in the square brackets because the integrand is odd in $[\varepsilon_3(\vec{q};v) - k_y]$. Focusing only on the first term, the remaining integrations are done by writing the expression as an antiderivative with respect to $c(v)$:

$$\Sigma^{\rm 1L}_{\rm 1,s}(\vec{q}) = \frac{2(d-2)i\left(N_c^2-1\right)\beta_d^2}{(d-1)\pi N_c N_f}\Gamma\left(\frac{d-2}{d-1}\right)\Gamma\left(\frac{1}{d-1}\right)w(v)\int_0^{c(v)} d\mathsf{c}\,\mathsf{c}^{d-2}\int_{\mathbb{R}^{d-1}}\frac{d\mathbf{K}}{(2\pi)^{d-1}}$$
$$\times\int_{\mathbb{R}}\frac{dk_y}{(2\pi)}\left[\left(\frac{[\varepsilon_3(\vec{q};v) - k_y]}{[\varepsilon_3(\vec{q};v) - k_y]^2 + \mathbf{K}^2}\right)\frac{|k_y|^{d-1}}{(|\mathbf{K}|^{d-1} + \mathsf{c}^{d-1}|k_y|^{d-1})^{\frac{2d-3}{d-1}}}\right]. \tag{D45}$$

The lower limit of the integration over c is determined from the fact that the integration over k_y in Eq. (D44) vanishes in the small $c(v)$ limit. The radial integration for $\mathbf{K}$ is divided into two regions: $K \equiv |\mathbf{K}| \in (0, |\varepsilon_3(\vec{q};v) - k_y|)$ and $K \in (|\varepsilon_3(\vec{q};v) - k_y|, \infty)$. In the first region, the fermionic contribution to the integrand varies slowly in $\mathbf{K}$ and can be Taylor expanded around the origin. Only the zeroth order term in the expansion becomes IR divergent when $\mathsf{c} = 0$, and thus, provides the leading order contribution to the integration in the small $c(v)$ limit. The contribution from the second region is regular and therefore is subleading in the small $c(v)$ limit. Keeping only the leading contribution in the small $c(v)$ limit, we obtain

$$\Sigma^{\rm 1L}_{\rm 1,s}(\vec{q}) = \frac{(d-2)i\left(N_c^2-1\right)\beta_d^2 w(v)}{2^{d-2}\pi^{\frac{d+1}{2}}N_c N_f}\frac{\Gamma\left(\frac{d-2}{d-1}\right)\Gamma\left(\frac{1}{d-1}\right)}{\Gamma\left(\frac{d+1}{2}\right)}\int_0^{c(v)} d\mathsf{c}\int_{\mathbb{R}}\frac{dk_y}{(2\pi)}\frac{[\varepsilon_3(\vec{q};v) - k_y]}{[\varepsilon_3(\vec{q};v) - k_y]^2}|k_y|\overline{\mathfrak{S}}'\left(d-2;\mathsf{c};\frac{|\varepsilon_3(\vec{q};v) - k_y|}{|k_y|}\right), \tag{D46}$$

where

$$|k_y|\overline{\mathfrak{S}}'\left(d-2;\mathsf{c};\frac{|\varepsilon_3(\vec{q};v) - k_y|}{|k_y|}\right) \equiv \int_0^{|\varepsilon_3(\vec{q};v) - k_y|} dK\,\frac{\mathsf{c}^{d-2}|k_y|^{d-1}K^{d-2}}{(K^{d-1} + \mathsf{c}^{d-1}|k_y|^{d-1})^{\frac{2d-3}{d-1}}}. \tag{D47}$$

While $\overline{\mathfrak{S}}'[d-2;\mathsf{c};|\varepsilon_3(\vec{q};v) - k_y|/|k_y|]$ depends on k_y and $\varepsilon_3(\vec{q};v)$, these dependencies are suppressed in the $d \to 2$ or $\mathsf{c} \to 0$ limits. In either of these limits, $\overline{\mathfrak{S}}'[d-2;\mathsf{c};|\varepsilon_3(\vec{q};v) - k_y|/|k_y|]$ reduces to $\mathfrak{S}(d-2;\mathsf{c})$ defined in Eq. (D13). From now on, we replace $\overline{\mathfrak{S}}'[d-2;\mathsf{c};|\varepsilon_3(\vec{q};v) - k_y|/|k_y|]$ with $\mathfrak{S}(d-2;\mathsf{c})$ in Eq. (D46). Integration over c can be done by using the following limits:

$$\lim_{\xi\to 0^+}\int da\,\mathfrak{S}(\xi;a) = a - a\log(a) \overset{a\ll 1}{=} \lim_{\xi\to 0^+} a\,\mathfrak{S}(\xi;a), \tag{D48}$$

$$\lim_{b\to 0}\int da\,\mathfrak{S}(\xi;ba) = \frac{a}{\xi} = a\lim_{a\to 0^+}\mathfrak{S}(\xi;a). \tag{D49}$$

This allows us to write Eq. (D46) as

$$\Sigma^{\rm 1L}_{\rm 1,s}(\vec{q}) = \frac{(d-2)i\left(N_c^2-1\right)\beta_d^2}{2^{d-2}\pi^{\frac{d+1}{2}}N_c N_f}\frac{\Gamma\left(\frac{d-2}{d-1}\right)\Gamma\left(\frac{1}{d-1}\right)}{\Gamma\left(\frac{d+1}{2}\right)} v\,\mathfrak{S}[d-2;c(v)]\varepsilon_3(\vec{q};v)\int_{\mathbb{R}}\frac{dk_y}{(2\pi)}\left(\frac{(1-k_y)}{(1-k_y)^2}\right)|k_y|. \tag{D50}$$

Here we have scaled out the external momentum through the change of variables $k_y \to |\varepsilon_3(\vec{q};v)|k_y$. The integration over k_y is UV divergent and we cut it off by $\widetilde{\Lambda}/|\varepsilon_3(\vec{q};v)|$. In the large $\widetilde{\Lambda}/|\varepsilon_3(\vec{q};v)|$ limit,

$$\int_{-\frac{\widetilde{\Lambda}}{|\varepsilon_3(\vec{q};v)|}}^{\frac{\widetilde{\Lambda}}{|\varepsilon_3(\vec{q};v)|}} \frac{dk_y}{(2\pi)}\left(\frac{1-k_y}{(1-k_y)^2}\right)|k_y| = \lim_{\delta\to 0}\left(\int_{-\frac{\widetilde{\Lambda}}{|\varepsilon_3(\vec{q};v)|}}^{1-\delta}\frac{dk_y}{(2\pi)} + \int_{1+\delta}^{\frac{\widetilde{\Lambda}}{|\varepsilon_3(\vec{q};v)|}}\frac{dk_y}{(2\pi)}\right)\left(\frac{1-k_y}{(1-k_y)^2}\right)|k_y| = \frac{1}{\pi}\log\left(\frac{|\varepsilon_3(\vec{q};v)|}{\widetilde{\Lambda}}\right). \tag{D51}$$

Hence, the divergent contribution to the spatial part of the one-loop fermion self-energy for the fermions at the $n=1$ hot spot is given by

$$\Sigma^{1L}_{1,s}(\vec{q}) = -\frac{(d-2)i\left(N_c^2-1\right)\beta_d^2}{2^{d-2}\pi^{\frac{d+3}{2}}N_cN_f}\frac{\Gamma\left(\frac{d-2}{d-1}\right)\Gamma\left(\frac{1}{d-1}\right)}{\Gamma\left(\frac{d+1}{2}\right)}v\mathfrak{S}[d-2;c(v)]\varepsilon_3(\vec{q};v)\log\left(\frac{\widetilde{\Lambda}}{|\varepsilon_3(\vec{q};v)|}\right) \tag{D52}$$

in the small v and large $\widetilde{\Lambda}/|\varepsilon_3(\vec{q};v)|$ limits. Introducing the value of β_d defined in Eq. (13) and combining this expression with the renormalization conditions in Eqs. (C5) and (C6) fixes the counter term coefficients A_2 and A_3 to the one-loop order,

$$A_2^{1L} = \frac{2(d-1)\left(N_c^2-1\right)\zeta(d)}{\pi N_cN_f}v\mathfrak{S}[d-2;c(v)]\log\left(\frac{\widetilde{\Lambda}}{\mu}\right), \tag{D53}$$

$$A_3^{1L} = -\frac{2(d-1)\left(N_c^2-1\right)\zeta(d)}{\pi N_cN_f}v\mathfrak{S}[d-2;c(v)]\log\left(\frac{\widetilde{\Lambda}}{\mu}\right), \tag{D54}$$

with $\zeta(d)$ defined in Eq. (23).

4. Two-loop fermion self-energy

We consider the two-loop fermion self-energy depicted in Fig. 9(a),

$$\delta\mathbf{\Gamma}^{(2,0)}_{2L} = \sum_{n=1}^{4}\sum_{\sigma=1}^{N_c}\sum_{j=1}^{N_f}\int dq\,\overline{\Psi}_{n,\sigma,j}(q)\Sigma^{2L}_n(q)\Psi_{n,\sigma,j}(q), \tag{D55}$$

where the two-loop fermion self-energy is given by

$$\Sigma^{2L}_n(k) = \frac{4\left(N_c^2-1\right)\beta_d^4v^2}{N_c^2N_f^2}\int dq\int dp\left[\gamma_{d-1}G^{(0)}_{\overline{n}}(k+q)\gamma_{d-1}G^{(0)}_n(k+q+p)\gamma_{d-1}G^{(0)}_{\overline{n}}(k+p)\gamma_{d-1}\right]D(p)D(q). \tag{D56}$$

Without loss of generality, we consider the $n=1$ hot spot contribution to the spatial piece of this quantum correction since its frequency part is strictly subleading with respect to the one-loop correction due to an additional factor of $w(v)=v/c(v)$. The self-energy at $\mathbf{K}=\mathbf{0}$ becomes

$$\begin{aligned}\Sigma^{2L}_{1,s}(\vec{k}) = &-\frac{4i\left(N_c^2-1\right)\beta_d^4v^2}{N_c^2N_f^2}\int dq\int dp\Bigg\{\frac{D(p)D(q)}{[\mathbf{P}^2+\varepsilon_3(\vec{k}+\vec{p};v)^2][\mathbf{Q}^2+\varepsilon_3(\vec{k}+\vec{q};v)^2][(\mathbf{P}+\mathbf{Q})^2+\varepsilon_1(\vec{k}+\vec{q}+\vec{p};v)^2]}\\ &\times[(\mathbf{P}\cdot\mathbf{Q})\varepsilon_1(\vec{k}+\vec{p}+\vec{q};v)+\mathbf{Q}\cdot(\mathbf{P}+\mathbf{Q})\varepsilon_3(\vec{k}+\vec{p};v)+[\mathbf{P}\cdot(\mathbf{P}+\mathbf{Q})-\varepsilon_1(\vec{k}+\vec{p}+\vec{q};v)\varepsilon_3(\vec{k}+\vec{p};v)]\varepsilon_3(\vec{k}+\vec{q};v)]\Bigg\}.\end{aligned} \tag{D57}$$

We proceed by performing the scaling $p_x \to p_x/v$ and $q_x \to q_x/v$ and dropping the dependencies on p_y and q_y inside the boson propagators in the small v limit. In the small $c(v)$ limit, the integrations over p_x and q_x give

$$\begin{aligned}\Sigma^{2L}_{1,s}(\vec{k}) = &-\frac{4(d-2)^2i\left(N_c^2-1\right)\beta_d^4w(v)^2}{\pi^2N_c^2N_f^2}\Gamma\left(\frac{d-2}{d-1}\right)^2\Gamma\left(\frac{d}{d-1}\right)^2\mathfrak{S}[d-2;w(v)]^2\int_{\mathbb{R}^{d-1}}\frac{d\mathbf{Q}}{(2\pi)^{d-1}}\\ &\times\int_{\mathbb{R}^{d-1}}\frac{d\mathbf{P}}{(2\pi)^{d-1}}\int_{\mathbb{R}}\frac{dq_y}{(2\pi)}\int_{\mathbb{R}}\frac{dp_y}{(2\pi)}\Bigg\{\frac{|\mathbf{P}|^{2-d}|\mathbf{Q}|^{2-d}}{\{\mathbf{Q}^2+[\varepsilon_3(\vec{k};v)-q_y]^2\}\{(\mathbf{P}+\mathbf{Q})^2+[\varepsilon_1(\vec{k};v)+p_y+q_y]^2\}}\\ &\times\frac{1}{\{\mathbf{P}^2+[\varepsilon_3(\vec{k};v)-p_y]^2\}}[(\mathbf{P}\cdot\mathbf{Q})[\varepsilon_1(\vec{k};v)+p_y+q_y]+\mathbf{Q}\cdot(\mathbf{P}+\mathbf{Q})[\varepsilon_3(\vec{k};v)-p_y]\\ &+\{\mathbf{P}\cdot(\mathbf{P}+\mathbf{Q})-[\varepsilon_1(\vec{k};v)+p_y+q_y][\varepsilon_3(\vec{k};v)-p_y]\}[\varepsilon_3(\vec{k};v)-q_y]]\Bigg\},\end{aligned} \tag{D58}$$

where $\mathfrak{S}[d-2;w(v)]$ is defined in Eq. (D13). Here we ignore terms that are subleading in $c(v)$. We continue by making the change of variables $p_y \to p_y+\varepsilon_3(\vec{k};v)$ and $q_y \to q_y+\varepsilon_3(\vec{k};v)$ which makes the two-loop fermion self-energy depend on the

external spatial momentum only through $\delta(\vec{k};v)\equiv\varepsilon_1(\vec{k};v)+2\varepsilon_3(\vec{k};v)=3vk_x-k_y$. After an introduction of a single-variable Feynman parametrization, the integration over p_y yields

$$\Sigma^{2\mathrm{L}}_{1,\mathrm{s}}(\vec{k})=-\frac{i(d-2)^2\left(N_c^2-1\right)\beta_d^4 w(v)^2}{\pi^2 N_c^2 N_f^2}\Gamma\left(\frac{d-2}{d-1}\right)^2\Gamma\left(\frac{d}{d-1}\right)^2\mathfrak{S}[d-2;w(v)]^2\int_{\mathbb{R}^{d-1}}\frac{d\mathbf{Q}}{(2\pi)^{d-1}}\int_{\mathbb{R}^{d-1}}\frac{d\mathbf{P}}{(2\pi)^{d-1}}\int_0^1 dx$$
$$\times\int_{\mathbb{R}}\frac{dq_y}{(2\pi)}|\mathbf{P}|^{2-d}|\mathbf{Q}|^{2-d}\left[\frac{\mathcal{A}-q_y(\mathbf{P}^2+2(1-x)\mathbf{P}\cdot\mathbf{Q}+(1-x)\{\mathbf{Q}^2+x[q_y+\delta(\vec{k};v)]^2\})}{(\mathbf{P}^2+2(1-x)\mathbf{P}\cdot\mathbf{Q}+(1-x)\{\mathbf{Q}^2+x[q_y+\delta(\vec{k};v)]^2\})^{3/2}(q_y^2+\mathbf{Q}^2)}\right], \tag{D59}$$

with

$$\mathcal{A}=-q_y[\mathbf{P}\cdot(\mathbf{P}+\mathbf{Q})]+x(\mathbf{P}\cdot\mathbf{Q})[q_y+\delta(\vec{k};v)]+(1-x)[q_y+\delta(\vec{k};v)]\{\mathbf{Q}\cdot(\mathbf{Q}+\mathbf{P})+xq_y[q_y+\delta(\vec{k};v)]\}. \tag{D60}$$

By introducing a second single-variable Feynman parametrization, the integration over q_y yields

$$\Sigma^{2\mathrm{L}}_{1,\mathrm{s}}(\vec{k})=-\frac{i(d-2)^2\left(N_c^2-1\right)\delta(\vec{k};v)\beta_d^4 w(v)^2}{\pi^3 N_c^2 N_f^2}\Gamma\left(\frac{d-2}{d-1}\right)^2\Gamma\left(\frac{d}{d-1}\right)^2\mathfrak{S}[d-2;w(v)]^2$$
$$\times\int_{\mathbb{R}^{d-1}}\frac{d\mathbf{Q}}{(2\pi)^{d-1}}\int_{\mathbb{R}^{d-1}}\frac{d\mathbf{P}}{(2\pi)^{d-1}}\int_0^1 dx\int_0^1 dy\frac{|\mathbf{P}|^{2-d}|\mathbf{Q}|^{2-d}}{\sqrt{y+x(1-x)(1-y)}}\left(\frac{\mathcal{C}_1}{\mathcal{D}_1^2}\right), \tag{D61}$$

where

$$\mathcal{C}_1=\frac{\sqrt{1-y}}{x+x^2(y-1)+y-xy}(xy(\mathbf{P}\cdot\mathbf{Q})+(1-x)\{x(1-y)\mathbf{P}\cdot(\mathbf{P}+\mathbf{Q})+y\mathbf{Q}\cdot(\mathbf{P}+\mathbf{Q})$$
$$+x(1-y)[\mathbf{P}^2+2(1-x)(\mathbf{P}\cdot\mathbf{Q})+(1-x)\mathbf{Q}^2]\}), \tag{D62}$$

$$\mathcal{D}_1=(1-y)\mathbf{P}^2+2(1-x)(1-y)(\mathbf{P}\cdot\mathbf{Q})+[1-x(1-y)]\mathbf{Q}^2+\frac{(1-x)(1-y)xy}{y+(1-x)(1-y)x}\delta(\vec{k};v)^2. \tag{D63}$$

Integration over $\mathbf{P}$ is done by introducing a third single-variable Feynman parametrization. This process yields a $\mathbf{Q}$-dependent integrand that can be cast in the rotationally invariant way,

$$\Sigma^{2\mathrm{L}}_{1,\mathrm{s}}(\vec{k})=\frac{i(d-2)^2\left(N_c^2-1\right)\delta(\vec{k};v)\beta_d^4 w(v)^2}{2^{2d-2}\pi^{\frac{2d+3}{2}}N_c^2N_f^2}\frac{\Gamma\left(\frac{d-2}{d-1}\right)^2\Gamma\left(\frac{d}{d-1}\right)^2}{\Gamma\left(\frac{d-2}{2}\right)\Gamma\left(\frac{d-1}{2}\right)}\mathfrak{S}[d-2;w(v)]^2$$
$$\times\int_0^1 dx\int_0^1 dy\int_0^1 dz\frac{(1-z)z^{\frac{d-4}{2}}\sqrt{1-y}}{[y+x(1-x)(1-y)]^{3/2}[1-y(1-z)]^{\frac{d+1}{2}}}\int_0^{\frac{\Lambda}{|\delta(\vec{k};v)|}}dQ\left[\frac{(\mathcal{E}_1Q^2+\mathcal{E}_2)}{(\mathcal{H}_1Q^2+\mathcal{H}_2)^{3/2}}\right], \tag{D64}$$

where the integration over the angular components has been done, and the integration over $Q\equiv|\mathbf{Q}|$ has been cut off in the UV since it is logarithmically divergent. The coefficients $\mathcal{E}_i$ and $\mathcal{H}_i$ are defined as follows:

$$\mathcal{E}_1=\frac{1}{1-y(1-z)}\{(x-1)[2x^3(y-1)^2(z-1)(d(y-1)(z-1)-yz+y+2z-1)$$
$$+x^2(y-1)(-2d(y-1)(z-1)(y(z-1)-2z+1)+2y^2(z-1)^2-y(9z-4)(z-1)+z(8z-9)+2)$$
$$+x(y-1)(2(d-1)y^2(z-1)^2-y(z-1)(2d(z-1)-3z+2)+z(2d(z-1)-4z+3))+yz(y(z-1)+1)]\}, \tag{D65}$$

$$\mathcal{E}_2=\frac{2(d-1)(x-1)^2x^2(y-1)^2y(z-1)}{(x-1)x(y-1)+y}, \tag{D66}$$

$$\mathcal{H}_1=-\frac{(z-1)\left\{x^2(y-1)^2(z-1)-x(y-1)[y(z-1)-2z+1]+y(y-1)(z-1)+z\right\}}{y(z-1)+1}, \tag{D67}$$

$$\mathcal{H}_2=-\frac{(1-x)x(1-y)y(1-z)}{[(x-1)x(y-1)+y]}. \tag{D68}$$

For $\Lambda/|\delta(\vec{k};v)|\gg1$, the divergent contribution to the two-loop fermion self-energy is given by

$$\Sigma^{2\mathrm{L}}_{1,\mathrm{s}}(\vec{k})=-\frac{2i\beta_d^4\left(N_c^2-1\right)}{N_c^2N_f^2}\mathfrak{F}(d)w(v)^2\mathfrak{S}[d-2;w(v)]^2\delta(\vec{k};v)\log\left(\frac{\Lambda}{|\delta(\vec{k};v)|}\right), \tag{D69}$$

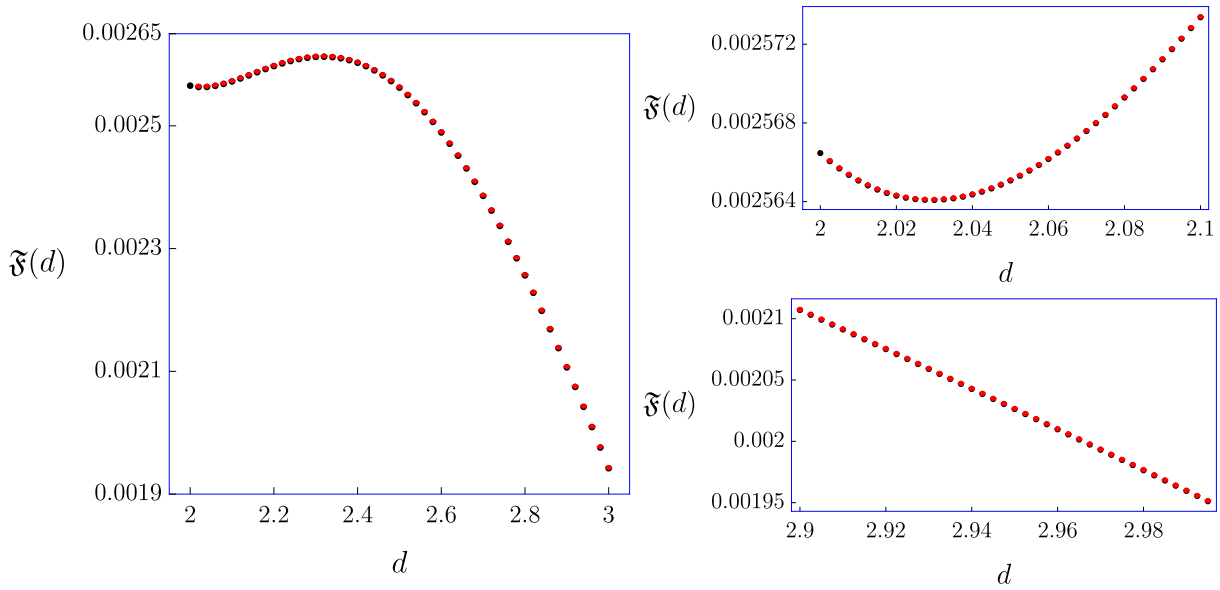

(a) $\mathfrak{F}(d)$ for $2 \leq d \leq 3$. (b) $\mathfrak{F}(d)$ near $d = 2$ (top) and $d = 3$ (bottom).

FIG. 11. (a) The function $\mathfrak{F}(d)$. Each point is computed numerically except for the one in $d = 2$ where it can be determined analytically. The (black) dots correspond the value of the numerical integration and the (red) error bars represent the numerical error in the computation. (b) Numerical evaluation near $d = 2$ (top) and $d = 3$ (bottom).

where the positive function $\mathfrak{F}(d)$ is given by

$$\begin{aligned}\mathfrak{F}(d) = \frac{(d-2)^2}{(2\pi)^{d+2}} \frac{\Gamma\left(\frac{d-2}{d-1}\right)^2 \Gamma\left(\frac{d}{d-1}\right)^2}{\Gamma(d-2)} \int_0^1 dx \int_0^1 dy \int_0^1 dz \frac{(1-x)\sqrt{1-y}z^{\frac{d-4}{2}}}{[1-y(1-z)]^{\frac{d}{2}}[y+(1-x)x(1-y)]^{3/2}\sqrt{1-z}} \\ \times \frac{(2x^3(y-1)^2(z-1)(d(y-1)(z-1)-yz+y+2z-1)}{((x(1-y)(1+y(-1+z)-2z)+x^2(-1+y)^2(-1+z)+(-1+y)y(-1+z)+z))^{3/2}} \\ + \frac{x^2(y-1)(-2d(y-1)(z-1)(y(z-1)-2z+1)+2y^2(z-1)^2-y(9z-4)(z-1)+z(8z-9)+2)}{((x(1-y)(1+y(-1+z)-2z)+x^2(-1+y)^2(-1+z)+(-1+y)y(-1+z)+z))^{3/2}} \\ + \frac{x(y-1)(2(d-1)y^2(z-1)^2-y(z-1)(2d(z-1)-3z+2)+z(2d(z-1)-4z+3))+yz(y(z-1)+1))}{((x(1-y)(1+y(-1+z)-2z)+x^2(-1+y)^2(-1+z)+(-1+y)y(-1+z)+z))^{3/2}}\Bigg].\end{aligned} \tag{D70}$$

Despite the multiplicative factor that vanishes in $d = 2$, Eq. (D70) does not vanish because the integration over z is divergent in $d = 2$. In this dimension, an explicit integration over the Feynman parameters gives rise to

$$\mathfrak{F}(2) = \frac{1}{4\pi^4} \int_0^1 dx \int_0^1 dy \frac{(1-x)x}{[y+(1-y)(1-x)x]^2} = \frac{1}{4\pi^4}. \tag{D71}$$

This agrees with the result obtained in Ref. [72]. For $d > 2$, the expression is computed numerically as shown in Fig. 11. From Eq. (D69) and the renormalization conditions in Eqs. (C5) and (C6) the two-loop counter term coefficients are determined to be

$$A_2^{2L} = \frac{6\left(N_c^2-1\right)\beta_d^4}{N_c^2 N_f^2} \mathfrak{F}(d) w(v)^2 \mathfrak{S}[d-2; w(v)]^2 \log\left(\frac{\Lambda}{\mu}\right), \tag{D72}$$

$$A_3^{2L} = -\frac{2\left(N_c^2-1\right)\beta_d^4}{N_c^2 N_f^2} \mathfrak{F}(d) w(v)^2 \mathfrak{S}[d-2; w(v)]^2 \log\left(\frac{\Lambda}{\mu}\right). \tag{D73}$$

Combining this result with Eqs. (D53) and (D54) it follows that the counter term coefficients Z_2 and Z_3 are given, to the leading order in v, by

$$Z_2 = 1 + \frac{\left(N_c^2-1\right)}{N_c N_f}\left[\frac{2(d-1)}{\pi}\zeta(d) v \mathfrak{S}[d-2; c(v)] \log\left(\frac{\widetilde{\Lambda}}{\mu}\right) + \frac{6\beta_d^4}{N_c N_f} \mathfrak{F}(d) w(v)^2 \mathfrak{S}[d-2; w(v)]^2 \log\left(\frac{\Lambda}{\mu}\right)\right], \tag{D74}$$

$$Z_3 = 1 - \frac{\left(N_c^2-1\right)}{N_c N_f}\left[\frac{2(d-1)}{\pi}\zeta(d)v\mathfrak{S}[d-2;c(v)]\log\left(\frac{\widetilde{\Lambda}}{\mu}\right) + \frac{2\beta_d^4}{N_c N_f}\mathfrak{F}(d)w(v)^2\mathfrak{S}[d-2;w(v)]^2\log\left(\frac{\Lambda}{\mu}\right)\right]. \quad \text{(D75)}$$

5. One-loop vertex correction

We consider the one-loop vertex correction in Fig. 8(b),

$$\delta\mathbf{\Gamma}_{1\mathrm{L}}^{(2,1)} = \frac{i\beta_d\sqrt{v}}{\sqrt{N_f}}\sum_{n=1}^{4}\sum_{\sigma,\sigma'=1}^{N_c}\sum_{j=1}^{N_f}\int dk\int dq\,\overline{\Psi}_{\bar{n},\sigma,j}(k+q)\Phi_{\sigma\sigma'}(q)\Gamma_n^{(2,1),1\mathrm{L}}(k,q)\Psi_{n,\sigma',j}(k), \quad \text{(D76)}$$

where the one-loop vertex function is given by

$$\Gamma_n^{(2,1),1\mathrm{L}}(k,q) = \frac{2\beta_d^2 v}{N_c N_f}\int dp\left[\gamma_{d-1}G_{\bar{n}}^{(0)}(p+k+q)\gamma_{d-1}G_n^{(0)}(p+k)\gamma_{d-1}\right]D(p). \quad \text{(D77)}$$

In view of the renormalization condition in Eq. (C7), we consider the vertex function at $k=0$ and $\vec{q}=0$,

$$\Upsilon_n^{1\mathrm{L}}(\mathbf{Q}) = \tfrac{1}{2}\mathrm{Tr}\left[\gamma_{d-1}\Gamma_n^{(2,1),1\mathrm{L}}(k,q)\right]\big|_{k=0,\vec{q}=\vec{0}}. \quad \text{(D78)}$$

For $n=1$, Eq. (D78) becomes

$$\Upsilon_1^{1\mathrm{L}}(\mathbf{Q}) = \frac{2\beta_d^2 v}{N_c N_f}\int dp\left(\frac{\mathbf{P}\cdot(\mathbf{P}+\mathbf{Q}) - \left(v^2p_x^2 - p_y^2\right)}{[\mathbf{P}^2+(vp_x+p_y)^2][(\mathbf{P}+\mathbf{Q})^2+(vp_x-p_y)^2]}\right)D(p). \quad \text{(D79)}$$

Following the same steps used in Appendixes D 2 and D 4, we obtain

$$\begin{aligned}\Upsilon_1^{1\mathrm{L}}(\mathbf{Q}) = {}& \frac{2(d-2)\beta_d^2 w(v)}{\pi N_c N_f}\Gamma\left(\frac{d-2}{d-1}\right)\Gamma\left(\frac{d}{d-1}\right)\mathfrak{S}[d-2;w(v)] \\ & \times\int_{\mathbb{R}^{d-1}}\frac{d\mathbf{P}}{(2\pi)^{d-1}}\int_{\mathbb{R}}\frac{dp_y}{(2\pi)}|\mathbf{P}|^{2-d}\left(\frac{\mathbf{P}\cdot(\mathbf{P}+\mathbf{Q})+p_y^2}{\left(\mathbf{P}^2+p_y^2\right)\left[(\mathbf{P}+\mathbf{Q})^2+p_y^2\right]}\right)\end{aligned} \quad \text{(D80)}$$

to leading order in the small v limit. Here $\mathfrak{S}[d-2;w(v)]$ is defined in Eq. (D13).

We introduce a two-variable Feynman parametrization that allows a straightforward integration over p_y,

$$\begin{aligned}\Upsilon_1^{1\mathrm{L}}(\mathbf{Q}) = {}& \frac{(d-2)\beta_d^2 w(v)}{d\pi^{\frac{3}{2}}N_c N_f}\frac{\Gamma\left(\frac{d-2}{d-1}\right)\Gamma\left(\frac{d}{d-1}\right)\Gamma\left(\frac{d+2}{2}\right)\Gamma\left(\frac{d-1}{2}\right)}{\Gamma\left(\frac{d}{2}\right)\Gamma\left(\frac{d-2}{2}\right)}\mathfrak{S}[d-2;w(v)]\int_0^1 dx_1\int_0^{1-x_1}dx_2 \\ & \times\int_{\mathbb{R}^{d-1}}\frac{d\mathbf{P}}{(2\pi)^{d-1}}\frac{(1-x_1-x_2)^{\frac{d-4}{2}}}{(x_1+x_2)^{\frac{3}{2}}}\frac{\left[\mathbf{P}^2-(d-1)(x_1+x_2)\mathbf{P}\cdot(\mathbf{P}+\mathbf{Q})+x_2\mathbf{Q}\cdot(\mathbf{Q}+2\mathbf{P})\right]}{\left(\mathbf{P}^2+2x_2\mathbf{P}\cdot\mathbf{Q}+x_2\mathbf{Q}^2\right)^{\frac{d+1}{2}}}.\end{aligned} \quad \text{(D81)}$$

The integration over $\mathbf{P}$ is logarithmically divergent, and in the large $\Lambda/|\mathbf{Q}|$ limit one obtains

$$\Upsilon_1^{1\mathrm{L}}(\mathbf{Q}) = \frac{(2-d)\beta_d^2 w(v)}{2^{d-2}N_c N_f\pi^{\frac{d+1}{2}}}\frac{\Gamma\left(\frac{d-2}{d-1}\right)\Gamma\left(\frac{d}{d-1}\right)}{\Gamma\left(\frac{d-1}{2}\right)}\mathfrak{S}[d-2;w(v)]\log\left(\frac{\Lambda}{|\mathbf{Q}|}\right). \quad \text{(D82)}$$

From Eq. (13) and the renormalization condition in Eq. (C7), we obtain a counter term for the vertex with

$$Z_6 = 1 - \frac{(d-1)\zeta(d)}{N_c N_f}w(v)\mathfrak{S}[d-2;w(v)]\log\left(\frac{\Lambda}{\mu}\right), \quad \text{(D83)}$$

with $\zeta(d)$ defined in Eq. (23).

APPENDIX E: DERIVATION OF THE LOW-ENERGY FIXED POINT

The self-consistent equation for the dynamically generated boson velocity reads

$$c(v)^{d-1} = \frac{4\beta_d^4\mathfrak{B}(d)}{(3-d)N_c N_f}\frac{v}{c(v)}\mathfrak{S}\left(d-2;\frac{v}{c(v)}\right), \quad \text{(E1)}$$

where $\mathfrak{S}[d-2;v/c(v)]$ its given in Eq. (D13). It is easy to see that

$$c(v) = \left(\frac{4\beta_d^4\mathfrak{B}(d)}{(3-d)N_c N_f}\right)^{\frac{1}{d}}v^{\frac{1}{d}}\mathfrak{S}\left(d-2;v^{\frac{(d-1)}{d}}\right)^{\frac{1}{d}} \quad \text{(E2)}$$

solves Eq. (E1) to the leading order in $v/c(v)$ both in the $v/c(v)\to 0$ limit with $d>2$ and in the $d\to 2$ limit. This follows from the fact that $\mathfrak{S}[d-2;v/c(v)]\sim 1/(d-2)$

in the $v/c(v) \to 0$ limit with $d > 2$, and $\mathfrak{S}[d-2; v/c(v)] \sim -\log[v/c(v)]$ in $d = 2$.

Now we compute the beta function for v in $2 \leqslant d < 3$. Equations (C3) and (C11), and the fact that the bare velocity is independent of the running energy scale μ, yield the beta function for v as a solution to the equation

$$\beta_v = v\left(\frac{1}{Z_3}\frac{\partial Z_3}{\partial \log \mu} - \frac{1}{Z_2}\frac{\partial Z_2}{\partial \log \mu}\right) + v\beta_v\left(\frac{1}{Z_3}\frac{\partial Z_3}{\partial v} - \frac{1}{Z_2}\frac{\partial Z_2}{\partial v}\right). \tag{E3}$$

From the counter term coefficients Z_2 and Z_3 that are obtained to the leading order in the small v limit, the beta function becomes

$$\beta_v \equiv \frac{\partial v}{\partial \ln \mu} = \frac{4\left(N_c^2-1\right)}{N_c N_f} v\left[\frac{(d-1)}{\pi}\zeta(d) v \mathfrak{S}[d-2; c(v)] + \frac{2\beta_d^4}{N_c N_f}\mathfrak{F}(d) w(v)^2 \mathfrak{S}[d-2; w(v)]^2\right]. \tag{E4}$$

In any $2 \leqslant d < 3$, $\beta_v > 0$ for $v \ll 1$. This implies that v decreases as energy is lowered once the bare value of v is small. Since our calculation is controlled in the small v limit, we conclude that $v \to 0$ limit is a stable fixed point with a finite basin of attraction.

Factoring out the first term in the square brackets we can use

$$\frac{2\pi\beta_d^4 \mathfrak{F}(d)}{N_c N_f (d-1)\zeta(d)} \frac{w(v)^2}{v} \frac{\mathfrak{S}[d-2; w(v)]^2}{\mathfrak{S}[d-2; c(v)]} \approx v^{\frac{(d-2)}{d}} \mathfrak{S}\left(d-2; v^{\frac{d-1}{d}}\right)^{\frac{(d-2)}{d}}, \tag{E5}$$

close to $d = 2$, to rewrite the beta function as

$$\beta_v = \frac{4(d-1)\left(N_c^2-1\right)}{\pi N_c N_f}\zeta(d) v^2 \mathfrak{S}\left(d-2; v^{\frac{d-1}{d}}\right) \times \left[1 + v^{\frac{(d-2)}{d}} \mathfrak{S}\left(d-2; v^{\frac{d-1}{d}}\right)^{\frac{(d-2)}{d}}\right]. \tag{E6}$$

Equation (E5) follows from Eq. (E1) and the fact that $\mathfrak{S}[d-2; c(v)] \approx \mathfrak{S}[d-2; w(v)] \approx \mathfrak{S}(d-2; v^{\frac{d-1}{d}})$ close to $d = 2$. In Eq. (E5) we use the numerical coefficient evaluated at $d = 2$ because the second term in the square brackets of Eq. (E4) is only important in the low-energy limit in $d = 2$.

We define the logarithmic length scale $l = \log(\Lambda/\mu)$, where Λ is a UV energy scale. The IR beta function that describes the flow of v with increasing length scale can be rewritten as

$$\frac{dv(l)}{dl} = -\frac{4(d-1)\left(N_c^2-1\right)}{\pi N_c N_f}\zeta(d) v(l)^2 \mathfrak{S}\left[d-2; v(l)^{\frac{d-1}{d}}\right] \times \left\{1 + v(l)^{\frac{(d-2)}{d}} \mathfrak{S}\left[d-2; v(l)^{\frac{d-1}{d}}\right]^{\frac{(d-2)}{d}}\right\}, \tag{E7}$$

with a boundary condition $v(0) = v_0$. We note that the term in square brackets is merely a constant in the small v limit in $d \geqslant 2$. On the other hand, $\mathfrak{S}[d-2; v(l)^{\frac{d-1}{d}}]$ provides, at most, a logarithmic correction in $d = 2$. With the l dependence of $v(l)$ ignored inside logarithms, the solution to Eq. (E7) can be cast in the following implicit form:

$$v(l) = \frac{1}{\frac{1}{v_0} + \mathbb{F}[v(l)] l},$$

$$\mathbb{F}[v(l)] = \frac{4(d-1)\left(N_c^2-1\right)\zeta(d)}{\pi N_c N_f}\mathfrak{S}\left[d-2; v(l)^{\frac{d-1}{d}}\right] \times \left\{1 + v(l)^{\frac{(d-2)}{d}} \mathfrak{S}\left[d-2; v(l)^{\frac{d-1}{d}}\right]^{\frac{(d-2)}{d}}\right\}. \tag{E8}$$

This equation for $v(l)$ can be solved iteratively in the low-energy limit. The initial condition naturally provides the logarithmic length scale $l_0^{-1} = v_0 \mathbb{F}(v_0) \sim \frac{\left(N_c^2-1\right)}{N_c N_f} v_0 \mathfrak{S}(d-2; v_0^{\frac{d-1}{d}})$ below which the solution in Eq. (E8) becomes independent of v_0 and reduces to the universal form:

$$v(l) = \frac{\pi N_c N_f}{4(d-1)\left(N_c^2-1\right)} \frac{1}{\zeta(d)} \frac{1}{l} \frac{1}{\mathfrak{S}\left(d-2; l^{-\frac{(d-1)}{d}}\right)} \times \left[\frac{1}{1 + l^{-\frac{(d-2)}{d}}}\right]. \tag{E9}$$

Equation (E9) continuously interpolates the form of $v(l)$ found in two and close to three dimensions [53,72]. In obtaining Eq. (E9) we used the limiting forms of Eq. (D13) repeatedly to discard subleading terms in the $l \gg l_0$ limit.

APPENDIX F: CRITICAL EXPONENTS AND PHYSICAL OBSERVABLES

From Eqs. (C10) and (C12) the dynamical critical exponent and the anomalous dimensions of the fields, defined as the deviations from the interaction-driven scaling, are given by

$$z = 1 - \frac{d}{d \log \mu}(\log Z_3 - \log Z_1), \tag{F1}$$

$$\eta_\Psi = \frac{1}{2}\frac{d}{d \log \mu}[d \log Z_3 - (d-1)\log Z_1], \tag{F2}$$

$$\eta_\Phi = \frac{1}{2}\frac{d}{d \log \mu}[2\log Z_6 - 2(d-1)\log Z_1 - \log Z_2 + (2d-3)\log Z_3]. \tag{F3}$$

At low energies, v flows to zero faster than the ratio $w(v) = v/c(v)$. The dominant contributions to z and η_Ψ come from Z_1 in the small v limit, while η_Φ is dominated by Z_6 and Z_1. To the leading order in v, the dynamical critical exponent and the anomalous scaling dimensions are given by

$$z = 1 + \frac{\left(N_c^2-1\right)}{N_c N_f}\zeta(d) w(v), \tag{F4}$$

$$\eta_\Psi = -\frac{\left(N_c^2-1\right)}{N_c N_f}\frac{(d-1)\zeta(d)}{2} w(v), \tag{F5}$$

$$\eta_\Phi = \frac{(d-1)\zeta(d)}{N_c N_f}\left\{\mathfrak{S}[d-2; w(v)] - \left(N_c^2-1\right)\right\} w(v). \tag{F6}$$

The scaling forms of the two-point functions are dictated by the renormalization group equation,

$$\left[z\mathbf{K}\cdot\boldsymbol{\nabla}_{\mathbf{K}}+\vec{k}\cdot\boldsymbol{\nabla}_{\vec{k}}-\beta_v\frac{\partial}{\partial v}+D_{\mathsf{a}}\right]\Gamma^{(2)}_{\mathsf{a}}(k,v;\mu)=0. \tag{F7}$$

Here $\mathsf{a}=\mathsf{b},\mathsf{f}$ labels the bosonic and fermionic cases, respectively. D_{a} denotes the total scaling dimension of the operator given by

$$D_{\mathsf{f}}=2\eta_\Psi+z(d-1)-d, \tag{F8}$$

$$D_{\mathsf{b}}=2\eta_\Phi+z(d-1)-2(d-1). \tag{F9}$$

Equation (F7) can be written as

$$\left[\mathbf{K}\cdot\boldsymbol{\nabla}_{\mathbf{K}}+\frac{\vec{k}}{z(l)}\cdot\boldsymbol{\nabla}_{\vec{k}}+\frac{d}{dl}+\frac{D_{\mathsf{a}}(l)}{z(l)}\right]\Gamma^{(2)}_{\mathsf{a}}(k,v(l))=0, \tag{F10}$$

where $v(l)$ is the solution of

$$\frac{dv(l)}{dl}=-\frac{\beta_v}{z(l)},\quad v(0)=v_0, \tag{F11}$$

and $l=l(\Lambda/\mu)$ is a logarithmic length scale. The solution to Eq. (F10) can be written as

$$\Gamma^{(2)}_{\mathsf{a}}(\mathbf{K},\vec{k},v_0)=\exp\left(\int_0^l d\ell\frac{D_{\mathsf{a}}(\ell)}{z(\ell)}\right)\times\Gamma^{(2)}_{\mathsf{a}}\left[e^l\mathbf{K},\exp\left(\int_0^l\frac{d\ell}{z(\ell)}\right)\vec{k},v(l)\right]. \tag{F12}$$

Here $z(\ell)$ and $D_{\mathsf{a}}(\ell)$ should be viewed as functions of the logarithmic length scale, where $w(v)$ in Eqs. (F4), (F5), (F6), and (F9) are replaced by

$$w(l)=\frac{\pi N_cN_f}{4(d-1)\left[\zeta(d)\left(N_c^2-1\right)\right]^{\frac{d-1}{d}}}\left[\frac{(3-d)(d-1)}{\pi\beta_d^4\mathfrak{B}(d)}\right]^{\frac{1}{d}}\times\left[\frac{1}{1+l^{-\frac{(d-2)}{d}}}\right]^{\frac{d-1}{d}}\frac{1}{l^{\frac{d-1}{d}}}\frac{1}{\mathfrak{S}\left(d-2;l^{-\frac{d-1}{d}}\right)}, \tag{F13}$$

in the large l limit. Similarly, the scale-dependent velocity of the collective mode is given by

$$c(l)=\left(\frac{\pi\beta_d^4\mathfrak{B}(d)}{(3-d)(d-1)\left(N_c^2-1\right)\zeta(d)}\right)^{\frac{1}{d}}\left[\frac{1}{1+l^{-\frac{(d-2)}{d}}}\right]^{\frac{1}{d}}\frac{1}{l^{\frac{1}{d}}}. \tag{F14}$$

In order to compute Eq. (F12) for the fermionic two-point function, we consider

$$\frac{D_{\mathsf{f}}(l)}{z(l)}=\frac{2\eta_\Psi(l)+z(l)(d-1)-d}{z(l)}=-\frac{1}{z(l)}+\frac{2\eta_\Psi(l)+(d-1)[z(l)-1]}{z(l)}, \tag{F15}$$

where the contribution from the dynamical critical exponent and that from the net anomalous scaling dimension of the fermion field are separated. The crossover function in Eq. (F12) is determined by

$$I_z(l)=\int_0^l\frac{d\ell}{z(\ell)}\quad\text{and}$$

$$I_\Psi(l)=\int_0^l d\ell\left(\frac{2\eta_\Psi(\ell)+(d-1)[z(\ell)-1]}{z(\ell)}\right). \tag{F16}$$

Since the critical exponents are controlled by $w(v)=v/c(v)\gg v$ it follows that, to the leading order in v, the contribution from the dynamical critical exponent is dominated by the counter term coefficient Z_1 and, consequently,

$$I_z(l)=\int_0^l d\ell\left(1-\frac{\left(N_c^2-1\right)}{N_cN_f}\zeta(d)w(\ell)\right)=l-\mathfrak{F}_z(d)\left(N_c^2-1\right)^{\frac{1}{d}}\left[\frac{1}{1+l^{-\frac{(d-2)}{d}}}\right]^{\frac{d-1}{d}}\times\frac{l^{\frac{1}{d}}}{\mathfrak{S}\left(d-2;l^{-\frac{(d-1)}{d}}\right)}, \tag{F17}$$

where $\mathfrak{S}(\xi;a)$ is defined in Eq. (D13), $\mathfrak{F}_z(d)$ is defined in Eq. (31), and the last equality follows from taking the $l\to\infty$ limit. Similarly, the contribution from the net anomalous scaling dimension is dominated by Z_3 at low energies,

$$I_\Psi(l)=\frac{\left(N_c^2-1\right)}{N_cN_f}\int_0^l d\ell\left[\frac{2(d-1)}{\pi}\zeta(d)v(\ell)\mathfrak{S}[d-2;c(\ell)]+\frac{2\beta_d^4}{N_cN_f}\mathfrak{F}(d)w(\ell)^2\mathfrak{S}[d-2;w(\ell)]^2\right]. \tag{F18}$$

From Eq. (E9) we use

$$v(l)\mathfrak{S}\left[d-2;v(l)^{\frac{d-1}{d}}\right]\approx\frac{\pi N_cN_f}{4(d-1)\left(N_c^2-1\right)}\frac{1}{\zeta(d)}\times\left[\frac{1}{1+l^{-\frac{(d-2)}{d}}}\right]\frac{1}{l} \tag{F19}$$

to write

$$I_\Psi(l)=\frac{1}{2}\left[\frac{1}{1+l^{-\frac{(d-2)}{d}}}\right]\left[\log l+\mathfrak{S}\left(d-2;l^{-\frac{1}{d}}\right)\right] \tag{F20}$$

in the large l limit. In obtaining Eq. (F20) from Eq. (F18) one has to use the expression for $v(l)$ without dropping the term depending on v_0 prior to the integration. Only after the integration is done, the terms depending on v_0 can be thrown away safely. Since the fermion two-point function reduces to the bare one in the small v limit, the two-point function for nonzero v is given by

$$\Gamma^{(2,0)}_n(\mathbf{K},\vec{k})=\Gamma^{(2)}_{\mathsf{f}}(\mathbf{K},\vec{k})=F_\Psi(|\mathbf{K}|)[iF_z(|\mathbf{K}|)\boldsymbol{\Gamma}\cdot\mathbf{K}+i\gamma_{d-1}\varepsilon_n(\vec{k};v_{|\mathbf{K}|})] \tag{F21}$$

for $e^{I_z(\log[\Lambda/|\mathbf{K}|])}\vec{k}$ fixed. Here $v_{|\mathbf{K}|} = v(\log[\Lambda/|\mathbf{K}|])$. The universal functions,

$$F_z(|\mathbf{K}|) = \exp\left(\mathfrak{F}_z(d)\left(N_c^2-1\right)^{\frac{1}{d}}\left[\frac{1}{1+[\log(\Lambda/|\mathbf{K}|)]^{-\frac{(d-2)}{d}}}\right]^{\frac{d-1}{d}} \times \frac{[\log(\Lambda/|\mathbf{K}|)]^{\frac{1}{d}}}{\mathfrak{S}\left(d-2;[\log(\Lambda/|\mathbf{K}|)]^{-\frac{(d-1)}{d}}\right)}\right), \tag{F22}$$

$$F_\Psi(|\mathbf{K}|) = \exp\left(\frac{1}{2}\left[\frac{1}{1+[\log(\Lambda/|\mathbf{K}|)]^{-\frac{(d-2)}{d}}}\right]\left[\log\log(\Lambda/|\mathbf{K}|) + \mathfrak{S}\left(d-2;[\log(\Lambda/|\mathbf{K}|)]^{-\frac{1}{d}}\right)\right]\right), \tag{F23}$$

capture the deviations of the dynamical critical exponent and the anomalous scaling dimension of the fermion field from their values at the low-energy fixed point.

For the bosonic two-point function in Eq. (F12), we consider

$$\frac{D_\mathrm{b}(l)}{z(l)} = \frac{2\eta_\Phi(l)+z(l)(d-1)-2(d-1)}{z(l)} = -\frac{(d-1)}{z(l)} + \frac{2\eta_\Phi(l)+[z(l)-1](d-1)}{z(l)}, \tag{F24}$$

where we have separated the contribution from the dynamical critical exponent and the net anomalous dimension of the bosonic field. The latter contribution to the two-point function is captured by

$$I_\Phi(l) = \int_0^l d\ell \frac{\{2\eta_\Phi(\ell)+(d-1)[z(\ell)-1]\}}{z(\ell)}. \tag{F25}$$

$I_\Phi(l)$ is dominated by the counter terms Z_6 and Z_1 in the small v limit, and we can write

$$I_\Phi(l) = \frac{\mathfrak{F}_\Phi(d)}{\left(N_c^2-1\right)^{\frac{d-1}{d}}}\left[\frac{1}{1+l^{-\frac{(d-2)}{d}}}\right]^{\frac{d-1}{d}} l^{\frac{1}{d}} \times\left(1-\frac{\left(N_c^2-1\right)}{2\mathfrak{S}\left(d-2;l^{-\frac{(d-1)}{d}}\right)}\right), \tag{F26}$$

where $\mathfrak{F}_\Phi(d)$ is defined in Eq. (33). Using Eqs. (F12) and (F17) and taking into account the fact that the bosonic two-point vertex function reduces to Eq. (15) for $v \ll 1$, we obtain

$$\Gamma^{(0,2)}(\mathbf{Q},\vec{q}) = \Gamma_\mathrm{b}^{(2)}(\mathbf{Q},\vec{q}) = F_\Phi(|\mathbf{Q}|)\left[F_z(|\mathbf{Q}|)^{d-1}|\mathbf{Q}|^{d-1} + c_{|\mathbf{Q}|}^{d-1}(|q_x|^{d-1}+|q_y|^{d-1})\right] \tag{F27}$$

for $e^{I_z(\log[\Lambda/|\mathbf{Q}|])}\vec{q}$ fixed. Here

$$F_\Phi(|\mathbf{Q}|) = \exp\left\{\frac{\mathfrak{F}_\Phi(d)[\log(\Lambda/|\mathbf{Q}|)]^{\frac{1}{d}}}{\left(N_c^2-1\right)^{\frac{d-1}{d}}}\left[\frac{1}{1+[\log(\Lambda/|\mathbf{Q}|)]^{-\frac{(d-2)}{d}}}\right]^{\frac{d-1}{d}} \times\left[1-\frac{\left(N_c^2-1\right)}{2\mathfrak{S}\left(d-2;[\log(\Lambda/|\mathbf{Q}|)]^{-\frac{(d-1)}{d}}\right)}\right]\right\}, \tag{F28}$$

and $c_{|\mathbf{Q}|} = c(\log[\Lambda/|\mathbf{Q}|])$ capture the scale-dependent anomalous dimension and the velocity of the collective mode.

[1] S. Sachdev, *Quantum Phase Transitions*, 2nd ed. (Cambridge University Press, Cambridge, 2011).
[2] N. Seiberg, Phys. Lett. B **318**, 469 (1993).
[3] R. Rattazzi, V. S. Rychkov, E. Tonni, and A. Vichi, J. High Energy Phys. 12 (2008) 031.
[4] S. El-Showk, M. F. Paulos, D. Poland, S. Rychkov, D. Simmons-Duffin, and A. Vichi, J. Stat. Phys. **157**, 869 (2014).
[5] T. Holstein, R. E. Norton, and P. Pincus, Phys. Rev. B **8**, 2649 (1973).
[6] J. A. Hertz, Phys. Rev. B **14**, 1165 (1976).
[7] P. A. Lee, Phys. Rev. Lett. **63**, 680 (1989).
[8] M. Y. Reizer, Phys. Rev. B **40**, 11571 (1989).
[9] P. A. Lee and N. Nagaosa, Phys. Rev. B **46**, 5621 (1992).
[10] A. J. Millis, Phys. Rev. B **48**, 7183 (1993).
[11] B. L. Altshuler, L. B. Ioffe, and A. J. Millis, Phys. Rev. B **50**, 14048 (1994).
[12] Y. B. Kim, A. Furusaki, X.-G. Wen, and P. A. Lee, Phys. Rev. B **50**, 17917 (1994).
[13] C. Nayak and F. Wilczek, Nucl. Phys. B **417**, 359 (1994).
[14] J. Polchinski, Nucl. Phys. B **422**, 617 (1994).
[15] A. Abanov and A. V. Chubukov, Phys. Rev. Lett. **84**, 5608 (2000).
[16] G. R. Stewart, Rev. Mod. Phys. **73**, 797 (2001).
[17] A. Abanov, A. V. Chubukov, and J. Schmalian, Adv. Phys. **52**, 119 (2003).
[18] A. Abanov and A. Chubukov, Phys. Rev. Lett. **93**, 255702 (2004).
[19] H. v. Löhneysen, A. Rosch, M. Vojta, and P. Wölfle, Rev. Mod. Phys. **79**, 1015 (2007).
[20] T. Senthil, Phys. Rev. B **78**, 035103 (2008).
[21] S.-S. Lee, Phys. Rev. B **80**, 165102 (2009).
[22] D. F. Mross, J. McGreevy, H. Liu, and T. Senthil, Phys. Rev. B **82**, 045121 (2010).
[23] M. A. Metlitski and S. Sachdev, Phys. Rev. B **82**, 075127 (2010).
[24] M. A. Metlitski and S. Sachdev, Phys. Rev. B **82**, 075128 (2010).
[25] S. A. Hartnoll, D. M. Hofman, M. A. Metlitski, and S. Sachdev, Phys. Rev. B **84**, 125115 (2011).
[26] E. Abrahams and P. Wölfe, Proc. Natl. Acad. Sci. USA **109**, 3238 (2012).
[27] H.-C. Jiang, M. S. Brock, R. V. Mishmash, J. R. Garrison, D. Sheng, O. I. Motrunich, and M. P. Fisher, Nature (London) **493**, 39 (2013).
[28] A. L. Fitzpatrick, S. Kachru, J. Kaplan, and S. Raghu, Phys. Rev. B **88**, 125116 (2013).

[29] D. Dalidovich and S.-S. Lee, Phys. Rev. B **88**, 245106 (2013).
[30] J. Lee, P. Strack, and S. Sachdev, Phys. Rev. B **87**, 045104 (2013).
[31] P. Strack and P. Jakubczyk, Phys. Rev. X **4**, 021012 (2014).
[32] S. Sur and S.-S. Lee, Phys. Rev. B **90**, 045121 (2014).
[33] A. A. Patel and S. Sachdev, Phys. Rev. B **90**, 165146 (2014).
[34] S. Sur and S.-S. Lee, Phys. Rev. B **91**, 125136 (2015).
[35] S. P. Ridgway and C. A. Hooley, Phys. Rev. Lett. **114**, 226404 (2015).
[36] T. Holder and W. Metzner, Phys. Rev. B **92**, 041112 (2015).
[37] A. A. Patel, P. Strack, and S. Sachdev, Phys. Rev. B **92**, 165105 (2015).
[38] C. M. Varma, Phys. Rev. Lett. **115**, 186405 (2015).
[39] A. Eberlein, Phys. Rev. B **92**, 235146 (2015).
[40] S. A. Maier and P. Strack, Phys. Rev. B **93**, 165114 (2016).
[41] Y. Schattner, S. Lederer, S. A. Kivelson, and E. Berg, Phys. Rev. X **6**, 031028 (2016).
[42] S. Sur and S.-S. Lee, Phys. Rev. B **94**, 195135 (2016).
[43] Z. H. Liu, X. Y. Xu, Y. Qi, K. Sun, and Z. Y. Meng, Phys. Rev. B **98**, 045116 (2018).
[44] X. Y. Xu, K. Sun, Y. Schattner, E. Berg, and Z. Y. Meng, Phys. Rev. X **7**, 031058 (2017).
[45] Z. H. Liu, X. Y. Xu, Y. Qi, K. Sun, and M. Z. Yang, arXiv:1801.00127.
[46] D. Chowdhury, Y. Werman, E. Berg, and T. Senthil, Phys. Rev. X **8**, 031024 (2018).
[47] C. M. Varma, W. J. Gannon, M. C. Aronson, J. A. Rodriguez-Rivera, and Y. Qiu, Phys. Rev. B **97**, 085134 (2018).
[48] E. Berg, S. Lederer, Y. Schattner, and S. Trebst, arXiv:1804.01988.
[49] L. D. Landau, Zh. Eksp. Teor. Fiz. **30**, 1058 (1956) [Sov. Phys. JETP **3**, 920 (1957)].
[50] S. Chakravarty, R. E. Norton, and O. F. Syljuåsen, Phys. Rev. Lett. **74**, 1423 (1995).
[51] I. Mandal and S.-S. Lee, Phys. Rev. B **92**, 035141 (2015).
[52] For an earlier implementation of dimensional regularization that tunes the codimension of the Fermi surface for a superconducting QCP, see Ref. [76].
[53] P. Lunts, A. Schlief, and S.-S. Lee, Phys. Rev. B **95**, 245109 (2017).
[54] S.-S. Lee, Annu. Rev. Condens. Matter Phys. **9**, 227 (2018).
[55] K. G. Wilson and M. E. Fisher, Phys. Rev. Lett. **28**, 240 (1972).
[56] K. G. Wilson, Phys. Rev. D **7**, 2911 (1973).
[57] L. Di Pietro, Z. Komargodski, I. Shamir, and E. Stamou, Phys. Rev. Lett. **116**, 131601 (2016).
[58] L. Di Pietro and E. Stamou, J. High Energy Phys. 12 (2017) 054.
[59] L. Di Pietro and E. Stamou, Phys. Rev. D **97**, 065007 (2018).
[60] V. S. de Carvalho and H. Freire, Nucl. Phys. B **875**, 738 (2013).
[61] V. S. de Carvalho and H. Freire, Ann. Phys. **348**, 32 (2014).
[62] E. Berg, M. Metlitski, and S. Sachdev, Science **338**, 1606 (2012).
[63] Z.-X. Li, F. Wang, H. Yao, and D.-H. Lee, Sci. Bull. **61**, 925 (2016).
[64] Y. Schattner, M. H. Gerlach, S. Trebst, and E. Berg, Phys. Rev. Lett. **117**, 097002 (2016).
[65] M. H. Gerlach, Y. Schattner, E. Berg, and S. Trebst, Phys. Rev. B **95**, 035124 (2017).
[66] X. Wang, Y. Schattner, E. Berg, and R. M. Fernandes, Phys. Rev. B **95**, 174520 (2017).
[67] Z.-X. Li, F. Wang, H. Yao, and D.-H. Lee, Phys. Rev. B **95**, 214505 (2017).
[68] X. Wang, Y. Wang, Y. Schattner, E. Berg, and R. M. Fernandes, Phys. Rev. Lett. **120**, 247002 (2018).
[69] T. Helm, M. V. Kartsovnik, I. Sheikin, M. Bartkowiak, F. Wolff-Fabris, N. Bittner, W. Biberacher, M. Lambacher, A. Erb, J. Wosnitza, and R. Gross, Phys. Rev. Lett. **105**, 247002 (2010).
[70] K. Hashimoto, K. Cho, T. Shibauchi, S. Kasahara, Y. Mizukami, R. Katsumata, Y. Tsuruhara, T. Terashima, H. Ikeda, M. A. Tanatar, H. Kitano, N. Salovich, R. W. Giannetta, P. Walmsley, A. Carrington, R. Prozorov, and Y. Matsuda, Science **336**, 1554 (2012).
[71] T. Park, F. Ronning, H. Yuan, M. Salamon, R. Movshovich, J. Sarrao, and J. Thompson, Nature (London) **440**, 65 (2006).
[72] A. Schlief, P. Lunts, and S.-S. Lee, Phys. Rev. X **7**, 021010 (2017).
[73] Y. Huh and S. Sachdev, Phys. Rev. B **78**, 064512 (2008).
[74] C. M. Varma, P. B. Littlewood, S. Schmitt-Rink, E. Abrahams, and A. E. Ruckenstein, Phys. Rev. Lett. **63**, 1996 (1989).
[75] C. Varma, Z. Nussinov, and W. van Saarloos, Phys. Rep. **361**, 267 (2002).
[76] T. Senthil and R. Shankar, Phys. Rev. Lett. **102**, 046406 (2009).